

Organic aerosol source apportionment in Zurich using an extractive electrospray ionization time-of-flight mass spectrometry (EESI-TOF): Part II, biomass burning influences in winter

Lu Qi^{1,2}, Mindong Chen², Giulia Stefenelli¹, Veronika Pospisilova¹, Yandong Tong¹, Amelie Bertrand¹,
5 Christoph Hueglin³, Xinlei Ge², Urs Baltensperger¹, André S. H. Prévôt¹, Jay G. Slowik¹

¹Laboratory of Atmospheric Chemistry, Paul Scherrer Institute (PSI), Switzerland

²Nanjing University of Information Science & Technology, 21000 Nanjing, China

³EMPA, Dübendorf 8600, Switzerland

Correspondence to: Jay G. Slowik (jay.slowik@psi.ch) and André S. H. Prévôt (andre.prevot@psi.ch)

Abstract.

Real-time, in situ molecular composition measurements of the organic fraction of fine particulate matter (PM_{2.5}) remain challenging, hindering a full understanding of the climate impacts and health effects of PM_{2.5}. In particular, the thermal decomposition and ionization-induced fragmentation affecting current techniques has limited a detailed investigation of secondary organic aerosol (SOA), which typically dominates OA. Here we deploy a novel extractive electrospray ionization time-of-flight mass spectrometer (EESI-TOF-MS) during winter 2017 in downtown Zurich, Switzerland, which overcomes these limitations, together with an Aerodyne high resolution time of flight aerosol mass spectrometer (HR-TOF-AMS) and supporting instrumentation. Positive matrix factorization (PMF) implemented within the Multilinear Engine (ME-2) was applied to the EESI-TOF data to quantify the primary and secondary contributions to OA. An 11-factor solution was selected as the best representation of the data, including 5 primary and 6 secondary factors. Primary factors showed influence from cooking, cigarette smoke, biomass burning (2 factors) and a special local unknown event occurred only during two nights. Secondary factors were affected by biomass burning (3 factors, distinguished by temperature and/or wind direction), organonitrates, monoterpene oxidation, and undetermined regional processing, in particular the contributions of wood combustion. While the AMS attributed slightly over half the OA mass to SOA but did not identify its source, the EESI-TOF showed that most (> 70 %) of the SOA was derived from biomass burning. Together with significant contributions from less aged biomass burning factors identified by both AMS and EESI-TOF, this firmly establishes biomass burning as the single most important contributor to OA mass at this site during winter. High correlation was obtained between EESI-TOF and AMS PMF factors where specific analogues existed, as well as between total signal and POA/SOA apportionment. This suggests the EESI-TOF apportionment in the current study can be approximately taken at face value, despite ion-by-ion differences in relative sensitivity. The apportionment of specific ions measured by the EESI-TOF (e.g. levoglucosan, nitrocatechol, and selected organic acids), and utilization of a cluster analysis-based approach to identify key marker ions for the EESI-TOF factors are investigated. The interpretability of the EESI-TOF results and improved source separation relative to the AMS within this pilot campaign validate the EESI-TOF as a promising approach to source apportionment and atmospheric composition research.

25 1 Introduction

Organic aerosol (OA) is relevant due to its roles in several atmospheric processes including radiative forcing, visibility, heterogeneous reactions, and uncertain effects on human health (Nel, 2005; Docherty et al., 2008; Stocker, 2013). OA sources are typically classified as either directly emitted primary organic aerosol (POA) or secondary organic aerosol (SOA) formed from gas-to-particle conversion after chemical reactions. SOA is estimated to comprise approximately 20 % to 90 % of OA, depending on location and time of year (Jimenez et al., 2009; Hallquist et al., 2009). Many studies have successfully linked POA to specific sources, but the level of chemical characterization achieved by conventional online instrumentation has been

in most cases proven insufficient for quantitative resolution of SOA source contributions and/or formation pathways. Therefore, the effects of individual SOA sources on health and climate remain poorly constrained, hampering the design of efficient emissions control policies.

A range of methods to measure molecular composition of aerosol particles have so far mostly been conducted offline, using filter samples (Wang et al., 2009; Daellenbach et al., 2017; Wang et al., 2017). Compared to online methods, offline methods have low time resolution typically integrating aerosol over hours and introducing sampling/storage artifacts (Timkovsky et al., 2015). Moreover, offline measurement techniques like gas chromatography-mass spectrometry (GC-MS) or liquid chromatography-mass spectrometry (LC-MS), are chemically highly specific, but often struggle with the fraction of mass that can be characterized (typically < 20 % of the total OA), which hinders our understanding of the SOA.

Currently available online speciation techniques to measure aerosol particle composition often rely on some type of thermal desorption and/or hard ionization leading to thermal decomposition and/or ionization-induced fragmentation of the original molecules. For example, the Aerodyne aerosol mass spectrometer (AMS) vaporizes molecules at 600 C followed by electron ionization at 70 eV, facilitating quantification but yielding extensive decomposition and fragmentation (Jayne et al., 2000; Sasaki et al., 2001; Samy et al., 2011; Hayes et al., 2013). The chemical analysis of aerosol online-proton transfer reaction mass spectrometer (CHARON-PTR-MS) has no significant thermal decomposition but **the ionization scheme fragments typical SOA molecules** (Eichler et al., 2015; Muller et al., 2017). Several semi-continuous methods have also been developed, including the thermal desorption aerosol-GC (TAG-MS, **GC-family**, Williams et al., 2006) and gas and aerosols-chemical ionization time-of-flight mass spectrometer (FIGAERO-CIMS, Lopez-Hilfiker et al., 2014). However, these systems remain subject to some degree of thermal decomposition, as well as potential reaction on the collection substrate, and significantly lower time resolution. Above all, an online instrument able to detect the original OA and resolve its chemical composition at the molecular level with higher time resolution is needed. The Paul Scherrer Institute (PSI) has developed such an instrument, i.e., the extractive electrospray ionization time-of-flight mass spectrometer (EESI-TOF), measuring particles at molecule level with a time resolution of seconds while overcoming the usual limitations, e.g. thermal decomposition, ionization-induced fragmentation, semi-continuous operation (**Lopez-Hilfiker et al., 2019**).

Due to the lacking ability to apportion SOA to specific sources, a terminology based on properties rather than sources was previously introduced, such as the AMS-based discrimination into semi-volatile and low-volatility oxygenated organic aerosol (SV-OOA and LV-OOA, respectively). The current state-of-the art SOA source apportionment is to be improved based on large laboratory experiments which generate a “library” of species of the SOA products (Zhang et al., 2015; Bianchi et al., 2017; Nakao et al., 2011; Nah et al., 2016; Zhang et al., 2017a). An isoprene-OA source was identified based on fragments in AMS and ACSM (Aerosol Chemical Speciation Monitor) mass spectra that are consistent with those of laboratory-generated isoprene SOA (via reactive uptake of epoxydiols (IEPOX), Xu et al., 2015; Zhang et al., 2017b). Offline analysis identified winter OOA and summer OOA which to some extent appears to be linked to sources (Daellenbach et al., 2017; Daellenbach et al., 2016; Bozzetti et al., 2016), even though the corresponding sources cannot be retrieved (**Lu et al., in prep**). Zhang et al.,

(2018) combined the offline GC-MS method and online FIGAERO-CIMS measurements to better characterize summertime monoterpene SOA.

Domestic wood combustion has been identified as a major source of OA in central Europe (Lanz et al., 2010; Herich et al., 2014), as well as in Asia (Sun et al., 2013; Quan et al., 2014). Recent studies have been devoted to the chemical characterization of the gas and particle-phase emissions from biomass burning in the laboratory, to provide information for a better source apportionment of primary and secondary biomass burning OA (Iinuma et al., 2010; Nakao et al., 2011; Ofner et al., 2011; Chan et al., 2005; Bruns et al., 2017; Bertrand et al., 2018). Various tracer compounds for biomass burning were reported, including levoglucosan, which is a sugar anhydride compound produced from the pyrolysis of cellulose and hemicellulose (Fine et al., 2001), or methoxyphenols (e.g. guaiacol and syringol), derived from the pyrolysis of lignin (Coeur-Tourneur et al., 2009; Veres et al., 2010; He et al., 2018), and methyl-nitrocatechols, nitrated aromatic compounds from biomass burning (Iimuma et al., 2010a). Furthermore, biomass burning has been shown to produce significant SOA in laboratory measurements (Bruns et al., 2016; Nakao et al., 2011; Yee et al., 2013; Stefenelli et al., 2019), but this component has not yet been resolved in the field with the partial exception of winter OOA.

Here, we report on a study in Zurich, a mid-size city in Central Europe, utilizing the EESI-TOF, complemented with AMS source apportionment results for a winter case. Summer measurement and source apportionment are presented in the companion paper (Stefenelli et al., 2019). In both cases, due to the enhanced chemical resolution of the EESI-TOF we are able to resolve more POA and SOA sources than in previous studies at the same site.

2 Methodologies

2.1 Measurement Campaign

Measurements were performed from 25 January to 5 February, 2017 at the Swiss National Air Pollution Monitoring Network (NABEL) station at Zurich Kaserne, Switzerland (Richard et al., 2011). The station is located in the center of the metropolitan area of Zurich (1.3 million inhabitants). It is characterized as an urban background site, although several restaurants are nearby (Lanz et al., 2007). Long-term measurements at the site include ambient meteorological data such as temperature, relative humidity (RH), solar radiation, wind speed and direction, trace gas measurements comprising nitrogen oxides (NO_x, Thermo Environmental Instruments 42i, Thermo Electro Corp., Waltham, MA) and ozone (O₃, Thermo Environmental Instruments 49C, Thermo Electro Corp., Waltham, MA), and particle measurements which include size distributions (scanning mobility particle sizer, SMPS, TSI) and number concentration (condensation particle counter, CPC). Although the measurement period is relatively short (12 days), the similarity of the AMS results obtained in the current study to previous AMS and ACSM measurements at the same site (Lanz et al., 2007, Canonaco et al., 2013, Richard et al., 2011, Daellenbach et al., 2016) give us high confidence that the sampled aerosol is representative of typical wintertime conditions. Exceptions to this are resolved by the source apportionment into unique event-driven factors, as discussed in the results section.

For the intensive campaign, an EESI-TOF, an HR-TOF-AMS (Aerodyne Research Inc.) and an SMPS were additionally deployed. The sampling was performed in a mobile trailer installed outside the NABEL station. Ambient air was sampled through a PM_{2.5} cyclone to remove coarse particles (~75 cm above the trailer roof and ~5 m above ground). The air passed through a stainless steel (~6 mm) tube into the AMS, EESI-TOF, and SMPS, installed on the same line and in close proximity.

5 2.2 Instrumentation

2.2.1 Extractive Electrospray Ionization Time-of-flight Mass Spectrometer (EESI-TOF)

The extractive electrospray ionization time-of-flight mass spectrometer (EESI-TOF) is a novel instrument for real-time measurement of organic aerosol without thermal decomposition or ionization-induced fragmentation. The instrument is discussed in detail elsewhere (Lopez-Hilfiker et al., 2019) and a brief overview is presented here. Ambient aerosol is continuously sampled at 900 cm³ min⁻¹, either directly or through a particle filter to yield a background measurement. In this study, 10 mins ambient air sampling was alternated with 2 mins through the filter with spectra recorded with 40 s time resolution. The flow then passes through a 5 cm long 6 mm outer diameter (OD) multi-channel extruded carbon denuder housed in a stainless steel tube, which removes most trace gas phase species. The denuder eliminates artifacts from semi-volatile species desorbing from the filter, and also improves detection limits by reducing the gas-phase background. The particle-laden flow then intersects a spray of charged droplets generated by a conventional electrospray capillary. Particles collide with the electrospray droplets and the soluble components are extracted, ionized by Coulomb explosion of the charged droplets, and detected by TOF-MS (resolution ~4000 at mass to charge ratio (m/z) 185). The electrospray droplets are generated by a commercially available 360 μm OD untreated fused silica capillary with an inner diameter of 50 μm (BGB Analytic). The sample flow remains unheated until after extraction of aerosol material into the electrospray droplets, minimizing volatilization of labile particle phase components and thermal decomposition. The droplets then enter the mass spectrometer through a capillary heated to 250 C, however, the very short residence time in this capillary means that the effective temperature experienced by the analyze is much lower and no thermal decomposition is observed. The electrospray working solution is a 50/50 water/acetonitrile (> 99.9 %, Sigma-Aldrich) mixture, which has less background signal compared to the water/methanol mixture, with 100 ppm of sodium iodide (NaI) as a charge carrier. Spectra are recorded in positive ion mode, in nearly all cases as adducts with Na⁺. Depending on voltage settings in the ion transfer optics (i.e. collision energy), clusters with acetonitrile can potentially be detected, however these clusters were observed to be negligible during the current study. The recorded signals are linear with mass and free of detectable matrix effects, in part due to the suppression of ionization pathways other than Na⁺ adduct formation (Lopez-Hilfiker et al., 2019). Here we report the signal measured by the EESI-TOF in terms of the mass flux of ions to the microchannel plate detector (attograms s⁻¹, neglecting Na⁺), calculated as shown in Eq. 1.

$$30 \quad M_x = I_x \cdot (MW_x - MW_{cc}) \quad (1)$$

Here M_x is the mass flux of ions united in ag s⁻¹, x represents the measured molecular composition. I_x is the recorded signal measured by EESI-TOF. MW_x and MW_{cc} represent the molecular weight of the ion and the charge carrier (e.g. H⁺, Na⁺),

respectively. Note that this measured mass flux can be related to ambient concentration by the instrument flow rate, EESI extraction/ionization efficiency, declustering probability, and ion transmission, where several of these parameters are ion-dependent (Lopez-Hilfiker et al., 2019). A comparison of the EESI-TOF mass flux to the AMS signal in terms of total signal or mass, bulk properties, and source apportionment results in section 3.5.

5 With the EESI-TOF, we almost continuously collected data from 25 January to 5 February, 2017 (84.6 %), missing a few time points due to instrumental calibration and issues such as cleaning the electrospray capillary due to lost or unstable signal. EESI-TOF stability and linearity with mass were confirmed by periodic measurement of nebulized levoglucosan aerosol with quantification of the mass concentration with an SMPS.

Data processing was executed using Tofware version 2.5.7 (Tofwerk AG, Thun, Switzerland). The total number of 1125 fitted ions (including 882 Na⁺ adducts, one H⁺ adduct, and 242 unknown ions) between m/z 135 and 400 were identified. Negligible signal was detected below m/z 135 due to the selected mass spectrometer transmission window. Data were pre-averaged to 1 min time resolution, and high resolution peak fitting was performed. Individual 1-min spectra were classified as either ambient measurements, background sampling (through the particle filter), or transitional measurements immediately after switching between ambient/background sampling. Transitional measurements were excluded from further analysis. Background spectra were averaged across each 2-min filter period, and these filter periods were interpolated to estimate the background spectrum during each ambient sampling period. The estimated backgrounds were subtracted from individual ambient spectra to yield the final ion time series of difference spectra. Ions with a mean signal-to-noise ratio (SNR) below 2 were removed from further analysis. No corrections for the relative sensitivity of individual ions or drift in instrument sensitivity were applied. For the Multilinear engine (ME-2) source apportionment analysis (Sect. 2.3), data were re-averaged to 2 mins. The corresponding error matrix σ_{ij} , which has the same dimensions as the data matrix, follows the model of Allan et al. (2003), which calculation includes the uncertainty deriving from electronic noise, ion-to-ion variability at the detector and ion counting statistics. The error estimates in this case incorporate the uncertainties related to both the ambient measurements (δ_i) (direct ambient sampling period) and the background (β_{ij}) (filter blank measuring period, both are processed with Tofware), which are combined in quadrature according to Eq. 2:

$$25 \quad \sigma_{ij} = \sqrt{\delta_{ij}^2 + \beta_{ij}^2} \quad (2)$$

The final data matrix and error matrix has the size of 10165 (time series) \times 892 (variables).

2.2.2 Aerosol Mass spectrometer (AMS)

30 An HR-TOF-AMS was deployed for online measurements of non-refractory (NR) PM_{2.5} (with an inline PM_{2.5} cyclone). A detailed description of the instrument can be found elsewhere (Jayne et al., 2000; DeCarlo et al., 2006). The AMS recorded data with 1 min time resolution, of which 30 s was spent recording the ensemble mass spectrum (mass spectrum (MS) mode) and 30 s recording size-resolved mass spectra (“particle time-of-flight (ePTof) mode”). A Nafion dryer was used to dry the

sampled air stream, which kept the relative humidity (RH) of air below 30 % within the AMS. Particles are continuously sampled ($\sim 0.8 \text{ L min}^{-1}$) through a $100 \mu\text{m}$ critical orifice and are focused by a recently developed $\text{PM}_{2.5}$ aerodynamic lens (Williams et al., 2013). The particles impact on a heated tungsten surface (heated to 600°) at $\sim 10^{-7}$ Torr and the NR components are flash vaporized. The resulting gases are ionized by electron ionization (EI, $\sim 70 \text{ eV}$) and the m/z values of the resulting fragments are determined by the TOF mass spectrometer. The AMS was calibrated for inlet flow, ionization efficiency (IE) at the beginning, middle and end of the campaign following standard protocols.

AMS data were analyzed in Igor Pro 6.36 using the SQUIRREL (version 1.57) and PIKA (1.16) analysis software (Donna Sueper, ToF-AMS High Resolution Analysis Software). The collection efficiency (CE) was estimated using a composition-dependent collection efficiency (CDCE) algorithm (Middlebrook et al., 2012) implemented in SQUIRREL. A CE=0.5 was assumed except in the case of strongly acidic aerosols, and high ammonium nitrate content where the approach by Middlebrook et al. (2012) was applied.

For ME-2 analysis, the input matrices consisted of the time series of fitted ions from high resolution mass spectral analysis, together with their corresponding uncertainties (Allan et al., 2003). According to the recommendations of Ulbrich et al. 2009, a minimum error value was added to the error matrix and ions were assessed and treated according to their signal-to-noise ratio (SNR) as follows: ions with an SNR less than 0.2 were excluded from ME-2 analysis, while those with an SNR between 0.2 and 2 were down-weighted by increasing their uncertainties by a factor of 2. Further, ions that were not independently fit but rather calculated from CO_2^+ were removed to avoid overweighting CO_2^+ . Likewise, isotopes were not included in the matrices to avoid overweighting the parent ions. The source apportionment input matrices consisted of 257 ions between m/z 12 and 120.

2.3 Source apportionment techniques

Source apportionment was performed on the organic AMS and EESI-TOF data separately using PMF as implemented by the multilinear engine (ME-2) (Paatero, 1997) and with model configuration and analysis executed via the SoFi (Source Finder, version 6.39) interface (Canonaco et al., 2013), coded in Igor Pro (WaveMetrics 6.37). PMF represents the input data matrix as a linear combination of characteristic factor profiles and their time-dependent contributions, which can be expressed in matrix notation as:

$$\mathbf{X} = \mathbf{G} \times \mathbf{F} + \mathbf{E} \quad (3)$$

The measured \mathbf{X} is an $m \times n$ matrix, representing m measurements of n m/z . \mathbf{G} and \mathbf{F} are $m \times p$ and $p \times n$ matrices, respectively, where p is the number of factors contained in a given model solution and is selected by the user.

Equation (3) is solved using a least squares algorithm that iteratively minimizes the quantity Q (Eq. 4), defined as the sum of the squared residuals weighted by their respective uncertainties, where the uncertainty may contain the measurements and model uncertainty:

$$Q = \sum_i \sum_j \left(\frac{e_{ij}}{\sigma_{ij}} \right)^2 \quad (4)$$

Here, e_{ij} represents the residuals (elements of \mathbf{E}), with i and j denoting respectively the time and m/z indices, and σ_{ij} is the corresponding measurement uncertainty. Rotations are explored by using the a -value approach, here implemented by constraining one or more output factor profiles to resemble a selected source, improving source separation (Crippa et al., 2014; Canonaco et al., 2013). The a -value (ranging from 0 to 1) determines how much the constrained factor (f_j , solution) is allowed to vary from its anchor (f_j), as defined in Eq. (5).

$$f_{j,solution} = f_j \pm a \cdot f_j \quad (5)$$

Execution of PMF analysis on separated AMS and EESI-TOF datasets minimizes the complexity of the analysis, while maximizing the factor resolution ability of the EESI-TOF. Factor related to traffic was constrained for the AMS analysis, while a factor related to cigarette smoke was constrained for the EESI-TOF. Details are presented in Sect. 3.1 and 3.2. Different factors were constrained in the two datasets due to the fundamental differences between the AMS and EESI-TOF measurements. Specifically, the absence of fragmentation in the EESI-TOF allowed clear separation of cooking without the need for constraints, while separation of a cigarette smoke factor was only achieved for the EESI-TOF. In addition, constraining an AMS cigarette smoke factor was attempted but failed.

2.4 Wind regression analysis

Wind regression analysis has been developed as a means of using meteorological and pollutant data to estimate the percent of a given pollutant originating from a specific wind sector. This study utilizes the Sustained Wind Incidence Method (SWIM), a quantitative model that estimates the weighted pollutant concentrations and uncertainties from a given wind direction and speed (Henry et al., 2009; Olson et al., 2012). The expected concentration (E) of a pollutant for each wind direction/wind speed pair (θ, u) is calculated as a weighted average of the concentration data in a window around (θ, u) represented by smoothing parameters σ and h using a weighting function $\mathbf{K}(\theta, u, \sigma, h) = \mathbf{K}_1(\theta, \sigma) \mathbf{K}_2(u, h)$, given by Eq (6):

$$E(C|\theta, u) = \frac{\sum_{i=1}^N K_1\left(\frac{\theta - W_i}{\sigma}\right) \cdot K_2\left(\frac{u - U_i}{h}\right) \cdot C_i}{\sum_{i=1}^N K_1\left(\frac{\theta - W_i}{\sigma}\right) \cdot K_2\left(\frac{u - U_i}{h}\right)} \quad (6)$$

$$K_1(x) = \frac{1}{\sqrt{2\pi}} \cdot e^{-0.5 \cdot x^2}, -\infty < x < \infty \quad (7)$$

$$K_2(x) = 0.75 \cdot (1 - x^2), -1 < x < 1 \quad (8)$$

$$W_i = \frac{C_i U_i}{\max(C_i U_i)} \cdot \frac{(\overline{\sigma \theta_i})}{\sigma \theta_i} \quad (9)$$

where C_i , U_i , and W_i are the observed concentration of a particular pollutant, resultant wind speed and directional standard deviation, respectively, N is the total number of observations; \mathbf{K}_1 (Eq (7)) and \mathbf{K}_2 (Eq (8)) are smoothing Gaussian kernel and

the Epanechnikov kernel, σ and h are smoothing parameters for wind direction and wind speed, respectively. The conditional probability of pollutant concentration (Eq (6)) is then weighted by the frequency of the wind using a joint probability of wind speed and wind direction, resulting in the following expression for the mean value of the pollutant concentration associated with winds from the sector defined by the intervals U ($U = [u_1, u_2]$) and θ ($\theta = [\theta_1, \theta_2]$).

$$S(\theta, U) = \int_{u_1}^{u_2} \int_{\theta_1}^{\theta_2} f(\theta, u) E(C|\theta, u) d\theta du \quad (10)$$

The joint probability of wind speed and wind direction (f) is calculated by using a kernel density, estimated as:

$$f(\theta, u) = \frac{1}{N\sigma h} \sum_{i=1}^N K_1\left(\frac{(\theta - \theta_i)}{\sigma}\right) K_2\left(\frac{(u - u_i)}{h}\right) \quad (11)$$

Calculations have been performed on Igor Pro with ZeFir package (Petit et al., 2017).

2.5 Identification of source-specific ions

- 10 To determine ions characteristic of individual factors (or groups of related factors), agglomerative hierarchical clustering was conducted on the EESI-TOF matrix of PMF profiles and standardizing data along the ions, clustering first along the columns (producing row-clustered groups of factor), and then along the rows (producing the clustered ions to each group) in the matrix data. In hierarchical cluster analysis, a dendrogram, used to show relationships between members of a group, i.e., a family tree with the oldest common ancestor at the base and branches for various divisions of lineage was generated with the following
- 15 steps (Matlab R2017b): (1) Calculate the distance by using Euclidean distance to find the similarity or dissimilarity between every ion and every pair of factors in our data set. (2) Link pairs of ions and factors that are in close proximity using the average linkage function. (3) Use the cluster function to prune branches off the bottom of hierarchical tree, and assign all the objects below each cut to a single cluster. Here, the clustergram function transforms the standardized values so that the mean is 0.

20 3 Results and Discussion

- Results of AMS and EESI-TOF PMF analyses are presented in sections 3.1 and 3.2, respectively. Section 3.3 focuses on the EESI-TOF PMF results are then exploited to assess the apportionment of specific ions related to key marker compounds (section 3.3) and to identify groups of molecules uniquely characteristic of the retrieved factors (section 3.4). However, quantitative interpretation of the EESI-TOF PMF results is complicated by differences in the relative sensitivity of the EESI-
- 25 TOF to different molecules. Therefore section 3.5 presents a comparison of the EESI-TOF and AMS results in terms of total signal, bulk atomic composition, and relative apportionment to the different factors.

3.1 AMS source apportionment

The AMS PMF analysis yielded seven OA factors: hydrocarbon-like OA (HOA_{AMS}), cooking-related OA (COA_{AMS}), biomass burning OA (BBOA_{AMS}), two oxygenated OA factors (less oxygenated ($\text{LO-OOA}_{\text{AMS}}$) and more oxygenated ($\text{MO-OOA}_{\text{AMS}}$)), nitrogen-containing OA (NOA_{AMS}), and a factor due to an isolated local event ($\text{EVENT}_{\text{AMS}}$). Factor mass spectra are shown in Fig. 1, while Fig. S1 shows factor time series, together with selected external tracers, and diurnal cycles which may be less convinced due to the short period of the measurement. Salient characteristics of these factors are discussed below; HOA_{AMS} , COA_{AMS} , BBOA_{AMS} , $\text{LO-OOA}_{\text{AMS}}$, and $\text{MO-OOA}_{\text{AMS}}$ are similar to factors frequently observed in other studies (Crippa et al., 2013a; Zhang et al., 2011; Young et al., 2016).

HOA_{AMS} was constrained using a factor mass spectrum from Paris (Crippa et al., 2013b) and an a -value of 0.1 (the a -value was selected according to the correlations between the time series of HOA with the traffic species NO_x), yielding a factor with a low O:C ratio (0.04) and high H:C ratio (1.8), consistent with a dominant contribution from aliphatic hydrocarbons. Strong signals from C_xH_y^+ ions are evident, especially C_3H_5^+ , C_3H_7^+ , C_4H_7^+ , and C_4H_9^+ ions. Consistent with previous studies, the HOA mass spectrum is similar to vehicle emission studies (Zhang et al., 2005; Sun et al., 2012; Young et al., 2016).

The COA_{AMS} mass spectrum is similar to primary cooking emissions (Crippa et al., 2013b) and exhibits a unique diurnal pattern peaking during lunch and dinner time. The COA_{AMS} spectrum is characterized by a high ratio of $\text{C}_4\text{H}_7^+:\text{C}_4\text{H}_9^+$ ratio and a high fraction of $\text{C}_3\text{H}_3\text{O}^+$ and C_4H_7^+ , consistent with COA_{AMS} factors previously identified at urban locations (Crippa et al., 2013a; Ge et al., 2012; Mohr et al., 2012).

BBOA_{AMS} has been identified as a significant source of aerosol in previous wintertime source apportionment studies in Switzerland and Central Europe (Lanz et al., 2008; Daellenbach et al., 2017). Similar to previous studies, BBOA_{AMS} shows a high fraction $\text{C}_2\text{H}_4\text{O}_2^+$ at m/z 60 and $\text{C}_3\text{H}_5\text{O}_2^+$ at m/z 73 and explains most of the variation of these ions (77 %, 65 %, respectively). A strong diurnal trend is evident, with concentrations peaking overnight and decreasing during the day.

$\text{LO-OOA}_{\text{AMS}}$ and $\text{MO-OOA}_{\text{AMS}}$ mass spectra are characterized by dominant peaks at m/z 28 (CO^+), 44 (CO_2^+), similar to OOA_{AMS} factors observed at other sites (Sun et al., 2011; Ng et al., 2010). The main difference between the $\text{LO-OOA}_{\text{AMS}}$ and $\text{MO-OOA}_{\text{AMS}}$ mass spectra is the relative contribution of $\text{C}_2\text{H}_3\text{O}^+$ compared to CO_2^+ , with $\text{C}_2\text{H}_3\text{O}^+$ enhanced in $\text{LO-OOA}_{\text{AMS}}$. Also enhanced in LO-OOA are ions at m/z 39 (C_3H_3^+), 41 (C_3H_5^+), 55 (C_4H_7^+). Further insight into the OOA_{AMS} factors is obtained through the EESI analysis (Sect. 3.2).

NOA_{AMS} exhibits a significantly higher N:C ratio (0.04) than the other factors and explains most of the organic nitrogen signal. This factor includes a strong signal from $\text{C}_5\text{H}_{10}\text{N}^+$ signal (m/z 84), which is consistent with N-methyl-pyrrolidine which has previously been identified in AMS spectra as a tracer for cigarette smoke (Struckmeier et al., 2016). This ion is also observed in the EI mass spectra of nicotine (NIST, <https://webbook.nist.gov/cgi/cbook.cgi?ID=C54115&Mask=200#Mass-Spec>). However, other spectral features (e.g. the high CO_2^+ signal) are not typical of primary cigarette smoke and suggest a contribution from secondary formation processes. This interpretation is consistent with correlations of NOA_{AMS} with EESI-TOF factors, suggesting NOA_{AMS} to be a mixed factor, as discussed in Sect. 3.2 and 3.4.

EVENT_{AMS} factor is a special case in our study as the mass spectrum is dominated by m/z 15 (CH_3^+), 27 (C_2H_3^+), 31 (CH_3O^+), and 43 ($\text{C}_2\text{H}_3\text{O}^+$). The time series only contributes during two nights (28 January and 29 January) from 00:00 am to 07:00 am with the concentrations peaking at $3.8 \mu\text{g m}^{-3}$ but being below $0.2 \mu\text{g m}^{-3}$ for the rest of the study. No associations with any markers are evident.

5 3.2 EESI-TOF source apportionment

An 11-factor solution was selected as the best representation of the EESI-TOF data, with 5 factors attributed mostly to POA and 6 to SOA. The POA factors include cooking-related OA (COA_{EESI}), two less aged biomass burning factors ($\text{LABB1}_{\text{EESI}}$ and $\text{LABB2}_{\text{EESI}}$) which are mostly dominated by primary organic aerosol compounds, cigarette smoke-influenced OA ($\text{CS-OA}_{\text{EESI}}$), and a factor related to an isolated special event ($\text{EVENT}_{\text{EESI}}$). The SOA factors consist of 3 more aged biomass burning factors dominated by secondary organic aerosol compounds and distinguished by mean daily temperature ($\text{MABB_LOW}_{\text{EESI}}$, $\text{MABB_HIGH}_{\text{EESI}}$, and $\text{MABB_TRANS}_{\text{EESI}}$, corresponding to low temperature, high temperature, and transition periods, respectively), two additional SOA factors lacking a clear attribution to biomass burning ($\text{SOA1}_{\text{EESI}}$ and $\text{SOA2}_{\text{EESI}}$), and nitrogen-containing SOA ($\text{NSOA}_{\text{EESI}}$). This solution was obtained by constraining the CS-OA_{EESI} factor with an α -value of 0.1, and all other factors unconstrained. This constraining approach and the solution selection criteria are discussed in Sect. 3.2.1, while the POA and SOA factors are discussed in Sect. 3.2.2 and 3.2.3, respectively. A detailed investigation of the factor mass spectra is presented in Sect. 3.4.

3.2.1 Selection of PMF solution

In selecting the PMF solution that best represents the EESI-TOF dataset, we considered both mathematical diagnostics (e.g. Q/Q_{exp} and residuals) as a function of the number of factors, as well as the interpretability of the retrieved factors. Interpretability was judged according to the following criteria:

- i. Correlation of the time series and diurnal patterns between the AMS and EESI-factors.
- ii. Comparison of factor profiles with mass spectra retrieved from less and more aged biomass burning exhaust from simulation chamber experiments at PSI (Bertrand et al., submitted).
- iii. Similarities to EESI-TOF factor mass spectra retrieved from summer measurements at the same site in Zurich (Stefenelli et al., 2019)
- iv. Identification of key ions in the factor profiles, including ions contributing a major fraction of the total factor signal, ions apportioned predominantly to a certain factor or related to a set of factors, and ions established in the literature as known tracers for specific sources/processes.
- v. Interpretation of the temporal behavior in terms of meteorological data, including temperature, solar radiation, and wind speed/direction.

For the EESI-TOF source apportionment, we considered unconstrained solutions from 7 to 20 factors (see Fig. S2a). Of these solutions, a 10-factor solution was found to best explain the data at a preliminary stage. This was preferred to lower-order solutions because all factors were interpretable according to the above criteria. Solutions with more factors lead to additional factors related to more aged biomass burning without obvious additional information. In addition, the investigation of Q/Q_{exp} as a function of the number of factors (Fig. S2b) did not show any significant change with the increase of the a -value from 7 factors. Fig. S3 and Fig. S4 show the mass spectra and time series of the 8- to 11-factor solutions.

Nonetheless, the unconstrained 10-factor solution revealed evidence of factor mixing, as the cooking-related (COA_{EESI}) factor mass spectrum had a strong contribution from m/z 163 ($\text{C}_{10}\text{H}_{15}\text{N}_2$, nicotine), which should rather be associated with cigarette smoke (Fig. S5). This suggests that at least one more factor remains to be resolved. The difficulty in separating these factors, despite their expected chemical differences, is likely due to strong temporal correlation between cooking and cigarette-smoking emissions due to the proximity of local restaurants (Fig. S6, the diurnal patterns of nicotine and COA_{EESI} factors), where people gather outside to smoke during mealtimes. We therefore attempted to obtain a clean cigarette smoking signature from the dataset to serve as an anchor profile with which to constrain this source. For solutions with fifteen to twenty factors, a factor was retrieved with an MS dominated by nicotine and to which $> 90\%$ of nicotine was apportioned. We therefore constructed a profile (average from 15-20 factors) for this nicotine-containing factor (apportioned to cigarette smoke, i.e. $\text{CS-OA}_{\text{EESI}}$). This profile was then constrained in an 11-factor solution (based on the selection of a 10-factor unconstrained solution, as discussed above) using an a -value approach (from 0 to 1 with steps of 0.1, 0.1 was chosen finally). The main criterion of the constraint was the fraction of nicotine apportioned to the constrained factor. Also in our case, the R^2 (Pearson) for the correlations between the time series of the solutions was constructed with the final 11-factor solution. Based on these considerations, we concluded that the source apportionment solution with eleven factors was the optimal solution.

3.2.2 EESI-TOF Factors: Primary Organic Aerosols (POA)

Figure 2a shows the time series of the five EESI-TOF factors attributed to primary organic aerosol: COA_{EESI} , $\text{LABB1}_{\text{EESI}}$, $\text{LABB2}_{\text{EESI}}$, $\text{CS-OA}_{\text{EESI}}$, and $\text{EVENT}_{\text{EESI}}$. Also shown are relevant ancillary measurements, including AMS PMF factors and meteorological parameters. Figure 2b shows the corresponding factor mass spectra, colored by the number of nitrogen atoms. A discussion of each factor follows. Figure 3a shows the diurnal patterns of the $\text{LABB}_{\text{EESI}}$ factors, as well as COA_{EESI} and COA_{AMS} .

Less aged biomass burning ($\text{LABB1}_{\text{EESI}}$ and $\text{LABB2}_{\text{EESI}}$)

The LABB factors are both enhanced at night, consistent with domestic heating activities. Considering the full campaign time series (Fig. 2a), this repeating pattern, opposed to solar radiation, is evident for $\text{LABB1}_{\text{EESI}}$, while the time series of $\text{LABB2}_{\text{EESI}}$ is driven by intense events (~ 6.5 times higher than $\text{LABB1}_{\text{EESI}}$) during two nights: from 18:00 on 27 January to 08:00 on 28 January, and from 18:00 on 28 January to 08:00 on 29 January. As shown in Fig. 2b, both factor profiles are dominated by $\text{C}_6\text{H}_{10}\text{O}_5$ and $\text{C}_8\text{H}_{12}\text{O}_6$. $\text{C}_6\text{H}_{10}\text{O}_5$ is attributed primarily to levoglucosan, which is a well-established tracer for biomass burning. The mass spectrum features of both factors are very similar to less aged biomass burning emissions measured directly from a

domestic biomass combustion appliance in the PSI smog chamber (Bertrand et al., submitted). Figures 4a and 4b show Van Krevelen plots (i.e., atomic ratios H:C as a function of O:C) for LABB1_{EESI} and LABB2_{EESI}, respectively, with points colored by the number of atoms and sized by the fraction of each ion apportioned to the respective factor. Both LABB1_{EESI} and LABB2_{EESI} are dominated by ions with low H:C (1.04) and low O:C (0.35, excluding the sugars C₆H₁₀O₅ and C₈H₁₂O₆, which exhibit high variability, Table S1), suggesting a strong contribution from primary or slightly aged aromatics. The wind regression analysis of these two factors are shown in Fig. S7. LABB1_{EESI} does not correspond to a specific wind direction, in contrast, LABB2_{EESI} originates predominantly from a single wind direction, excluding the smaller source to the SE on the third day. Fig. S8 compares the BBOA_{AMS} factor (Fig. 2a) with LABB1_{EESI}, LABB2_{EESI}, and the sum of LABB1_{EESI} + LABB2_{EESI}, with R 0.59, 0.79, and 0.82, respectively. The correlation is generally good except during the first part of the campaign (25 January to 27 January) which as discussed later relates to the complexity of wood burning classification between the EESI-TOF and AMS. The correlation of BBOA_{AMS} with either LABB2_{EESI} or LABB1_{EESI}+LABB2_{EESI} is rather high at night (R=0.59 to 0.82), while the LABB_{EESI} factors are consistently lower than BBOA_{AMS} during the day. We assign the high correlation of LABB2_{EESI} with BBOA_{AMS} to the high abundance of levoglucosan which drives the variation in *f*₆₀ in the AMS. Some specific features of BBOA_{AMS} do not appear in any LABB factor because less aged and more aged biomass burning OA are not unambiguously separated in the AMS.

Cooking-related OA (COA_{EESI})

The COA_{EESI} and COA_{AMS} factor time series are strongly correlated (R=0.88), as shown in Fig. 2a. The diurnal variation of the COA_{EESI} is also similar to COA_{AMS}, with strong peaks at lunch and dinner time (Fig. 3a). In addition to this diurnal pattern, both COA_{EESI} and COA_{AMS} are significantly elevated during two periods: from 18:00 on 27 January to 01:00 on 28 January (Friday night), and from 18:00 on 28 January to 01:00 on 29 January (Saturday night). These periods occur on the same evening as the unknown special event giving rise to the EVENT_{AMS} and EVENT_{EESI} factors, but are slightly offset in time, with the COA factors peaking approximately four hours earlier. The distinct contribution from the COA_{EESI} factor is due in part to the location of several restaurants within a 100-m radius, including one adjacent to the site.

As shown in Fig. 2b, the COA_{EESI} mass spectrum is unique in having most of the mass at ions with higher *m/z*. Several of the dominant ions can be attributed to fatty acids and alcohols, which are associated with cooking emissions and oils. For example, C₁₃H₂₂O₄ (dibutyl itaconate), C₁₆H₃₀O₃ (2-oxo-tetradecanoic acid), and C₁₈H₃₄O₃ (ricinoleic acid), are prominent, and contributed 0.89 %, 1.7 %, and 2.0 %, respectively, of the total mass spectrum. Figure 3b shows a Van Krevelen plot of the COA_{EESI} factor mass spectrum, with points sized by the fraction of each ion apportioned to COA_{EESI} and colored by the number of carbon atoms. The dominant contribution of ions with higher carbon number (C13-C25) and high H:C ratio (greater than 1.5) but low O:C ratio (below 0.2) indicates that these ions are more consistent with fatty acids or alcohols rather than aromatic-derived ions.

Special event (Event_{EESI})

The time series of $\text{EVENT}_{\text{EESI}}$ is highly correlated with $\text{EVENT}_{\text{AMS}}$ ($R=0.99$, Fig. 2a). Both factors are near-zero except for two intense events beginning at approximately midnight and lasting till the early morning on 28 and 29 January, supporting the hypothesis of a unique event as opposed to variation in BBOA. The Zurich game festival was taking place at the weekend (the event is apparently held in a building on the SW side of the courtyard), though no human activities in the immediate vicinity of the sampling inlet were evident by inspection of the on-site camera. The EESI-TOF factor mass spectrum is dominated by an ion at m/z 174.08, tentatively assigned to $\text{C}_8\text{H}_{11}\text{N}_2\text{O}$. However, the EESI-TOF does not provide structural information and to our knowledge no compound with this formula has been reported as a major constituent of an atmospheric emission source, preventing its use as a diagnostic tracer. Other significant ions are $\text{C}_8\text{H}_{12}\text{O}_4$ and $\text{C}_8\text{H}_{18}\text{O}_5$. The $\text{C}_8\text{H}_{12}\text{O}_4$ ion likely represents 1,2-cyclohexane dicarboxylic acid diisononyl ester, a plasticizer for the manufacture of food packaging, belonging to the group of aliphatic esters from a chemical point of view. This indicates that the source may be from food plastic burning in a nearby restaurant.

Cigarette smoke-influenced OA ($\text{CS-OA}_{\text{EESI}}$)

Cigarette smoke-influenced OA ($\text{CS-OA}_{\text{EESI}}$) is a constrained factor, based on a reference profile retrieved from higher-order PMF solutions as described in Sect. 3.2.1. The mass spectrum of $\text{CS-OA}_{\text{EESI}}$ is dominated by the $\text{C}_{10}\text{H}_{14}\text{N}_2\text{H}^+$ ion (Fig. 2b). This ion is the only ion (out of 892 ions) that does not appear as an adduct with Na^+ . Instead, the observed molecular formula corresponds to that of nicotine with an extra hydrogen. As a reduced nitrogen compound, nicotine likely forms a stable ion by abstracting a hydrogen from water, leading to the observed cation. However, the time series and the mass flux of this ion should be interpreted with caution, because it is formed by a different ionization pathway than the majority of the spectrum, its relative sensitivity may be significantly different from that of the other ions. Additionally, we have not characterized such non-Na-adducts in terms of ion suppression or matrix effects and cannot rule out a nonlinear response to mass. However, the comparison of the $\text{CS-OA}_{\text{EESI}}$ factor with AMS PMF results and individual ions discussed below suggest that such nonlinear effects are not significant.

Oxidized organic nitrogen species such as $\text{C}_x\text{H}_y\text{N}_1\text{O}_z$ (34.9 %) and $\text{C}_x\text{H}_y\text{N}_2\text{O}_z$ (6.8 %) are also significant in the $\text{CS-OA}_{\text{EESI}}$ factor, as shown in Fig. 2b and Fig. 5a. $\text{CS-OA}_{\text{EESI}}$ is only slightly oxygenated ($\text{O:C}=0.31$) and has an H:C ratio of approximately 1.51 (Table S1). The $\text{CS-OA}_{\text{EESI}}$ time series exhibits two large evening peaks (27 Jan and 28 Jan). These peaks are likely associated with cigarette smoking outside the nearby restaurants. A high correlation is observed between the time series of $\text{CS-OA}_{\text{EESI}}$ and the AMS $\text{C}_5\text{H}_{10}\text{N}^+$ ion ($R=0.91$, Fig. 5b), which has been proposed as a tracer for nicotine (Struckmeier et al., 2016).

3.2.3 EESI-TOF Factors: Secondary Organic Aerosols

Here we discuss the EESI-TOF SOA factors in three groups: (1) more aged wood-burning related ($\text{MABB_LOW}_{\text{EESI}}$, $\text{MABB_TRANS}_{\text{EESI}}$, and $\text{MABB_HIGH}_{\text{EESI}}$); (2) non-source-specific SOA ($\text{SOA1}_{\text{EESI}}$ and $\text{SOA2}_{\text{EESI}}$); and (3) high nitrogen content ($\text{NSOA}_{\text{EESI}}$). Factor mass spectra for these factors are shown in Fig. 6a, with the spectra colored by the number of N atoms and normalized such that the sum of the peaks in each spectrum is 1. Figure 6b shows a stacked time series of all 6

EESI-TOF SOA factors, such that the sum of the stacked plot represents the total EESI-TOF mass flux attributed to SOA. For comparison, the time series of the estimated AMS SOA is shown, calculated as $LO\text{-}OOA_{AMS} + MO\text{-}OOA_{AMS}$. NOA_{AMS} is excluded from this calculation due to the contribution from primary cigarette smoke discussed above. The total EESI-TOF SOA and AMS SOA estimates are in general well-correlated ($R=0.90$), even though the EESI-TOF mass flux is proportionally lower during the first few days of the study.

More aged biomass burning-related factors ($MABB_LOW_{EESI}$, $MABB_TRANS_{EESI}$, and $MABB_HIGH_{EESI}$)

Three more aged biomass burning (MABB) factors are identified in this study: $MABB_LOW_{EESI}$, $MABB_TRANS_{EESI}$, and $MABB_HIGH_{EESI}$. Each $MABB_{EESI}$ factor is enhanced relative to the others during a different part of the campaign, which correspond to both changes in the daily temperature cycle and wind direction. As shown in Fig. 6b, the coldest part of the study, period 1, occurs from 25 to 27 January (mean -5.4° , min -6.4° , max -2.2°). During this period, $MABB_LOW_{EESI}$ contributes 84 % of the total MABB ($MABB_LOW_{EESI}/(MABB_LOW_{EESI} + MABB_TRANS_{EESI} + MABB_HIGH_{EESI})$). From 27 to 29 January, Period 2, temperature increases (mean 1.4° , min -2.2° , max 7.4°), and the $MABB_TRANS_{EESI}$ factor constitutes the dominant $MABB_{EESI}$ fraction (65 %). Period 3, from 29 January to the campaign end on 4 February, corresponds to higher temperatures (mean 5.7° , min 0.8° , max 8.7°), and the $MABB_{EESI}$ fraction is dominated by $MABB_HIGH_{EESI}$ (90 %) until a substantial precipitation event beginning on 31 January, after which relatively clean air is observed for the remainder of the campaign. Figure 7 shows the source-specific wind sectors determined by SWIM (see Sect. 2.4) for the three MABB factors. This analysis assigns the three factors to distinct wind vectors: NNE for $MABB_LOW_{EESI}$, NNW for $MABB_TRANS_{EESI}$, and SE for $MABB_HIGH_{EESI}$. Because each factor is predominantly observed during a single time period, it is difficult to assess the relative importance of temperature vs. source region for these three factors.

As shown in Fig. 6a, all three $MABB_{EESI}$ factor mass spectra are qualitatively similar, with many of the same ions enhanced. These spectra are also similar to the mass spectrum of aged biomass burning emissions retrieved from smog chamber experiment (Bertrand et al., submitted). For both the $MABB_{EESI}$ and chamber spectra, the major ions, $C_7H_{10}O_5$, $C_9H_{14}O_4$, $C_8H_{12}O_6$, are in common. The main difference between the EESI-TOF factors and the chamber mass spectrum is that the chamber data show a higher fraction of signal at lower m/z . This is likely due to the higher concentrations used during the chamber experiments, causing increased partitioning of semi-volatile compounds to the particle phase. $MABB_LOW_{EESI}$ also exhibits somehow enhanced intensities at lower m/z compared to the other $MABB_{EESI}$ factors. As $MABB_LOW_{EESI}$ is dominant during the coldest period 1, the $MABB_LOW_{EESI}$ factor is possibly separated from the other $MABB_{EESI}$ factors due to partitioning of semi-volatile material to the particle phase due to colder temperatures.

Further insight into the composition trends across the $MABB_{EESI}$ factors is obtained through Fig. 8 which represents the three $MABB_{EESI}$ mass spectra as the carbon oxidation state (OS_c) (Kroll et al., 2011) of each ion as a function of the carbon number (n_c). Data points are colored by the H:C ratio and sized by the fraction of each ion apportioned to the designated factor. The figure shows that $MABB_LOW_{EESI}$ is enhanced in ions with low n_c , consistent with condensation of semi-volatile OA ($C_5H_6O_4$, $C_8H_6O_4$, $C_5H_8O_7$) at low temperature. Otherwise, all three $MABB_{EESI}$ factors are rather similar. Figure 8 also shows the OS_c of non- $MABB_{EESI}$ (weighted average of $SOA1_{EESI} + SOA2_{EESI}$) and $LABB_{EESI}$ (weighted average of $LABB1_{EESI}$ and

LABB_{2EESI}) factors. Obviously, the non-MABB_{EESI} and LABB_{EESI} factors are less oxidized than the MABB factors, with lower OS_c.

Other SOA factors (SOA_{1EESI} and SOA_{2EESI})

The mass spectra of SOA_{1EESI} and SOA_{2EESI} are qualitatively similar to factors retrieved from PMF analysis of EESI-TOF data from Zurich during summer, when monoterpenes are the dominant SOA precursors (Stefenelli et al, 2019, Fig. S9). Major ions include C₈H₁₂O₄, C₉H₁₄O₄, C₁₀H₁₆O₄, C₁₀H₁₈O₄, C₁₀H₁₆O₅ and C₁₀H₁₆O₂, C₁₀H₁₆O₃, C₁₀H₁₈O₄, separately. In contrast to the MABB_{EESI} factors, the SOA_{EESI} factors have a negligible contribution from levoglucosan (C₆H₁₀O₅). Approximately 57 % of the total C10 ion signal is apportioned to the SOA_{EESI} factors. Figures 9a and 9b show the atomic ratio of H:C as a function of O:C for the two SOA_{EESI} factors. These H:C ratios are higher than typically observed from the oxidation of aromatic emissions and are instead consistent with monoterpene oxidation. The Van Krevelen plots show clear differences between these two factors, SOA_{2EESI} is less oxygenated than SOA_{1EESI} with lower O:C ratio and lower H:C ratio. The time series of SOA_{1EESI} shows a higher contribution during the period 1, 2, while SOA_{2EESI} has a more regular cycle contribution during daytime (Fig. 6b). Since we have clear evidence that these EESI-retrieved factors are related to secondary organic aerosol we call them SOA_{EESI}, in contrast to the OOA_{AMS} factors, where this evidence is less clear. The more detailed comparison between EESI-TOF_SOA factors and AMS_OOA factors will be discussed in Sect. 3.5.

Nitrogen-containing SOA factor (NSOA_{EESI})

As mentioned in Sect. 3.1, the EESI-TOF source apportionment also resolves a nitrogen-containing SOA factor (NSOA_{EESI}). NSOA_{EESI} is dominated by highly oxygenated organonitrate molecules, including C₈H₁₃NO₅, C₁₀H₁₅NO₆, C₁₀H₁₉NO₈. Ions like C₆H₁₀O₅, C₁₀H₁₆O₂ and C₈H₁₂O₆ are comprising another fraction of the NSOA_{EESI} signal, but are not unique to the NSOA_{EESI} factor and rather spread over many other factors. The significant contribution of organonitrates results in an N:C ratio (0.04) and suggests a secondary origin for this factor. Therefore, we call it NSOA_{EESI}, in contrast to NOA_{AMS} for which the primary/secondary origin is less certain. The time series of the factor is quite unique, shows maximum mass flux at the end of this campaign with the highest peak at night (3-4 February), and a smaller peak during the night of 28 to 29 February.

Figure S10 shows a comparison of the NSOA_{EESI} time series and CS-OA_{EESI} time series with the CHON ions from the EESI and CHN ions from the AMS, respectively. The group of EESI_CHON ions shows the same temporal variation as the NSOA_{EESI} factor (Fig. S10) while the AMS_CHN group is more correlated to the primary organic group.

3.3 Analysis of marker ions

Laboratory, as well as offline and semi-continuous field studies have identified a number of tracer molecules that are useful for the investigation of primary and secondary OA from various sources, including biomass burning. The real-time and in situ measurement of these compounds is a novel feature of the EESI-TOF, and their apportionment gives further insight into the nature of the factors described above. Here we investigate the apportionment of eight ions associated with compounds of interest: C₆H₁₀O₅ (approximately assigned to levoglucosan), C₇H₇NO₄ (methyl-nitrocatechol), C₉H₁₀O₅ (syringic acid), C₈H₈O₄ (vanillic acid), C₈H₆O₄ (phthalic acid), C₅H₆O₄ (glutaconic acid), C₇H₈O₄ (tetrahydroxy toluene) and C₇H₁₀O₅

(pentahydroxy toluene). Note that because the EESI-TOF can provide only a molecular formula, we cannot establish for certain the identity of a compound or assess the relative isomeric abundances. For example, $C_6H_{10}O_5$ is likely to consist not only of levoglucosan, but also other sugars such as mannosan and galactosan. The named compounds are thus provided for reference, but their identification should not be considered as conclusive and the ions cannot be assumed to be isomerically pure.

5 Nevertheless, as these assignments are based on molecular investigations of wood burning-related emissions they are likely to be qualitatively correct and provide a useful framework for interpreting molecular aspects of the source apportionment results.

Figure 10a shows a stacked time series of the mass flux of these compounds representing the contribution of each EESI-TOF PMF factor to the total mass flux (assuming no significant conformational isomers). Levoglucosan, which is derived from the pyrolysis of cellulose and hemicellulose, is commonly used as an indicator for the presence of primary aerosols originating from biomass combustion (Fine et al., 2001). Figure 10b shows that levoglucosan appears in both POA (total contribution, 62 %, mostly from $LABB1_{EESI}$ (22 %) and $LABB2_{EESI}$ (37 %), and minor contributions by COA_{EESI} , $CS-OA_{EESI}$, and $EVENT_{EESI}$) and SOA (total contribution, 38 %, of which 36 % related to the sum of $MABB_HIGH_{EESI}$, $MABB_TRANS_{EESI}$, $MABB_LOW_{EESI}$, plus minor contributions from $NSOA_{EESI}$). Due to the high biomass burning emission background and the lifetime of levoglucosan, it is inevitable to find a contribution of levoglucosan in the MABB factor, which is consistent with our aged biomass burning discussion above. In contrast, nitrocatechol ($C_7H_7NO_4$) has been established as a secondary species originating from the oxidation of biomass burning (Inuma et al., 2010; Finewax et al., 2018). Here 86 % of nitrocatechol is apportioned to the less aged (49 %) and more aged (37 %) biomass burning factors. Syringic acid and vanillic acid are phenolic acids derived from the oxidation of lignin decomposition products (He et al., 2018), which in turn are a major component of biomass combustion emissions, and are apportioned primarily to the $MABB_{EESI}$ factors (52 % for syringic acid and 66 % for vanillic acid).

Phthalic acid ($C_8H_6O_4$) and glutaconic acid ($C_5H_6O_4$) are apportioned to the SOA factors (91 % and 94 % in total, respectively), with main contributions from the $MABB_{EESI}$ factors and in particular the $MABB_LOW_{EESI}$ factor (53 % and 59 %, respectively). These dicarboxylic acids are ubiquitous water-soluble organic compounds which have been detected in a variety of aerosol samples, and originate from the combustion of biomass burning and fossil fuels, as well as from biogenic emission and photo-oxidation of organic gases. For example, phthalic acid has been identified based on field measurements, as a tracer of naphthalene oxidation (Kleindienst et al., 2012) or oxidation products from PAHs (Chan et al., 2009), and is also consistently found in combustion products of lignin, which is likely to explain the contribution in the MABB factors (Fu et al., 2010; Wang et al., 2007).

Tetrahydroxy toluene ($C_7H_8O_4$) and pentahydroxy toluene ($C_7H_8O_5$) are apportioned mainly to secondary factors (85 % and 78 %, respectively). Tetrahydroxy toluene and pentahydroxy toluene have been detected as dominant products both in the particle phase and gas phase under low-NO oxidation of toluene (Nakao et al., 2012; Schwantes et al., 2017). The *o*-cresol oxidation mechanism for tetrahydroxy toluene and pentahydroxy toluene is found in MCM v3.3.1, based on Olariu et al. (2002). This formation indicates that these two low-volatility ions are indeed secondary organic compounds, consistent with our results shown in Fig. 10. In addition, the temporal variation of the pentahydroxy toluene contribution is consistent with the one of

tetrahydroxy toluene except for the $\text{EVENT}_{\text{EESI}}$ factor, which may indicate that during this night event an isomer of pentahydroxy toluene was present.

3.4 EESI-TOF cluster analysis

As evidenced from the previous section and Figs. 2 and 6, many of the dominant ions in the EESI-TOF PMF analysis are shared by multiple factors. Here, we utilize a cluster analysis to identify ions unique or nearly unique to a single factor or group of factors. As discussed in Sect. 2.5, hierarchical agglomerative clustering is performed separately on the set of all EESI-TOF ions and **all EESI-TOF factor time series**. Figure 11 shows the resulting dendrogram of the ions and factors along the vertical and horizontal axes, respectively; the ion dendrogram is colored subjectively to guide the eye. Comparison of the ions to the factors yields a matrix, also shown in Fig. 11, which is colored by the z-score, with brown colors denoting high correlation. In this representation, an ion unique to a given factor is brown for one and only one rectangle in the horizontal dimension.

The factor dendrogram identifies several groups of EESI-TOF PMF factors consistent with the interpretations provided above: (1) more aged biomass burning factors ($\text{MABB_LOW}_{\text{EESI}}$, $\text{MABB_TRANS}_{\text{EESI}}$ and $\text{MABB_HIGH}_{\text{EESI}}$), (2) less aged biomass burning factors ($\text{LABB1}_{\text{EESI}}$ and $\text{LABB2}_{\text{EESI}}$), and (3) the cooking-related OA and cigarette smoking OA factors. The more aged and less aged biomass burning factor groups are themselves likewise grouped. This clustering is consistent with our interpretation of these factors, as discussed in the previous section. Ions are clustered to different groups using the standardized values. In each factor, there are distinguished molecules (lists of the specific ions (standardized value above 1.5) for each factor is shown in Table S2). The other two resolved groups, one group including SOA1 and EVENT factor, one group containing SOA2 and NSOA factor, apparently don't retrieve the common ions, which make less sense for the current study.”

For several of the factors, the uniquely assigned ions exhibit systematic patterns contributing to the identification or deconvolution of the factors. Figure 12a shows the mass defect, defined as the exact m/z minus the nearest integer m/z , as a function of m/z for the uniquely assigned ions for the five POA_{EESI} factors. Figure 12b shows the equivalent plot for the three $\text{MABB}_{\text{EESI}}$ factors and $\text{SOA1}_{\text{EESI}}$ ($\text{SOA2}_{\text{EESI}}$ and $\text{NSOA}_{\text{EESI}}$ have a high degree of scatter and are omitted to avoid masking trends in the other secondary factors). The displayed factors exhibit linear correlations or tight clusters of points; all factors are shown independently in Fig. S11). $\text{LABB1}_{\text{EESI}}$ and $\text{LABB2}_{\text{EESI}}$ have a lower mass defect and shallower slope than COA_{EESI} and $\text{CS-OA}_{\text{EESI}}$, consistent with increased aromaticity. The slopes are $(4.9 \pm 0.4) \cdot 10^{-4}$, $(5.9 \pm 0.6) \cdot 10^{-4}$, $(8 \pm 0.5) \cdot 10^{-4}$ and $(8 \pm 0.3) \cdot 10^{-4}$ for $\text{LABB1}_{\text{EESI}}$, $\text{LABB2}_{\text{EESI}}$, COA_{EESI} and $\text{CS-OA}_{\text{EESI}}$, respectively. The slopes of the two LABB factors as well as those of COA_{EESI} and $\text{CS-OA}_{\text{EESI}}$ are very similar to each other and have a high possibility to be consistent with CH addition for the former (i.e. $\text{C}_{10+x}\text{H}_{14+x}\text{O}_{4-5}$, theoretical slope $6 \cdot 10^{-4}$), and CH_2 addition for the latter (i.e. $\text{C}_{10+x}\text{H}_{20+2x}\text{O}_{3-5}$ for COA_{EESI} and $\text{C}_{10+y}\text{H}_{15+2y}\text{NO}_{3-5}$ for $\text{CS-OA}_{\text{EESI}}$ as nearly every CS-OA-specific ion contains a single N atom, theoretical slope $1.1 \cdot 10^{-3}$).

The MABB and LABB factors have similar slopes, despite different ion lists. The slopes of two MABB factors ($0.9 \cdot 10^{-3}$), as shown in Fig. 12b, are consistent with the addition of CHO functionality (theoretical slope = $0.1 \cdot 10^{-2}$). Due to the high

variability of the slopes of the MABB factors, it may also contain the other potential possibility for the added functionalities.

Both mass defect and slope are higher for MABB_LOW_{EESI} than for MABB_HIGH_{EESI}, which is consistent with our discussion in Sect. 3.2.3, assuming that the organics of the MABB_LOW_{EESI} factor are more oxidized than those of the MABB_HIGH_{EESI} factors. In addition, the MABB intercepts are more positive than those of LABB, consistent with the higher oxidation state shown above.

3.5 Comparison of AMS and EESI-TOF

Fig. 13a shows the sum of the mass flux of the ions measured by the EESI-TOF as a function of the OA concentration measured by the AMS, with the points colored by date and time. We apply no ion-dependent sensitivity corrections for the EESI-TOF, although ion-by-ion differences are known to exist (Lopez-Hilfiker et al., 2019). Note that the AMS signal includes the minor OA source, HOA_{AMS}, which is mostly insoluble in the electrospray droplets and thus expected to be basically undetectable by the EESI-TOF. Nevertheless, the two instruments are well-correlated ($R=0.94$). The strong correlation in Fig. 13a suggests that the overall EESI-TOF sensitivity to OA does not vary significantly throughout the study, and therefore it is unlikely that the major individual EESI-TOF PMF factors (which describe the compositional variability) have dramatically different response factors. We therefore interpret the EESI-TOF PMF results without correction of the data for factor-specific sensitivities. Several features are evident from dependence of the sensitivity on the mass flux of levoglucosan (Fig. 13b) which may explain the discrepancy in the first part of the campaign (period 1) vs. the rest of the campaign. An SOA-dominated period with low levoglucosan concentration (red line) toward the beginning of the campaign exhibits a lower sensitivity than during a period with higher levoglucosan concentrations (black line), which includes the events on 28.01.2017 and 29.01.2017 characteristic of EVENT_{EESI} (Lopez-Hilfiker et al., 2019). Figures 13c and 13d respectively show the O:C and H:C atomic ratios for the EESI-TOF as a function of those for the AMS. Here again no ion-dependent sensitivity corrections are applied. The EESI-TOF and AMS O:C ratios are correlated ($R=0.62$), however, the O:C ratios estimated by the EESI-TOF are systematically higher than those measured by the AMS. For H:C ratios, we do not observe a correlation. The EESI-TOF values are scattered around approximately 1.56, independent of the AMS H:C ratios which vary between 1.11 and 1.44. The cause for this discrepancy is not yet understood but may be related to differences in ion relative sensitivity (Bertrand et al., submitted). Fig. 14 shows the stacked time series of the EESI-TOF PMF factors (together with total AMS OA concentration) and of the AMS PMF factors. Also shown are pie charts denoting the mean OA PMF composition over the entire campaign from the EESI-TOF and AMS data. Despite uncertainties in the definition and resolution of primary vs. more aged biomass burning, the AMS and EESI-TOF are in relatively good agreement with respect to the total POA and SOA fractions. The SOA factors comprise 58.8 % of the mass flux for the EESI-TOF and 69.4 % of the mass for the AMS. The agreement may in fact be better than these values indicate: as noted above the NOA_{AMS} factor, comprising 17.9 % of the mass and fully associated to SOA in our solution, is likely composed of both POA (derived from cigarette smoke, as resolved in CS-OA_{EESI}) and SOA (from organonitrate-containing SOA, as resolved in NSOA_{EESI}), resulting in a low total POA fraction in the AMS solution. Since both CS-OA_{EESI} and NSOA_{EESI} are enriched with the nitrogen-containing ions, we compare in Fig. 15, the O:C and N:C ratios

for these two factors, where the size of the colored star and circle corresponds to the H:C ratio. A distinct separation between CS-OA_{EESI} and NSOA_{EESI} is evident due to a significantly higher O:C ratio for a given N:C ratio, i.e., higher degree of oxygenation for the NSOA_{EESI} factor and a higher abundance of organic-nitrate molecules in the NSOA_{EESI} factor. Moreover, this separation was not possible for AMS PMF.

- 5 Both AMS and EESI-TOF factors stacked time series (Fig. 14) show clearly that biomass burning is dominated by secondary fractions early in the campaign, mixed fractions in the middle of the campaign, and **a primary fractions** late in the campaign. As discussed in Sect 3.2.2, BBOA_{AMS} is a mixture of primary and secondary ions, and OOA_{AMS} is a mixture of biomass burning fragments and background SOA fragments from photochemistry production ions. Although the fraction of OOA comprised more than 50 % percent of total OA (Fig. 14), it is hard to define how much of AMS OOA is **BB-related** as a function of time.
- 10 The EESI-TOF separates the biomass burning factors into LABB_{EESI} and MABB_{EESI} and splits the background SOA factors into separate factors, which provides evidence that biomass burning is the single most important contributor to the organic aerosol at the measurement site during winter.

4 Conclusions

- 15 Real-time, near-molecular level measurements of OA composition were performed during winter in Zurich using a novel extractive electrospray ionization time-of-flight mass spectrometer (EESI-TOF). The lack of thermal decomposition or ionization-induced fragmentation in the EESI-TOF provides an improved description of SOA in particular, facilitating SOA source identification by PMF. We retrieve eleven factors, of which 5 are dominated by POA and 6 by SOA. The POA factors included cooking-influenced OA (COA_{EESI}, which strongly correlates with an equivalent AMS factor), cigarette smoke-
- 20 influenced OA (CS-OA_{EESI}, characterized by a strong contribution from nicotine) and a special event also captured by the AMS. Two less aged biomass burning factors are also resolved. Of the six SOA factors, three are clearly related to biomass burning and are distinguished by temperature and possibly wind direction. We also observe two SOA factors with no clear biomass burning signatures, one of which closely resembles monoterpene oxidation. Finally, we observe a minor factor with a high organonitrate fraction.
- 25 We performed cluster analysis of the EESI-TOF ions followed by correlation with the resolved factors, which identifies groups of ions characteristic of each factor. These characteristic ions represent potential tracers for future studies; they indicate strong aromatic influence in both **less aged** and more aged biomass burning, and support the primary / secondary assignment of biomass burning-influenced factors.

- The increased chemical specificity of the EESI-TOF allows for additional, meaningful factors to be resolved relative to the
- 30 AMS. Comparisons of bulk measurements, as well as of individual factors or groups of factors between the EESI-TOF and AMS indicate good agreement, **but with the differences in elemental ratios**. This suggests that, despite significant uncertainties in the relative response factors of individual ions measured by the EESI-TOF, responses at the level of the PMF factors are

relatively similar, with the main differences resulting from the high sensitivity to levoglucosan in the EESI. Furthermore, source apportionment of EESI-TOF provides more classification of SOA factors, separating EESI biomass burning factors as more/ less aged instead of primary / secondary, identifying organic nitrogen containing factors as primary-dominated nitrogen factor / organonitrate-containing secondary factor, which are not possible for AMS PMF. As a result, the EESI-TOF represents a promising new approach for source apportionment and atmospheric composition studies.

Author Contribution.

LQ was the main author. LQ, GS, VP, YT, and CH conducted the field campaign. MD, XG, JS, AP, and UB were the supervisors. All contributed to the corrections of the paper.

Competing interests.

The authors declare that they have no conflict of interest.

Acknowledgements.

This study was funded by the Swiss National Science Foundation (starting grant BSSGIO_155846), the National Natural Science Foundation of China (grant No. 91543115, 21577065), and the International ST Cooperation Program of China (2014DFA90780). We acknowledge the support by the Federal Office for the Environment. Mao Xiao is acknowledged for useful discussions. The authors gratefully acknowledge technical and logistical support from R. Richter (PSI).

Reference

- Bertrand, A., Stefenelli, G., Jen, C. N., Pieber, S. M., Bruns, E. A., Ni, H., Temime-Roussel, B., Slowik, J. G., Goldstein, A. H., El Haddad, I., Baltensperger, U., Prévôt, A. S. H., Wortham, H., and Marchand, N.: Evolution of the chemical fingerprint of biomass burning organic aerosol during aging, *Atmos. Chem. Phys.*, 18, 7607-7624, 10.5194/acp-18-7607-2018, 2018.
- Bianchi, F., Garmash, O., He, X., Yan, C., Iyer, S., Rosendahl, I., Xu, Z., Rissanen, M. P., Riva, M., Taipale, R., Sarnela, N., Petäjä, T., Worsnop, D. R., Kulmala, M., Ehn, M., and Junninen, H.: The role of highly oxygenated molecules (HOMs) in determining the composition of ambient ions in the boreal forest, *Atmos. Chem. Phys.*, 17, 13819-13831, 10.5194/acp-17-13819-2017, 2017.
- Bozzetti, C., Sosedova, Y., Xiao, M., Daellenbach, K. R., Ulevicius, V., Dudoitis, V., Mordas, G., Byčenkienė, S., Plauškaitė, K., Vlachou, A., Golly, B., Chazeanu, B., Besombes, J.-L., Baltensperger, U., Jaffrezo, J.-L., Slowik, J. G., and El-Haddad, I.,

- and Prévôt A. S. H. : Argon offline-AMS source apportionment of organic aerosol over yearly cycles for an urban, rural and marine site in Northern Europe, *Environ. Sci. Technol.*, 2016.
- Bruns, E. A., El Haddad, I., Slowik, J. G., Kilic, D., Klein, F., Baltensperger, U., and Prevot, A. S.: Identification of significant precursor gases of secondary organic aerosols from residential wood combustion, *Sci. Rep.*, 6, 27881, 10.1038/srep27881, 5 2016.
- Bruns, E. A., Slowik, J. G., El Haddad, I., Kilic, D., Klein, F., Dommen, J., Temime-Roussel, B., Marchand, N., Baltensperger, U., and Prévôt, A. S. H.: Characterization of gas-phase organics using proton transfer reaction time-of-flight mass spectrometry: fresh and aged residential wood combustion emissions, *Atmos. Chem. Phys.*, 17, 705-720, 10.5194/acp-17-705-2017, 2017.
- Canonaco, F., Crippa, M., Slowik, J. G., Baltensperger, U., and Prévôt, A. S. H.: SoFi, an IGOR-based interface for the efficient use of the generalized multilinear engine (ME-2) for the source apportionment: ME-2 application to aerosol mass spectrometer data, *Atmos. Meas. Tech.*, 6, 3649-3661, 10.5194/amt-6-3649-2013, 2013.
- Chan, A. W. H., Kautzman, K. E., Chhabra, P. S., Surratt, J. D., Chan, M. N., Crouse, J. D., Kürten, A., Wennberg, P. O., Flagan, R. C., and Seinfeld, J. H.: Secondary organic aerosol formation from photooxidation of naphthalene and alkylnaphthalenes: implications for oxidation of intermediate volatility organic compounds (IVOCs), *Atmos. Chem. Phys.*, 9, 15 3049-3060, 10.5194/acp-9-3049-2009, 2009.
- Chan, M. N., Choi, M. Y., Ng, N. L., and Chan, C. K.: Hygroscopicity of water-soluble organic compounds in atmospheric aerosols: Amino acids and biomass burning derived organic species, *Environ. Sci. Technol.*, 39, 1555-1562, Doi 10.1021/Es0495841, 2005.
- Coeur-Tourneur, C., Tomas, A., Guilloteau, A., Henry, F., Ledoux, F., Visez, N., Riffault, V., Wenger, J. C., and Bedjanian, Y.: Aerosol formation yields from the reaction of catechol with ozone, *Atmos. Environ.*, 43, 2360-2365, 20 10.1016/j.atmosenv.2008.12.054, 2009.
- Crippa, M., DeCarlo, P. F., Slowik, J. G., Mohr, C., Heringa, M. F., Chirico, R., Poulain, L., Freutel, F., Sciare, J., Cozic, J., Di Marco, C. F., Elsasser, M., Nicolas, J. B., Marchand, N., Abidi, E., Wiedensohler, A., Drewnick, F., Schneider, J., Borrmann, S., Nemitz, E., Zimmermann, R., Jaffrezo, J. L., Prévôt, A. S. H., and Baltensperger, U.: Wintertime aerosol chemical composition and source apportionment of the organic fraction in the metropolitan area of Paris, *Atmos. Chem. Phys.*, 13, 961- 25 981, 10.5194/acp-13-961-2013, 2013a.
- Crippa, M., El Haddad, I., Slowik, J. G., DeCarlo, P. F., Mohr, C., Heringa, M. F., Chirico, R., Marchand, N., Sciare, J., Baltensperger, U., and Prevot, A. S. H.: Identification of marine and continental aerosol sources in Paris using high resolution aerosol mass spectrometry, *J. Geophys. Res.*, 118, 1950-1963, 10.1002/jgrd.50151, 2013b.
- 30 Crippa, M., Canonaco, F., Lanz, V. A., Äijälä, M., Allan, J. D., Carbone, S., Capes, G., Ceburnis, D., Dall'Osto, M., Day, D. A., DeCarlo, P. F., Ehn, M., Eriksson, A., Freney, E., Hildebrandt Ruiz, L., Hillamo, R., Jimenez, J. L., Junninen, H., Kiendler-Scharr, A., Kortelainen, A. M., Kulmala, M., Laaksonen, A., Mensah, A. A., Mohr, C., Nemitz, E., O'Dowd, C., Ovadnevaite, J., Pandis, S. N., Petäjä, T., Poulain, L., Saarikoski, S., Sellegri, K., Swietlicki, E., Tiitta, P., Worsnop, D. R., Baltensperger,

- U., and Prévôt, A. S. H.: Organic aerosol components derived from 25 AMS data sets across Europe using a consistent ME-2 based source apportionment approach, *Atmos. Chem. Phys.*, 14, 6159-6176, 10.5194/acp-14-6159-2014, 2014.
- Daellenbach, K. R., Bozzetti, C., Křepelová, A., Canonaco, F., Wolf, R., Zotter, P., Fermo, P., Crippa, M., Slowik, J. G., Sosedova, Y., Zhang, Y., Huang, R. J., Poulain, L., Szidat, S., Baltensperger, U., El Haddad, I., and Prévôt, A. S. H.:
5 Characterization and source apportionment of organic aerosol using offline aerosol mass spectrometry, *Atmos. Meas. Tech.*, 9, 23-39, 10.5194/amt-9-23-2016, 2016.
- Daellenbach, K. R., Stefenelli, G., Bozzetti, C., Vlachou, A., Fermo, P., Gonzalez, R., Piazzalunga, A., Colombi, C., Canonaco, F., Hueglin, C., Kasper-Giebl, A., Jaffrezo, J.-L., Bianchi, F., Slowik, J. G., Baltensperger, U., El-Haddad, I., and Prévôt, A. S. H.: Long-term chemical analysis and organic aerosol source apportionment at nine sites in central Europe: source
10 identification and uncertainty assessment, *Atmos. Chem. Phys.*, 17, 13265-13282, 10.5194/acp-17-13265-2017, 2017.
- DeCarlo, P. F., Kimmel, J. R., Trimborn, A., Northway, M. J., Jayne, J. T., Aiken, A. C., Gonin, M., Fuhrer, K., Horvath, T., Docherty, K. S., Worsnop, D. R., and Jimenez, J. L.: Field-deployable, high-resolution, time-of-flight aerosol mass spectrometer, *Anal. Chem.*, 78, 8281-8289, 10.1021/Ac061249n, 2006.
- Docherty, K. S., Stone, E. A., Ulbrich, I. M., DeCarlo, P. F., Snyder, D. C., Schauer, J. J., Peltier, R. E., Weber, R. J., Murphy, S. M., Seinfeld, J. H., Grover, B. D., Eatough, D. J., and Jimenez, J. L.: Apportionment of primary and secondary organic
15 aerosols in southern California during the 2005 study of organic aerosols in riverside (SOAR-1), *Environ. Sci. Technol.*, 42, 7655-7662, Doi 10.1021/Es8008166, 2008.
- Eichler, P., Müller, M., Anna, B., and Wisthaler, A.: A novel inlet system for online chemical analysis of semi-volatile submicron particulate matter, *Atmos. Meas. Tech.*, 8, 1353-1360, 10.5194/amt-8-1353-2015, 2015.
- 20 Fine, P. M., Cass, G. R., and Simoneit, B. R. T.: Chemical characterization of fine particle emissions from fireplace combustion of woods grown in the northeastern United States, *Environ. Sci. Technol.*, 35, 2665-2675, 10.1021/es001466k, 2001.
- Finewax, Z., de Gouw, J. A., and Ziemann, P. J.: Identification and quantification of 4-nitrocatechol formed from OH and NO₃ radical-initiated reactions of catechol in air in the presence of NO_x: implications for secondary organic aerosol formation from biomass burning, *Environ. Sci. Technol.*, 52, 1981-1989, 10.1021/acs.est.7b05864, 2018.
- 25 Fu, P. Q., Kawamura, K., Pavuluri, C. M., Swaminathan, T., and Chen, J.: Molecular characterization of urban organic aerosol in tropical India: contributions of primary emissions and secondary photooxidation, *Atmos. Chem. Phys.*, 10, 2663-2689, 10.5194/acp-10-2663-2010, 2010.
- Ge, X. L., Setyan, A., Sun, Y., and Zhang, Q.: Primary and secondary organic aerosols in Fresno, California during wintertime: Results from high resolution aerosol mass spectrometry, *J. Geophys. Res.*, 117, D19301, 10.1029/2012jd018026, 2012.
- 30 Hallquist, M., Wenger, J. C., Baltensperger, U., Rudich, Y., Simpson, D., Claeys, M., Dommen, J., Donahue, N. M., George, C., Goldstein, A. H., Hamilton, J. F., Herrmann, H., Hoffmann, T., Iinuma, Y., Jang, M., Jenkin, M. E., Jimenez, J. L., Kiendler-Scharr, A., Maenhaut, W., McFiggans, G., Mentel, T. F., Monod, A., Prévôt, A. S. H., Seinfeld, J. H., Surratt, J. D., Szmigielski, R., and Wildt, J.: The formation, properties and impact of secondary organic aerosol: current and emerging issues, *Atmos. Chem. Phys.*, 9, 5155-5236, 10.5194/acp-9-5155-2009, 2009.

- Hayes, P. L., Ortega, A. M., Cubison, M. J., Froyd, K. D., Zhao, Y., Cliff, S. S., Hu, W. W., Toohey, D. W., Flynn, J. H., Lefer, B. L., Grossberg, N., Alvarez, S., Rappenglueck, B., Taylor, J. W., Allan, J. D., Holloway, J. S., Gilman, J. B., Kuster, W. C., De Gouw, J. A., Massoli, P., Zhang, X., Liu, J., Weber, R. J., Corrigan, A. L., Russell, L. M., Isaacman, G., Worton, D. R., Kreisberg, N. M., Goldstein, A. H., Thalman, R., Waxman, E. M., Volkamer, R., Lin, Y. H., Surratt, J. D., Kleindienst, T. E., Offenberg, J. H., Dusanter, S., Griffith, S., Stevens, P. S., Brioude, J., Angevine, W. M., and Jimenez, J. L.: Organic aerosol composition and sources in Pasadena, California, during the 2010 CalNex campaign, *J. Geophys. Res.*, 118, 9233-9257, 10.1002/jgrd.50530, 2013.
- He, X., Huang, X. H. H., Chow, K. S., Wang, Q., Zhang, T., Wu, D., and Yu, J. Z.: Abundance and sources of phthalic acids, benzene-tricarboxylic acids and phenolic acids in PM_{2.5}, *Earth Space Chem.*, 10.1021/, 2018.
- 10 Henry, R., Garya Norris, Ram Vedantham, and Turner, J. R.: Source region identification using Kernel smoothing, *Environ. Sci. Technol.*, 43, 4090-4097, 2009.
- Herich, H., Gianini, M. F. D., Piot, C., Močnik, G., Jaffrezo, J. L., Besombes, J. L., Prévôt, A. S. H., and Hueglin, C.: Overview of the impact of wood burning emissions on carbonaceous aerosols and PM in large parts of the Alpine region, *Atmos. Environ.*, 89, 64-75, 10.1016/j.atmosenv.2014.02.008, 2014.
- 15 Iinuma, Y., Boge, O., Grafe, R., and Herrmann, H.: Methyl-nitrocatechols: atmospheric tracer compounds for biomass burning secondary organic aerosols, *Environ. Sci. Technol.*, 44, 8453-8459, 10.1021/es102938a, 2010.
- Jayne, J. T., Leard, D. C., Zhang, X., Davidovits, P., Smith, K. A., Kolb, C. E., and Worsnop, D. R.: Development of an aerosol mass spectrometer for size and composition analysis of submicron particles, *Aerosol Sci. Technol.*, 33, 49 - 70, 10.1016/S0021-8502(98)00158-X, 2000.
- 20 Jimenez, J. L., Canagaratna, M. R., Donahue, N. M., Prevot, A. S. H., Zhang, Q., Kroll, J. H., DeCarlo, P. F., Allan, J. D., Coe, H., Ng, N. L., Aiken, A. C., Docherty, K. S., Ulbrich, I. M., Grieshop, A. P., Robinson, A. L., Duplissy, J., Smith, J. D., Wilson, K. R., Lanz, V. A., Hueglin, C., Sun, Y. L., Tian, J., Laaksonen, A., Raatikainen, T., Rautiainen, J., Vaattovaara, P., Ehn, M., Kulmala, M., Tomlinson, J. M., Collins, D. R., Cubison, M. J., Dunlea, E. J., Huffman, J. A., Onasch, T. B., Alfarra, M. R., Williams, P. I., Bower, K., Kondo, Y., Schneider, J., Drewnick, F., Borrmann, S., Weimer, S., Demerjian, K., Salcedo, D.,
- 25 Cottrell, L., Griffin, R., Takami, A., Miyoshi, T., Hatakeyama, S., Shimono, A., Sun, J. Y., Zhang, Y. M., Dzepina, K., Kimmel, J. R., Sueper, D., Jayne, J. T., Herndon, S. C., Trimborn, A. M., Williams, L. R., Wood, E. C., Middlebrook, A. M., Kolb, C. E., Baltensperger, U., and Worsnop, D. R.: Evolution of organic aerosols in the atmosphere, *Science*, 326, 1525-1529, 10.1126/science.1180353, 2009.
- Kleindienst, T. E., Jaoui, M., Lewandowski, M., Offenberg, J. H., and Docherty, K. S.: The formation of SOA and chemical tracer compounds from the photooxidation of naphthalene and its methyl analogs in the presence and absence of nitrogen oxides, *Atmos. Chem. Phys.*, 12, 8711-8726, 10.5194/acp-12-8711-2012, 2012.
- 30 Kroll, J. H., Donahue, N. M., Jimenez, J. L., Kessler, S. H., Canagaratna, M. R., Wilson, K. R., Altieri, K. E., Mazzoleni, L. R., Wozniak, A. S., Bluhm, H., Mysak, E. R., Smith, J. D., Kolb, C. E., and Worsnop, D. R.: Carbon oxidation state as a metric for describing the chemistry of atmospheric organic aerosol, *Nat. Chem.*, 3, 133-139, 10.1038/nchem.948, 2011.

- Lanz, V. A., Alfarra, M. R., Baltensperger, U., Buchmann, B., Hueglin, C., and Prévôt, A. S. H.: Source apportionment of submicron organic aerosols at an urban site by factor analytical modelling of aerosol mass spectra, *Atmos. Chem. Phys.*, 7, 1503-1522, 10.5194/acp-7-1503-2007, 2007.
- Lanz, V. A., Alfarra, M. R., Baltensperger, U., Buchmann, B., Hueglin, C., Szidat, S., Wehrli, M. N., Wacker, L., Weimer, S.,
5 Caseiro, A., Puxbaum, H., and Prevot, A. S. H.: Source attribution of submicron organic aerosols during wintertime inversions by advanced factor analysis of aerosol mass spectra, *Environ. Sci. Technol.*, 42, 214-220, 10.1021/es0707207, 2008.
- Lanz, V. A., Prévôt, A. S. H., Alfarra, M. R., Weimer, S., Mohr, C., DeCarlo, P. F., Gianini, M. F. D., Hueglin, C., Schneider, J., Favez, O., D'Anna, B., George, C., and Baltensperger, U.: Characterization of aerosol chemical composition with aerosol mass spectrometry in Central Europe: an overview, *Atmos. Chem. Phys.*, 10, 10453-10471, 10.5194/acp-10-10453-2010, 2010.
- 10 Lopez-Hilfiker, F. D., Mohr, C., Ehn, M., Rubach, F., Kleist, E., Wildt, J., Mentel, T. F., Lutz, A., Hallquist, M., Worsnop, D., and Thornton, J. A.: A novel method for online analysis of gas and particle composition: description and evaluation of a Filter Inlet for Gases and AEROsols (FIGAERO), *Atmos. Meas. Tech.*, 7, 983-1001, 10.5194/amt-7-983-2014, 2014.
- Lopez-Hilfiker, F. D., Pospisilova, V., Huang, W., Kalberer, M., Mohr, C., Stefenelli, G., Thornton, J. A., Baltensperger, U., Prevot, A. S. H., and Slowik, J. G.: An Extractive Electrospray Ionization Time-of-Flight Mass Spectrometer (EESI-TOF) for
15 online measurement of atmospheric aerosol particles, *Atmospheric Measurement Techniques Discussions*, 1-40, 10.5194/amt-2019-45, 2019.
- Middlebrook, A. M., Bahreini, R., Jimenez, J. L., and Canagaratna, M. R.: Evaluation of composition-dependent collection efficiencies for the Aerodyne aerosol mass spectrometer using field data, *Aerosol Sci. Technol.*, 46, 258-271, 10.1080/02786826.2011.620041, 2012.
- 20 Mohr, C., DeCarlo, P. F., Heringa, M. F., Chirico, R., Slowik, J. G., Richter, R., Reche, C., Alastuey, A., Querol, X., Seco, R., Peñuelas, J., Jiménez, J. L., Crippa, M., Zimmermann, R., Baltensperger, U., and Prévôt, A. S. H.: Identification and quantification of organic aerosol from cooking and other sources in Barcelona using aerosol mass spectrometer data, *Atmos. Chem. Phys.*, 12, 1649-1665, 10.5194/acp-12-1649-2012, 2012.
- Muller, M., Eichler, P., D'Anna, B., Tan, W., and Wisthaler, A.: Direct Sampling and Analysis of Atmospheric Particulate
25 Organic Matter by Proton-Transfer-Reaction Mass Spectrometry, *Anal Chem*, 89, 10889-10897, 10.1021/acs.analchem.7b02582, 2017.
- Nah, T., Sanchez, J., Boyd, C. M., and Ng, N. L.: Photochemical aging of alpha-pinene and beta-pinene secondary organic aerosol formed from nitrate radical oxidation, *Environ. Sci. Technol.*, 50, 222-231, 10.1021/acs.est.5b04594, 2016.
- Nakao, S., Clark, C., Tang, P., Sato, K., and Cocker I., D.: Secondary organic aerosol formation from phenolic compounds in
30 the absence of NO₃, *Atmos. Chem. Phys.*, 11, 10649-10660, 10.5194/acp-11-10649-2011, 2011.
- Nakao, S., Liu, Y., Tang, P., Chen, C. L., Zhang, J., and Cocker I., D. R.: Chamber studies of SOA formation from aromatic hydrocarbons: observation of limited glyoxal uptake, *Atmospheric Chemistry and Physics*, 12, 3927-3937, 10.5194/acp-12-3927-2012, 2012.
- Nel, A.: Air pollution-related illness: Effects of particles, *Science*, 308, 804-806, 10.1126/science.1108752, 2005.

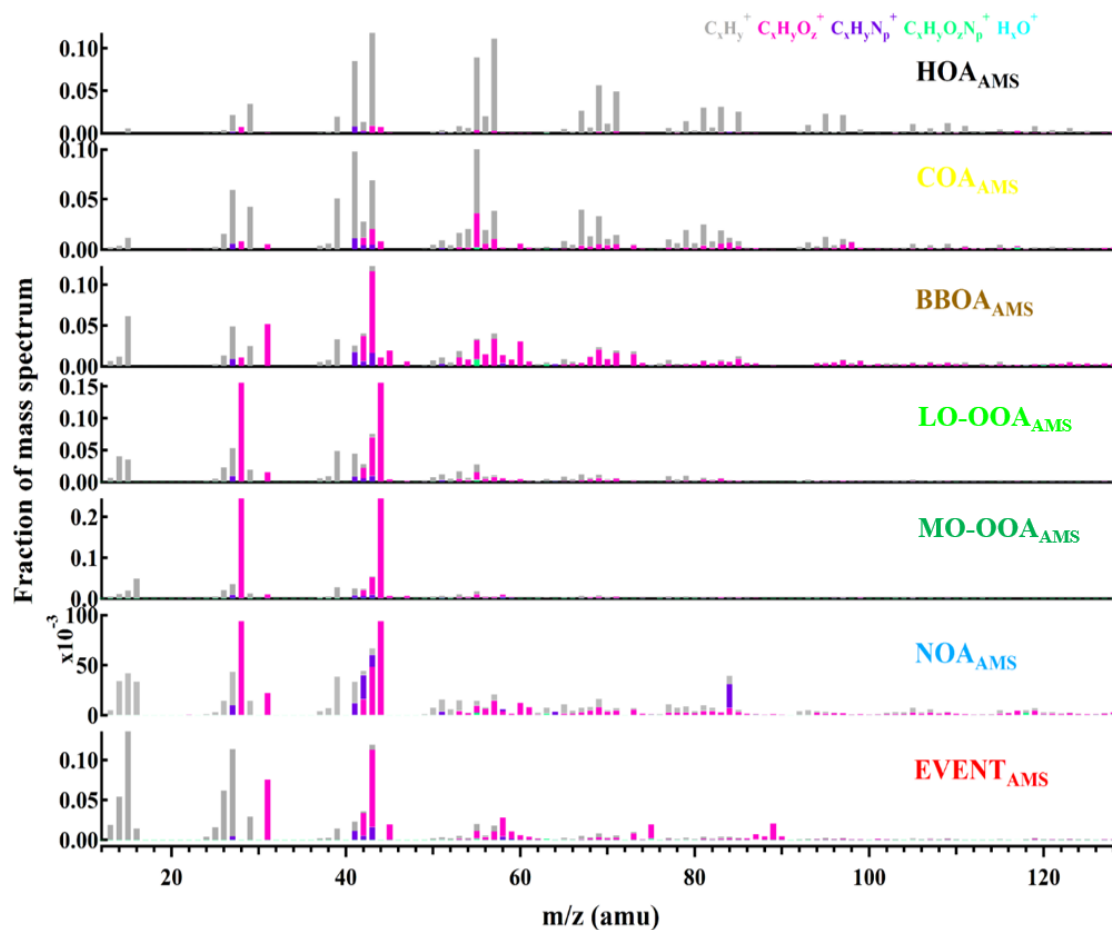
- Ng, N. L., Canagaratna, M. R., Zhang, Q., Jimenez, J. L., Tian, J., Ulbrich, I. M., Kroll, J. H., Docherty, K. S., Chhabra, P. S., Bahreini, R., Murphy, S. M., Seinfeld, J. H., Hildebrandt, L., Donahue, N. M., DeCarlo, P. F., Lanz, V. A., Prevot, A. S. H., Dinar, E., Rudich, Y., and Worsnop, D. R.: Organic aerosol components observed in Northern Hemispheric datasets from Aerosol Mass Spectrometry, *Atmos. Chem. Phys.*, 10, 4625-4641, 10.5194/acp-10-4625-2010, 2010.
- 5 Ofner, J., Krüger, H. U., Grothe, H., Schmitt-Kopplin, P., Whitmore, K., and Zetzsch, C.: Physico-chemical characterization of SOA derived from catechol and guaiacol - a model substance for the aromatic fraction of atmospheric HULIS, *Atmos. Chem. Phys.*, 11, 1-15, 10.5194/acp-11-1-2011, 2011.
- Olson, D. A., Vedantham, R., Norris, G. A., Brown, S. G., and Roberts, P.: Determining source impacts near roadways using wind regression and organic source markers, *Atmos. Environ.*, 47, 261-268, 10.1016/j.atmosenv.2011.11.003, 2012.
- 10 Paatero, P.: Least squares formulation of robust non-negative factor analysis, *Chemo. Intell. Lab. Syst.*, 37, 23-35, 10.1016/s0169-7439(96)00044-5, 1997.
- Petit, J. E., O. Favez, A. Albinet, and Canonaco, F.: A user-friendly tool for comprehensive evaluation of the geographical origins of atmospheric pollution: Wind and trajectory analyses, *Environ. Model. Soft.*, 88, 183-187, 10.1016/j.envsoft.2016.11.022, 2017.
- 15 Quan, J., Tie, X., Zhang, Q., Liu, Q., Li, X., Gao, Y., and Zhao, D.: Characteristics of heavy aerosol pollution during the 2012-2013 winter in Beijing, China, *Atmos. Environ.*, 88, 83-89, <http://dx.doi.org/10.1016/j.atmosenv.2014.01.058>, 2014.
- Richard, A., Gianini, M. F. D., Mohr, C., Furger, M., Bukowiecki, N., Minguillón, M. C., Lienemann, P., Flechsig, U., Appel, K., DeCarlo, P. F., Heringa, M. F., Chirico, R., Baltensperger, U., and Prévôt, A. S. H.: Source apportionment of size and time resolved trace elements and organic aerosols from an urban courtyard site in Switzerland, *Atmos. Chem. Phys.*, 11, 8945-8963, 2011.
- 20 10.5194/acp-11-8945-2011, 2011.
- Samy, S., Robinson, J., and Hays, M. D.: An advanced LC-MS (Q-TOF) technique for the detection of amino acids in atmospheric aerosols, *Anal. Bioanal. Chem.*, 401, 3103-3113, 10.1007/s00216-011-5238-2, 2011.
- Sasaki, T. A., Wilkins, J. M., Forehand, J. B., and Moldoveanu, S. C.: Analysis of heterocyclic amines in mainstream cigarette smoke using a new NCI GC-MS technique, *Anal. Lett.*, 34, 1749-1761, 10.1081/al-100105358, 2001.
- 25 Schwantes, R. H., Schilling, K. A., McVay, R. C., Lignell, H., Coggon, M. M., Zhang, X., Wennberg, P. O., and Seinfeld, J. H.: Formation of highly oxygenated low-volatility products from cresol oxidation, *Atmos. Chem. Phys.*, 17, 3453-3474, 10.5194/acp-17-3453-2017, 2017.
- Stefenelli, G., Jiang, J., Bertrand, A., Bruns, E. A., Pieber, S. M., Baltensperger, U., Marchand, N., Aksoyoglu, S., Prévôt, A. S. H., Slowik, J. G., and El Haddad, I.: Secondary organic aerosol formation from smoldering and flaming combustion of biomass: a box model parametrization based on volatility basis set, *Atmos. Chem. Phys. Diss.*, 1-41, 10.5194/acp-2018-1308, 2019.
- 30 Stefenelli, G., Pospisilova, V., Lopez-Hilfiker, F. D., Daellenbach, K. R., Hüglin, C., Tong, Y., Baltensperger, U., Prevot, A. S. H., and Slowik, J. G.: Organic aerosol source apportionment in Zurich using extractive electrospray ionization time-of-

- flight mass spectrometry (EESI-TOF): Part I, biogenic influences and day/night chemistry in summer, *Atmospheric Chemistry and Physics Discussions*, 1-36, 10.5194/acp-2019-361, 2019.
- Stocker, T. F., D. Qin, G.-K. Plattner, M. Tignor, S.K. Allen, J. Boschung, A. Nauels, Y. Xia, V. Bex, P. M. Midgley IPCC: Climate Change 2013: the Physical Science Basis. Contribution of Working Group to the Fifth Assessment Report of the Intergovernmental Panel on Climate Change, Cambridge University Press, Cambridge, UK, and NY, USA, 2013.
- Struckmeier, C., Drewnick, F., Fachinger, F., Gobbi, G. P., and Borrmann, S.: Atmospheric aerosols in Rome, Italy: sources, dynamics and spatial variations during two seasons, *Atmos. Chem. Phys.*, 16, 15277-15299, 10.5194/acp-16-15277-2016, 2016.
- Sun, Y. L., Zhang, Q., Schwab, J. J., Demerjian, K. L., Chen, W. N., Bae, M. S., Hung, H. M., Hogrefe, O., Frank, B., Rattigan, O. V., and Lin, Y. C.: Characterization of the sources and processes of organic and inorganic aerosols in New York city with a high-resolution time-of-flight aerosol mass spectrometer, *Atmos. Chem. Phys.*, 11, 1581-1602, 10.5194/acp-11-1581-2011, 2011.
- Sun, Y. L., Zhang, Q., Schwab, J. J., Chen, W. N., Bae, M. S., Hung, H. M., Lin, Y. C., Ng, N. L., Jayne, J., Massoli, P., Williams, L. R., and Demerjian, K. L.: Characterization of near-highway submicron aerosols in New York City with a high-resolution aerosol mass spectrometer, *Atmos. Chem. Phys.*, 12, 2215-2227, 10.5194/acp-12-2215-2012, 2012.
- Sun, Y. L., Wang, Z. F., Fu, P. Q., Yang, T., Jiang, Q., Dong, H. B., Li, J., and Jia, J. J.: Aerosol composition, sources and processes during wintertime in Beijing, China, *Atmos. Chem. Phys.*, 13, 4577-4592, 10.5194/acp-13-4577-2013, 2013.
- Timkovsky, J., Chan, A. W. H., Dorst, T., Goldstein, A. H., Oyama, B., and Holzinger, R.: Comparison of advanced offline and in situ techniques of organic aerosol composition measurement during the CalNex campaign, *Atmos. Meas. Tech.*, 8, 5177-5187, 10.5194/amt-8-5177-2015, 2015.
- Veres, P., Roberts, J. M., Burling, I. R., Warneke, C., de Gouw, J., and Yokelson, R. J.: Measurements of gas-phase inorganic and organic acids from biomass fires by negative-ion proton-transfer chemical-ionization mass spectrometry, *J. Geophys. Res.*, 115, 10.1029/2010jd014033, 2010.
- Wang, G., Kawamura, K., Xie, M., Hu, S., Cao, J., An, Z., Waston, J. G., and Chow, J. C.: Organic molecular compositions and size distributions of Chinese summer and autumn aerosols from Nanjing: Characteristic haze event caused by wheat straw burning, *Environ. Sci. Technol.*, 43, 6493-6499, 2009.
- Wang, L., Atkinson, R., and Arey, J.: Dicarbonyl products of the OH radical-initiated reactions of naphthalene and the C1- and C2-alkylnaphthalenes, *Environ. Sci. Technol.*, 41, 2803-2810, 10.1021/es0628102, 2007.
- Wang, X., Hayeck, N., Brüggemann, M., Yao, L., Chen, H., Zhang, C., Emmelin, C., Chen, J., George, C., and Wang, L.: Chemical characteristics of organic aerosols in Shanghai: A study by ultrahigh-performance liquid chromatography coupled with orbitrap mass spectrometry, *J. Geophys. Res.*, 122, 703-711, 10.1002/2017jd026930, 2017.
- Williams, B. J., Goldstein, A. H., Kreisberg, N. M., and Hering, S. V.: An in-situ instrument for speciated organic composition of atmospheric aerosols: Thermal Desorption Aerosol GC/MS-FID (TAG), *Aerosol Sci. Technol.*, 40, 627-638, 10.1080/02786820600754631, 2006.

- Williams, L. R., Gonzalez, L. A., Peck, J., Trimborn, D., McInnis, J., Farrar, M. R., Moore, K. D., Jayne, J. T., Robinson, W. A., Lewis, D. K., Onasch, T. B., Canagaratna, M. R., Trimborn, A., Timko, M. T., Magoon, G., Deng, R., Tang, D., de la Rosa Blanco, E., Prévôt, A. S. H., Smith, K. A., and Worsnop, D. R.: Characterization of an aerodynamic lens for transmitting particles greater than 1 micrometer in diameter into the Aerodyne aerosol mass spectrometer, *Atmos. Meas. Tech.*, 6, 3271-3280, 10.5194/amt-6-3271-2013, 2013.
- 5 Xu, L., Guo, H., Boyd, C. M., Klein, M., Bougiatioti, A., Cerully, K. M., Hite, J. R., Isaacman-VanWertz, G., Kreisberg, N. M., Knote, C., Olson, K., Koss, A., Hering, S. V., de Gouw, J., Baumann, K., Lee, S.-H., Nenes, A., Weber, R. J., and Ng, N. L.: Effects of anthropogenic emissions on aerosol formation from isoprene and monoterpenes in the southeastern United States, *P. Natl. Acad. Sci. USA*, 112, E4506-4507, 10.1073/pnas.1512277112, 2015.
- 10 Yee, L. D., Kautzman, K. E., Loza, C. L., Schilling, K. A., Coggon, M. M., Chhabra, P. S., Chan, M. N., Chan, A. W. H., Hersey, S. P., Crounse, J. D., Wennberg, P. O., Flagan, R. C., and Seinfeld, J. H.: Secondary organic aerosol formation from biomass burning intermediates: phenol and methoxyphenols, *Atmos. Chem. Phys.*, 13, 8019-8043, 10.5194/acp-13-8019-2013, 2013.
- Young, D. E., Kim, H., Parworth, C., Zhou, S., Zhang, X., Cappa, C. D., Seco, R., Kim, S., and Zhang, Q.: Influences of emission sources and meteorology on aerosol chemistry in a polluted urban environment: results from DISCOVER-AQ California, *Atmos. Chem. Phys.*, 16, 5427-5451, 10.5194/acp-16-5427-2016, 2016.
- 15 Zhang, H., Worton, D. R., Shen, S., Nah, T., Isaacman-VanWertz, G., Wilson, K. R., and Goldstein, A. H.: Fundamental time scales governing organic aerosol multiphase partitioning and oxidative aging, *Environ. Sci. Technol.*, 49, 9768-9777, 10.1021/acs.est.5b02115, 2015.
- 20 Zhang, H., Yee, L. D., Lee, B. H., Curtis, M. P., Worton, D. R., Isaacman-VanWertz, G., Offenberg, J. H., Lewandowski, M., Kleindienst, T. E., Beaver, M. R., Holder, A. L., Lonneman, W. A., Docherty, K. S., Jaoui, M., Pye, H. O. T., Hu, W., Day, D. A., Campuzano-Jost, P., Jimenez, J. L., Guo, H., Weber, R. J., de Gouw, J., Koss, A. R., Edgerton, E. S., Brune, W., Mohr, C., Lopez-Hilfiker, F. D., Lutz, A., Kreisberg, N. M., Spielman, S. R., Hering, S. V., Wilson, K. R., Thornton, J. A., and Goldstein, A. H.: Monoterpenes are the largest source of summertime organic aerosol in the southeastern United States, *P. Natl. Acad. Sci. USA*, 115, 2038-2043, 10.1073/pnas.1717513115, 2018.
- 25 Zhang, Q., Worsnop, D. R., Canagaratna, M. R., and Jimenez, J. L.: Hydrocarbon-like and oxygenated organic aerosols in Pittsburgh: insights into sources and processes of organic aerosols, *Atmos. Chem. Phys.*, 5, 3289-3311, 2005.
- Zhang, Q., Jimenez, J., Canagaratna, M., Ulbrich, I., Ng, N., Worsnop, D., and Sun, Y.: Understanding atmospheric organic aerosols via factor analysis of aerosol mass spectrometry: a review, *Anal. Bioanal. Chem.*, 401, 3045-3067, 10.1007/s00216-011-5355-y, 2011.
- 30 Zhang, X., Lambe, A. T., Upshur, M. A., Brooks, W. A., Gray Be, A., Thomson, R. J., Geiger, F. M., Surratt, J. D., Zhang, Z., Gold, A., Graf, S., Cubison, M. J., Groessl, M., Jayne, J. T., Worsnop, D. R., and Canagaratna, M. R.: Highly oxygenated multifunctional compounds in alpha-pinene secondary organic aerosol, *Environ. Sci. Technol.*, 51, 5932-5940, 10.1021/acs.est.6b06588, 2017a.

Zhang, Y., Tang, L., Sun, Y., Favez, O., Canonaco, F., Albinet, A., Couvidat, F., Liu, D., Jayne, J. T., Wang, Z., Croteau, P. L., Canagaratna, M. R., Zhou, H.-c., Prévôt, A. S. H., and Worsnop, D. R.: Limited formation of isoprene epoxydiols-derived secondary organic aerosol under NO_x-rich environments in Eastern China, *Geophys. Res. Lett.*, 10.1002/2016gl072368, 2017b.

Figures



5 Fig. 1. Factor profiles for the 7-factor AMS PMF solution. HOA_{AMS} is constrained by a -value 0.1. The total signal of each factor is normalized to unity. (HOA_{AMS} : Hydrocarbon OA, COA_{AMS} : Cooking-related OA, BBOA_{AMS} : Biomass burning OA, OOA_{AMS} : Oxygenated OA, NOA_{AMS} : Nitrogen containing OA, $\text{EVENT}_{\text{AMS}}$, an isolated local event)

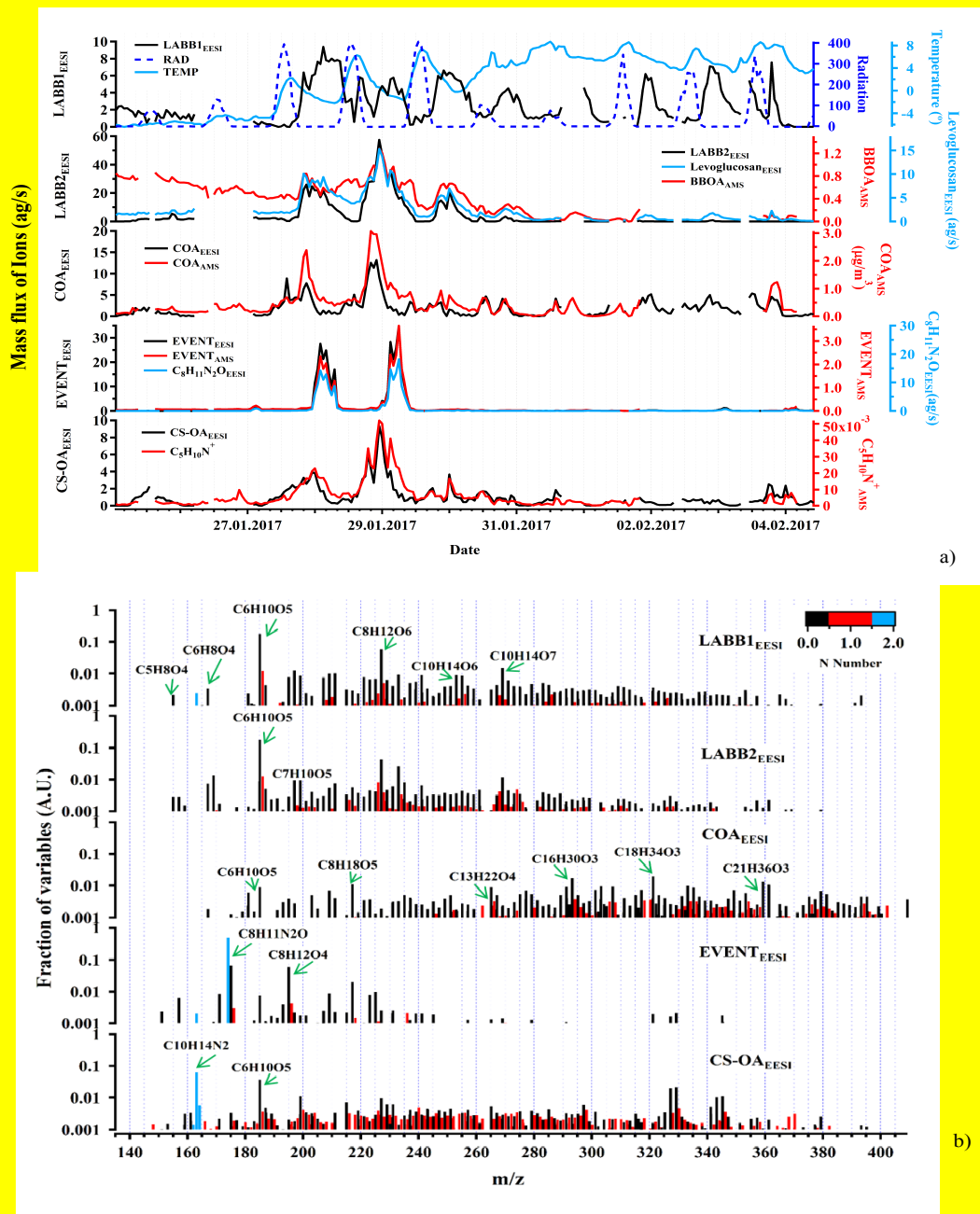
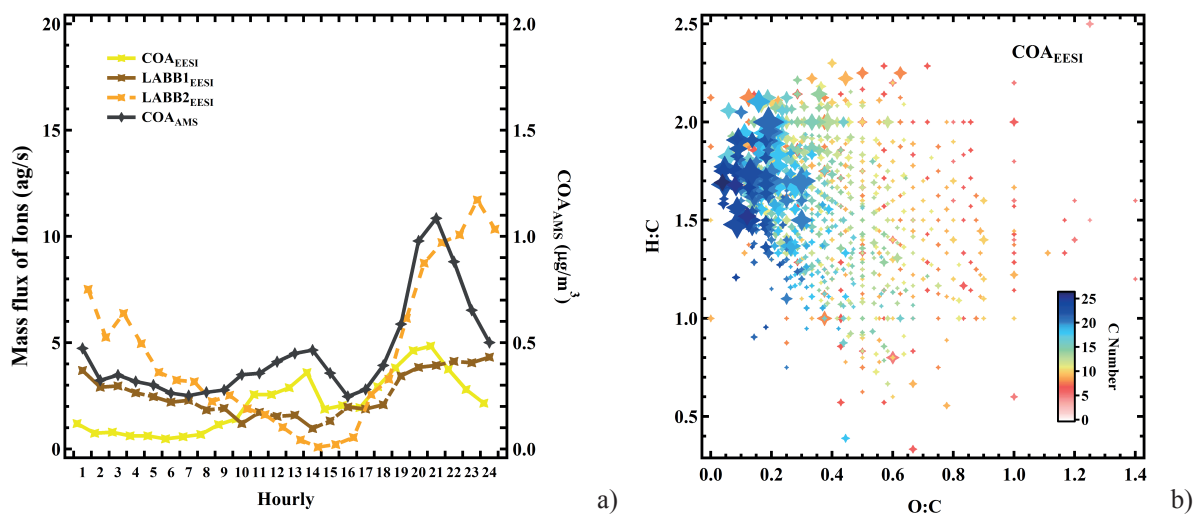
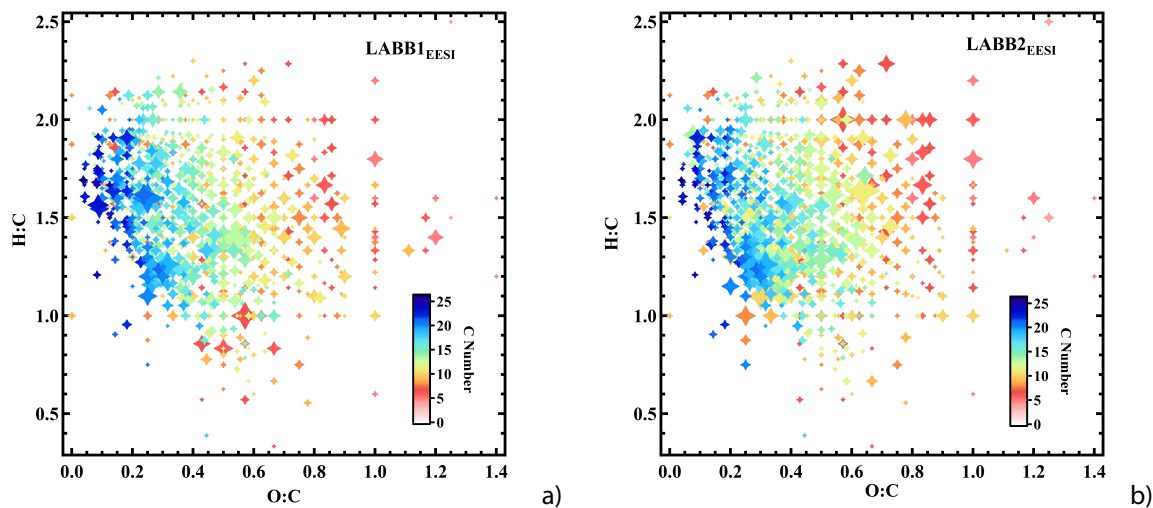


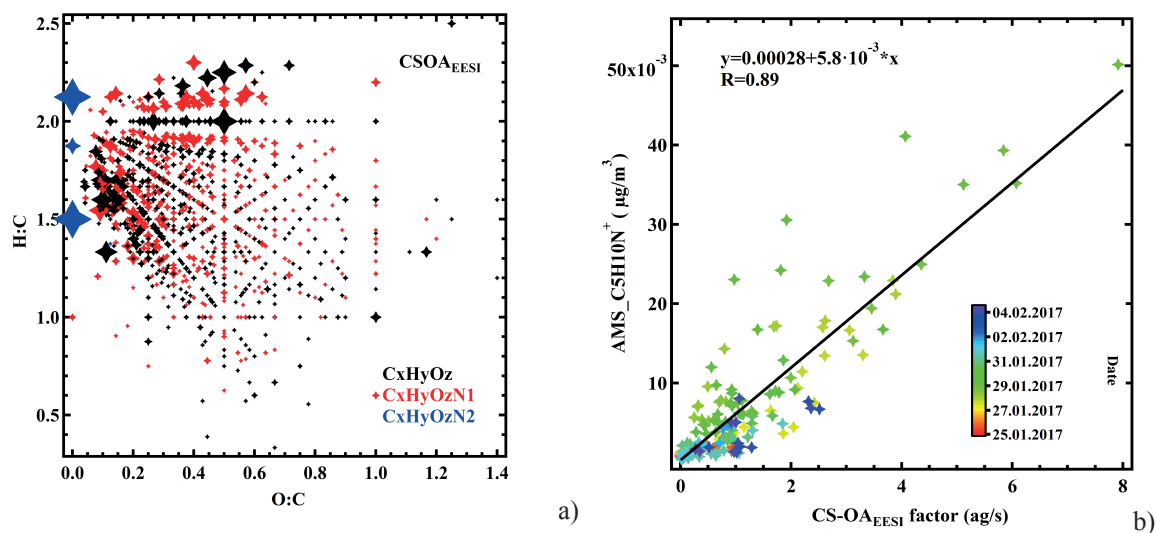
Fig. 2. Time series of the POA factors retrieved from EESI-TOF PMF analysis, along with ancillary data (a), and corresponding factor profiles (b). For all y-axes, EESI-TOF data are shown in mass flux (ag/s), AMS data are shown in $\mu\text{g m}^{-3}$, and other units are given. Factor profiles are molecular weighted and are normalized such that the sum of each profile is 1.



5 Fig. 3. a) Diurnal cycles of the EESI-TOF less aged biomass burning and cooking factors, together with AMS cooking. b) Van Krevelen plot (atomic H:C vs. O:C of each ion) for the COA_{EESI} factor mass spectrum, with points sized by the fraction of each ion apportioned to COA_{EESI} and colored by number of carbon atoms.



10 Fig. 4. a), b) Van Krevelen plot (atomic H:C vs. O:C ratio) of the LABB1_{EESI} and LABB2_{EESI} factor mass spectra. Points are sized by the fraction of each ion apportioned to LABB1_{EESI} and LABB2_{EESI} and colored by number of carbon atoms.



5 Fig. 5. a) Van Krevelen plot (atomic H:C vs. O:C ratio) of the cigarette smoking (CS-OA_{EESI}) factor mass spectrum. Points are sized by the fraction of each ion apportioned to CS-OA_{EESI}. Colors denote C_xH_yO_z, C_xH_yN₁O_z, and C_xH_yN₂O_z groups. b) Comparison of CS-OA_{EESI} and C5H10N⁺_{AMS}, colored by time.

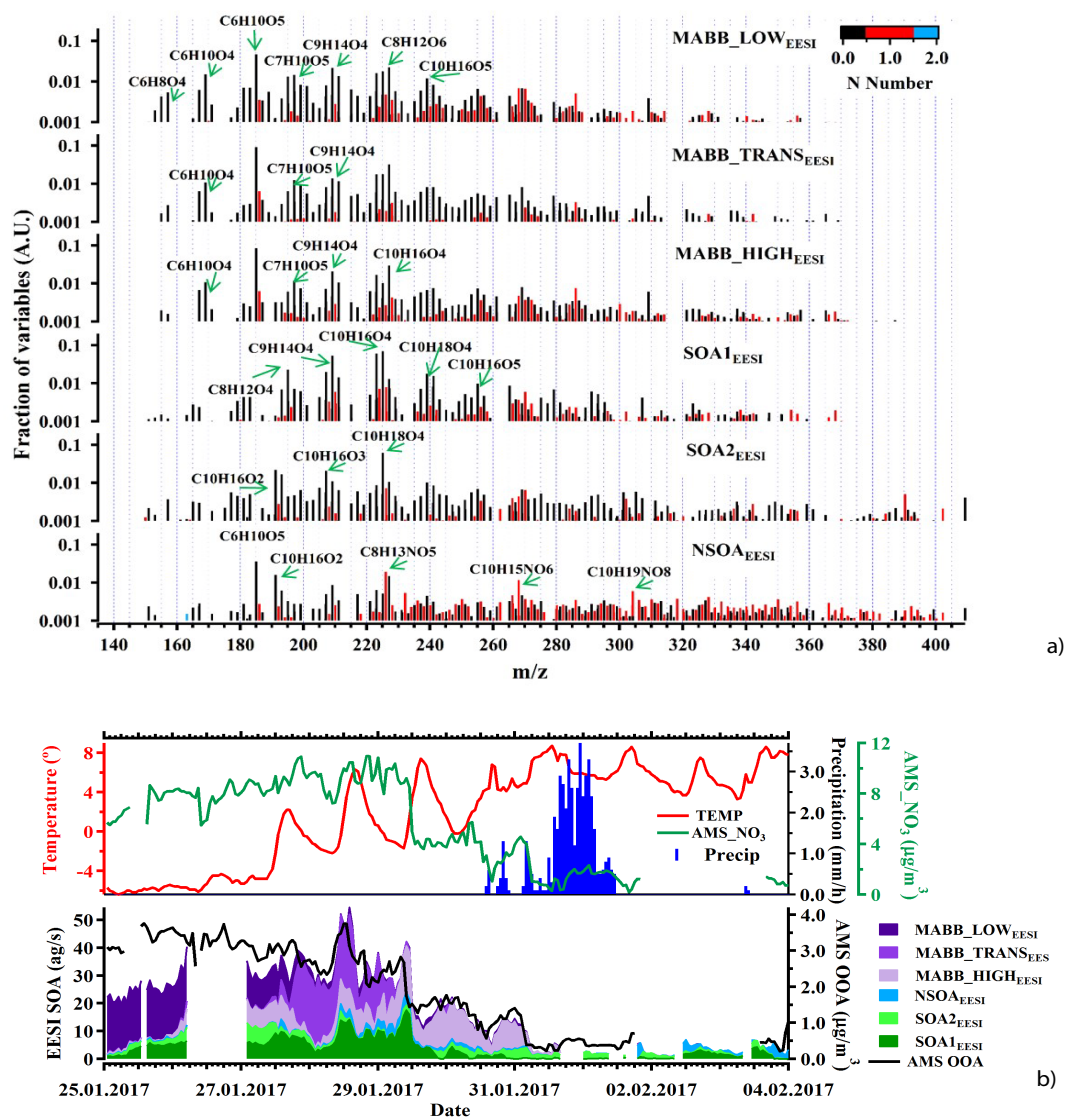
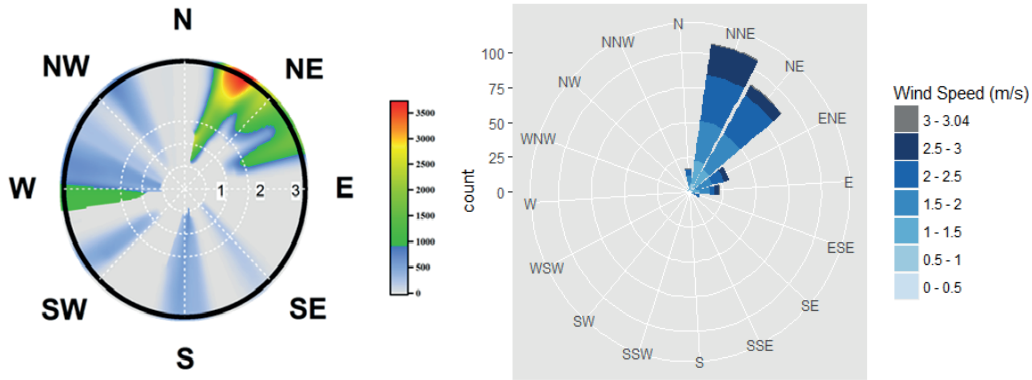
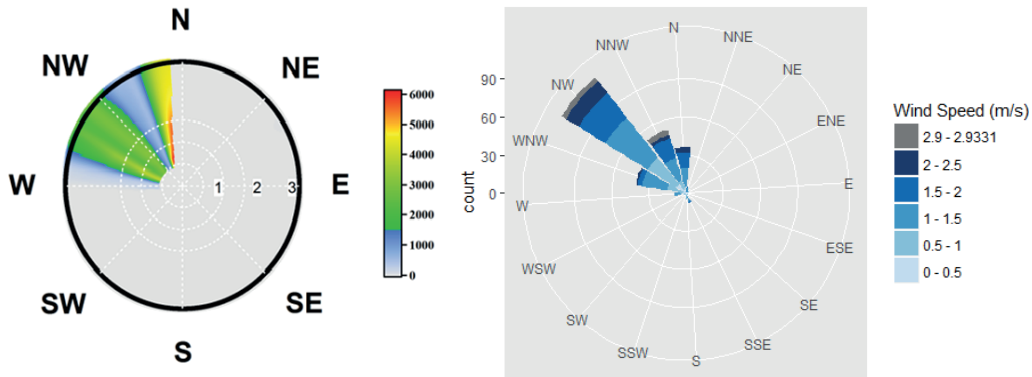


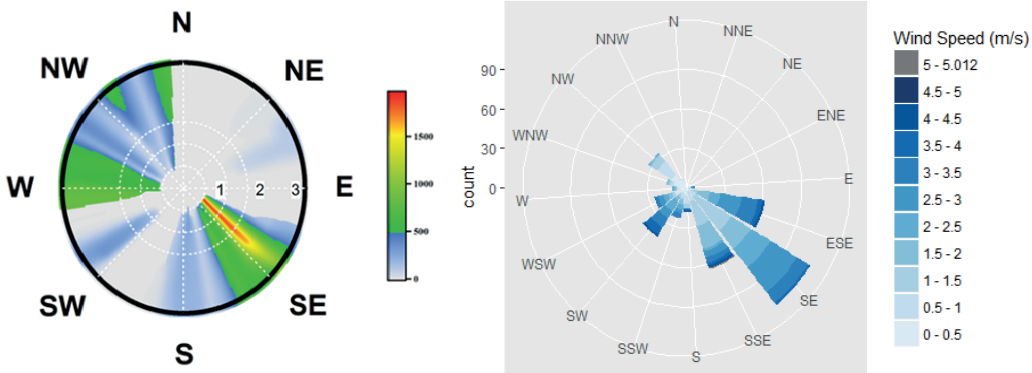
Fig. 6. Factor profiles (a) and stacked time series (b) of the 6 EESI-TOF SOA PMF factors, together with AMS OOA. The latter panel also shows meteorological data. All EESI-TOF data are plotted in mass flux (ag/s), AMS in $\mu\text{g m}^{-3}$, other units are included. Factor profiles (b) are molecular weighted and are normalized such that the sum of each profile is 1.



MABB_LOW_{EESI}

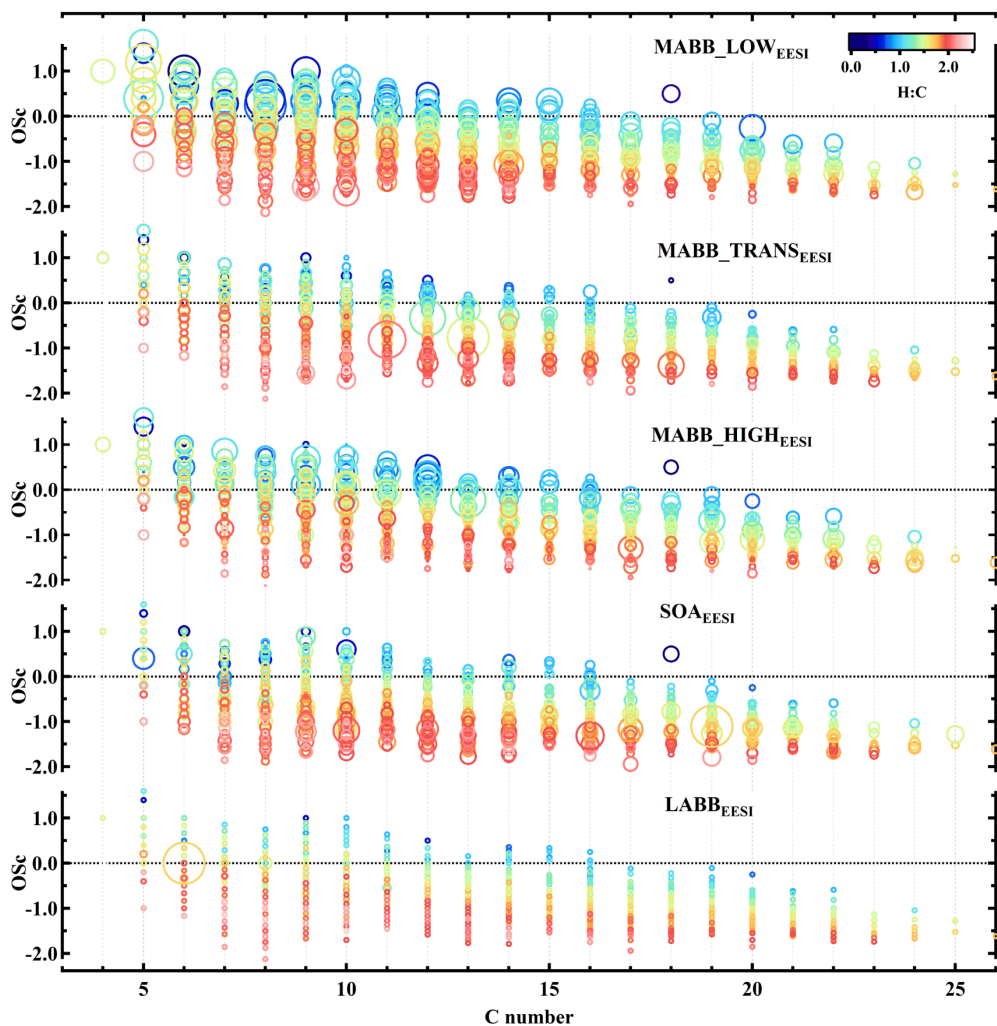


MABB_TRANS_{EESI}



MABB_HIGH_{EESI}

Fig. 7. Wind analysis results using the SWIM model on the concentrations of MABB_LOW_{EESI}, MABB_TRANS_{EESI}, MABB_HIGH_{EESI}. Left: wind direction combined with frequency, wind speed in m/s. Right: the wind speed and wind direction.



5 Fig. 8. Carbon oxidation state (Osc) as a function of number of carbons atoms for the factors, More Aged Biomass Burning_Low temperature, More Aged Biomass Burning_Transition, More Aged Biomass Burning_High temperature, Secondary organic aerosol, Less Aged Biomass Burning. Points are colored by atomic H:C ratio and sized by the fraction of each ion apportioned to the designated factor.

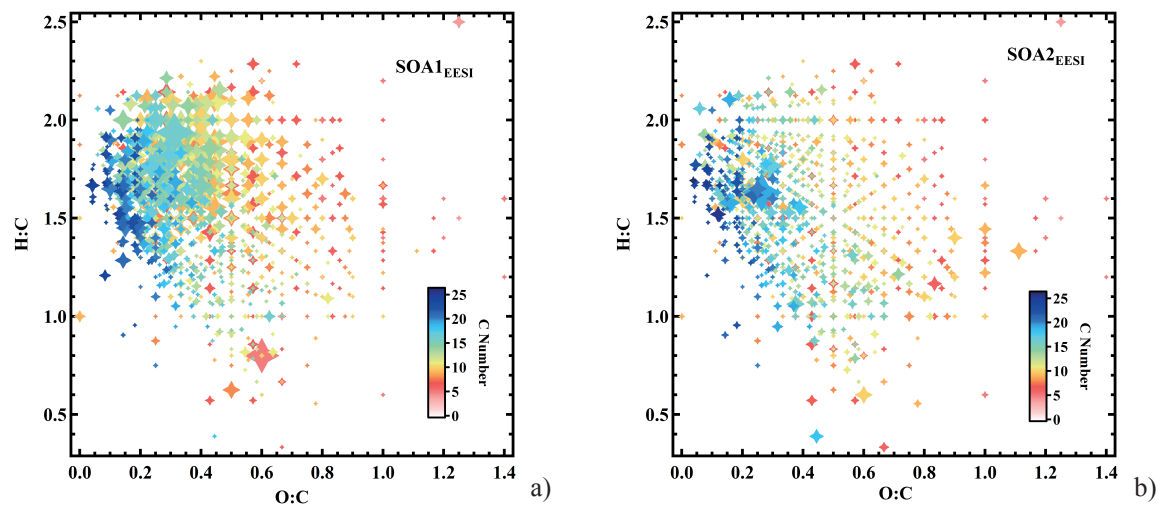
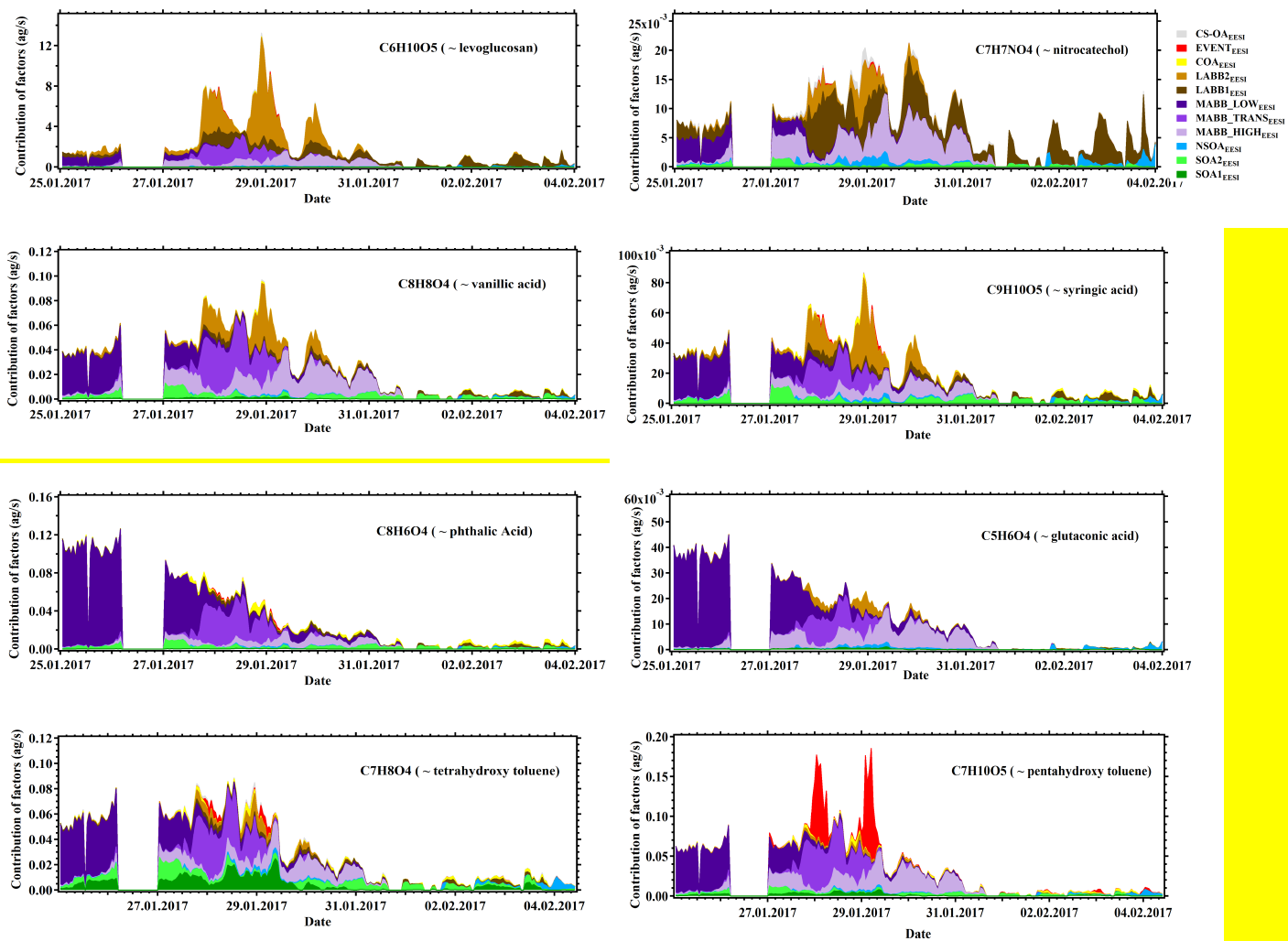


Fig. 9 Van Krevelen plots (atomic H:C vs. O:C) for the SOA1_{EESI} and SOA2_{EESI} factor mass spectra. The points are sized by the fraction of each ion apportioned to SOA1_{EESI} and SOA2_{EESI} and colored by the number of carbon atoms.



a)

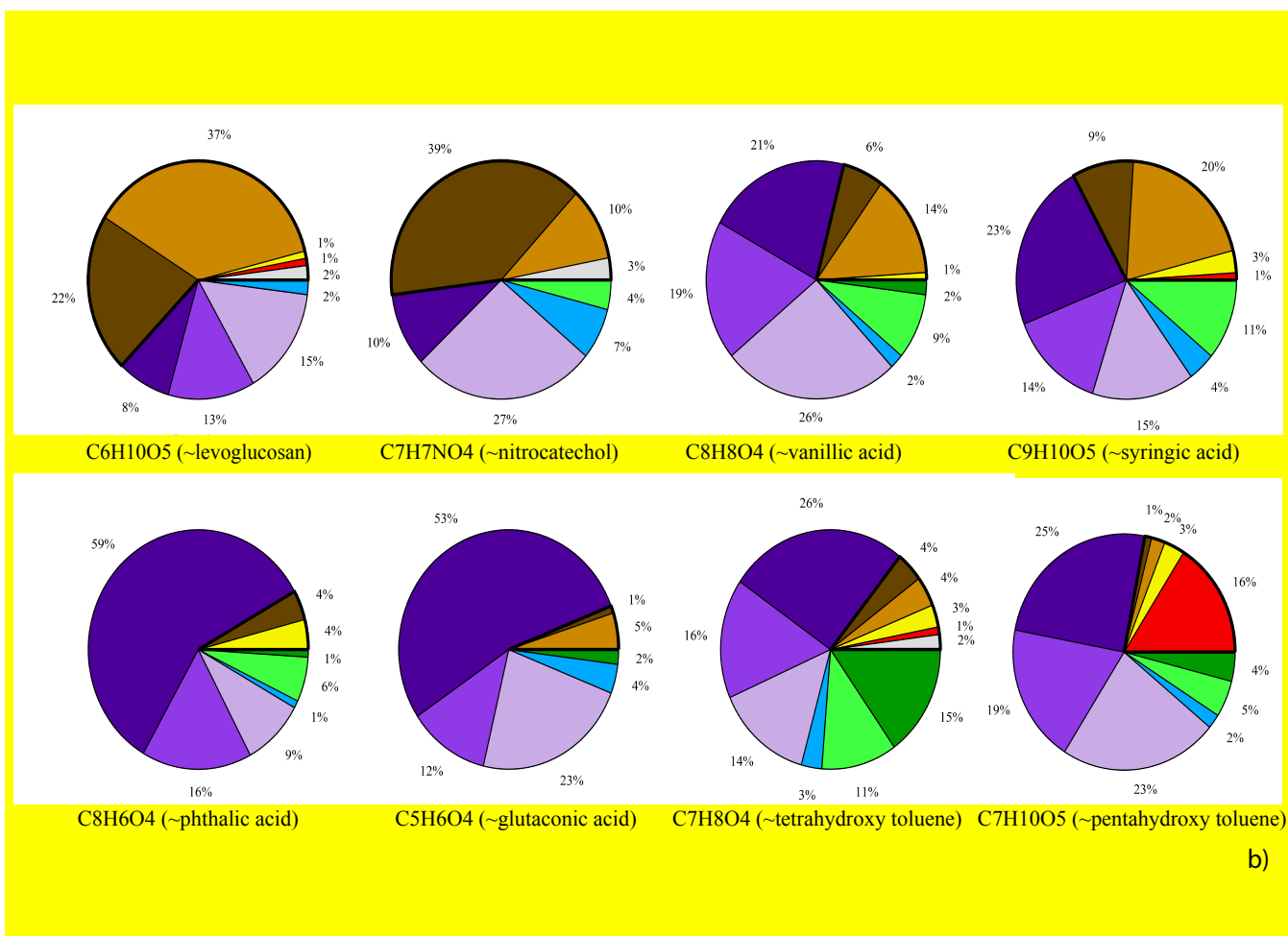


Fig. 10. Apportionment of selected ions by EESI-TOF PMF. (a) Time series of the mass flux (ag s^{-1}) and (b) mean fraction apportioned to each factor. Each ion is associated with a compound of interest having this molecular formula, however, the relative isomeric abundance of this compound cannot be confirmed by the EESI-TOF.

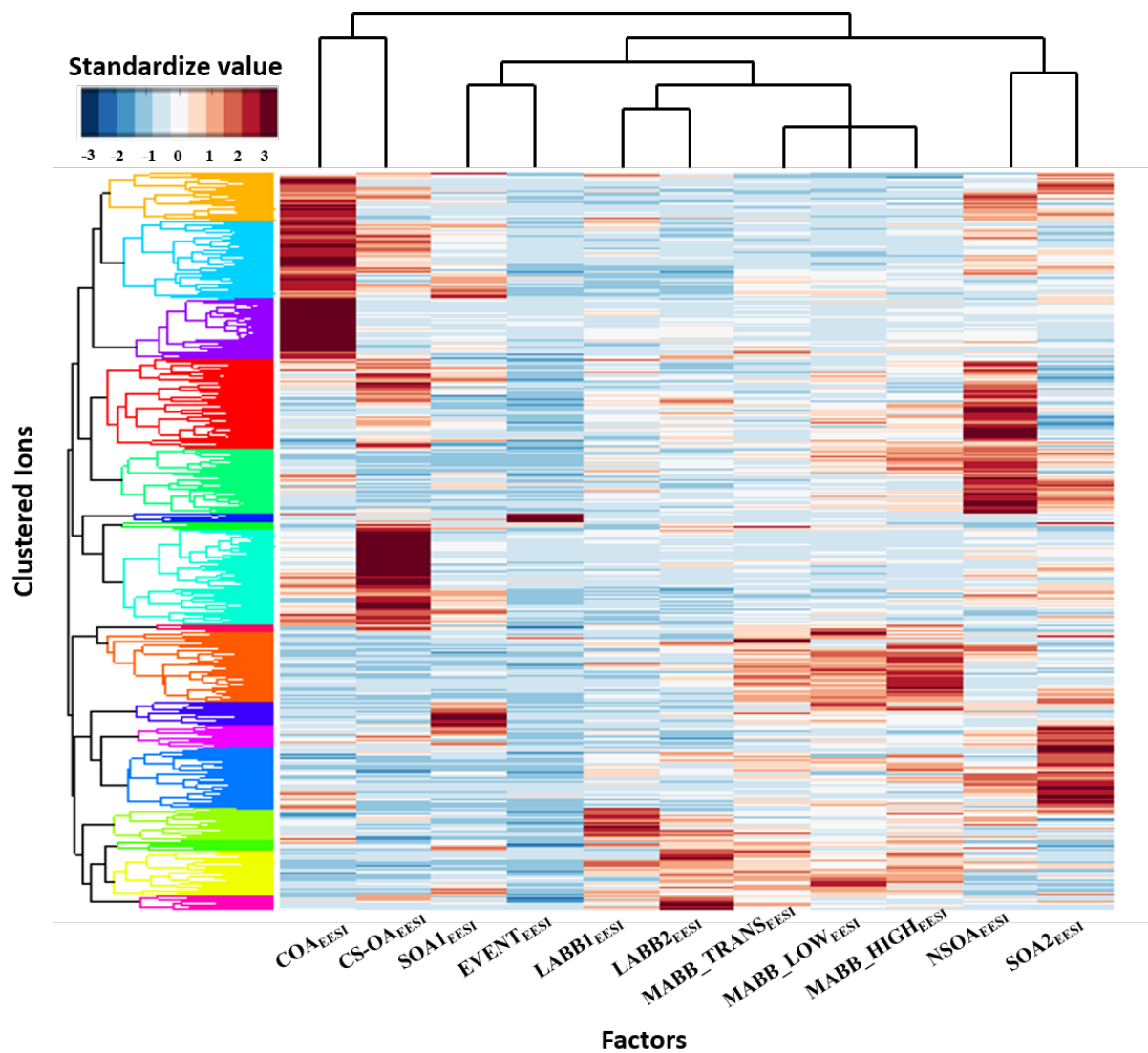


Fig. 11. Standardize matrix of individual EESI-TOF ions vs. EESI-TOF PMF factors. Ions and factors are sorted according to the results of their respective hierarchical clustering analysis; the resulting dendrograms are shown on the respective axes. The color of the compounds' groups in the dendrogram are chosen to make groupings convenient to read (color is random).

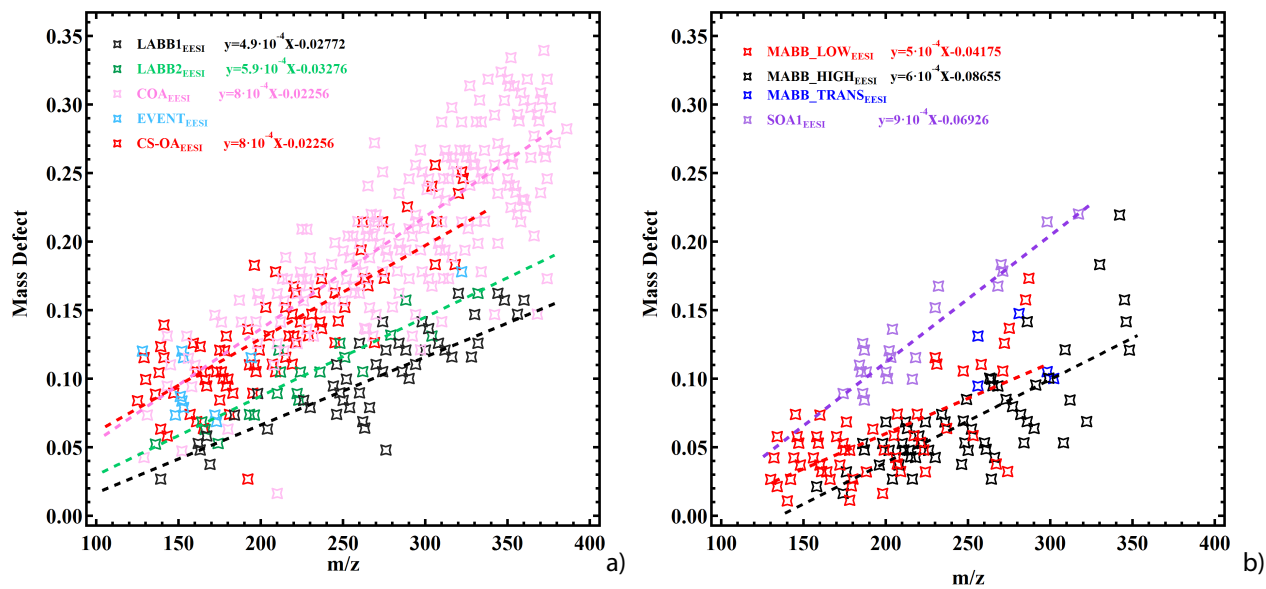


Fig. 12. Mass defect filtering plot of factor-specific ions (identified from the cluster analysis) for selected EESI-TOF POA (a) and SOA (b) factors.

5

10

15

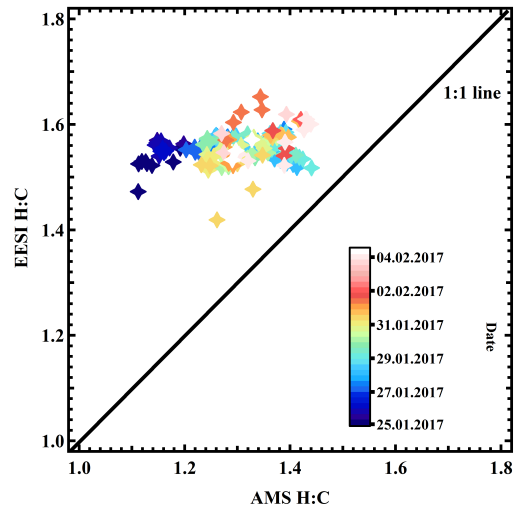
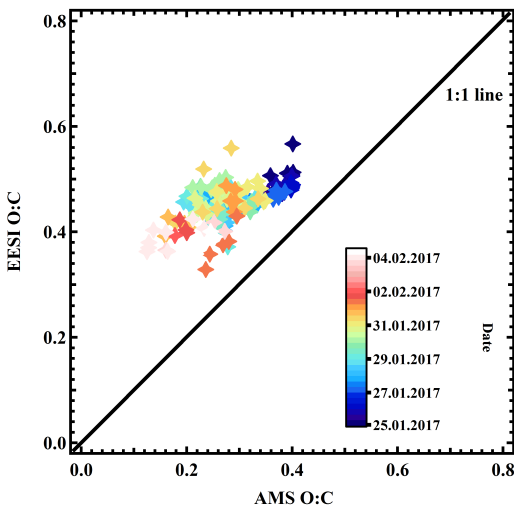
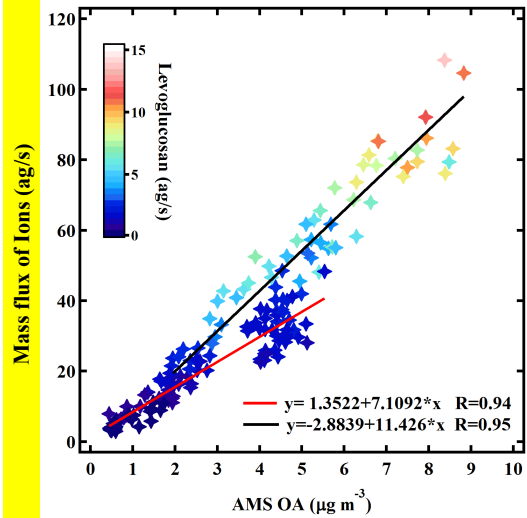
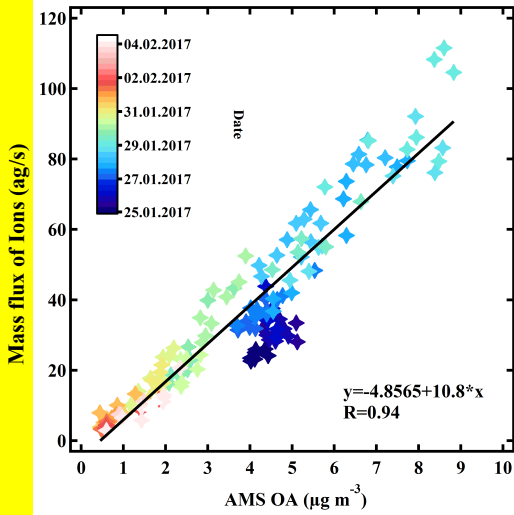
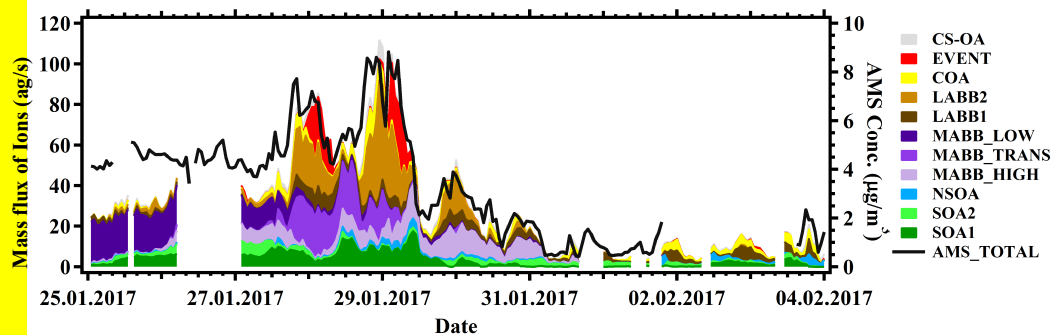
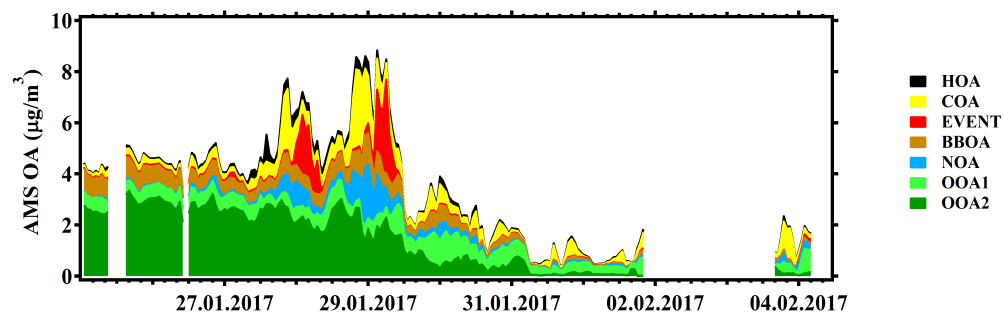


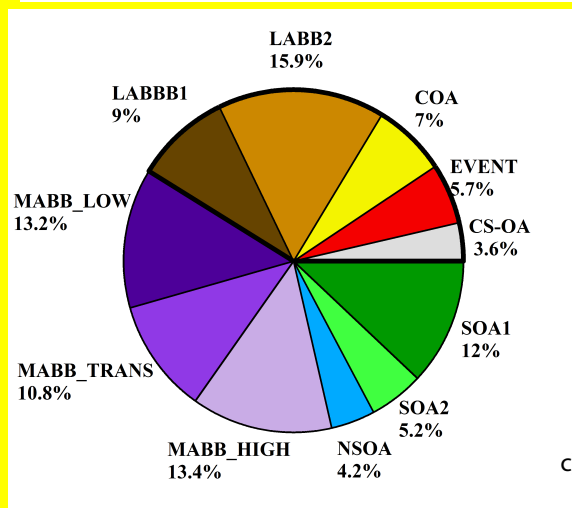
Fig. 13. Comparison of EESI-TOF and AMS. Total EESI-TOF mass flux (ag/s) as a function of AMS OA, points are colored by date (a) and the fraction of levoglucosan (b). The EESI-TOF and AMS comparison in terms of H:C (c) and O:C (d), points are colored by date.



a)



b)



c)

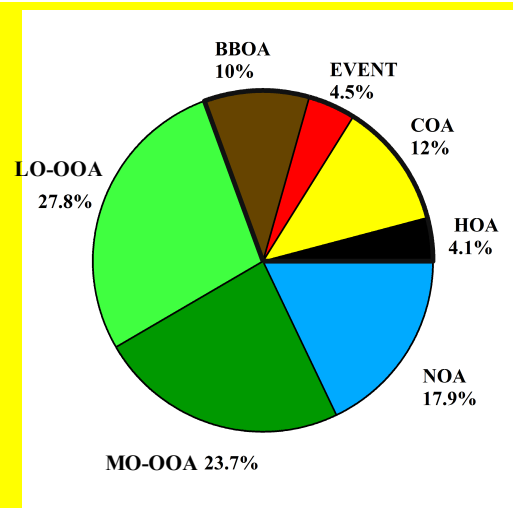


Fig. 14. Comparison between EESI factors and AMS factors: time series of the mass flux of each EESI PMF factors (a) and time series of concentrations of each AMS PMF factors (b). Pie charts of source apportionment results from the EESI (left) and AMS (right) (c). The thick block frame denotes the sum of the primary OA for both data sets.

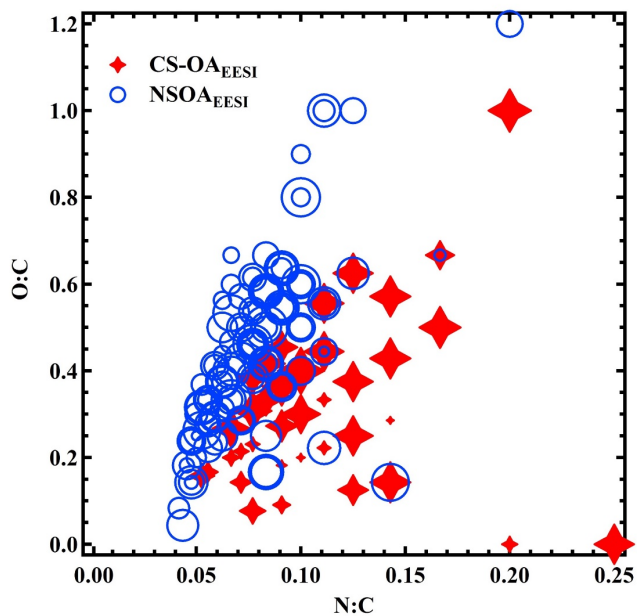


Fig. 15. The atomic O:C vs. N:C plot of the CS-OA_{EESI} and NSOA_{EESI} factors mass spectra. Points are sized by H:C value of each distinguished ion of the CS-OA_{EESI} and NSOA_{EESI}.

Response to the comments of anonymous referee #1

We thank the referee for the valuable comments which have greatly helped us improve the manuscript. Please find below our responses (in black) after the referee comments (in blue). The changes in the revised manuscript are written in *italic*.

General comments

The measurement campaign was very short (January 25 – February 5), so the authors should add a short discussion on the significance and representativeness of their results.

We agree with the comment that the period of the measurement campaign is short. However, the Zurich-Kaserne site has been extensively characterized in previous studies using AMS and ACSM. The general similarity of the AMS results obtained in the current study to previous publications gives us high confidence that the results obtained here are typical of wintertime conditions at the site (with the exception of the special events clearly separated by the $EVENT_{EESI}$ and $EVENT_{AMS}$ factors).

We add a short note in section 2.1 (P4, L27-31), “*Although the measurement period is relatively short (12 days), the similarity of the AMS results obtained in the current study to previous AMS and ACSM measurements at the same site (Lanz et al., 2007, Canonaco et al., 2013, Richard et al., 2011, Daellenbach et al., 2016) give us high confidence that the sampled aerosol is representative of typical wintertime conditions. Exceptions to this are resolved by the source apportionment into unique event-driven factors, as discussed in the results section.*”

Also a short note should be added on why PMF was done separately for AMS and EESI-TOF data, and if the authors expect results to differ for a combined approach (if possible at all).

A combined AMS/EESI-TOF PMF analysis is potentially of high interest and may facilitate quantitative interpretation of EESI-TOF data. However, such combined analyses are highly complex, requiring careful balancing of the explained variability within the two component datasets (Slowik et al., 2010; Crippa et al., 2013). In addition, such combined analyses tend to decrease the ability of the component datasets to retrieve factors resolvable by only a single instrument (such as HOA_{AMS} , or factors driven by chemical signatures observable only by the EESI-TOF). As a result, we focus here on exploring the ability of the novel EESI-TOF measurements to improve factor separation and design the source apportionment analysis to maximize this potential.

As requested, we address this in the manuscript (section 2.3) (P8, L8-9) as follows:

“Execution of PMF analysis on separated AMS and EESI-TOF datasets minimizes the complexity of the analysis, while maximizing the factor resolution ability of the EESI-TOF.”

Conclusions are a bit meager, and some effort could be taken in better describing the (atmospheric) implications of the results.

The following text has been added to the conclusion (P21, L1-4), “*Comparisons of bulk measurements, as well as of individual factors or groups of factors between the EESI-TOF and AMS indicate good agreement, but with the differences in elemental ratios. This suggests that, despite significant uncertainties in the relative response*

factors of individual ions measured by the EESI-TOF, responses at the level of the PMF factors are relatively similar, with the main differences resulting from the high sensitivity to levoglucosan in the EESI. Furthermore, source apportionment of EESI-TOF provides more classification of SOA factors, separating EESI biomass burning factors as more/ less aged instead of primary / secondary, identifying organic nitrogen containing factors as primary-dominated nitrogen factor / organonitrate-containing secondary factor, which are not possible for AMS PMF.”

A few important references are given as “in prep.” (also see specific comments below) – if these references are not available soon the authors should consider removing them and adding more information to the present manuscript.

We agree with the comment. In this manuscript, we presented four “in prep” references, and we modified as bellow:

1. “Lopez-Hilfiker et al., in prep”, now the paper is public on AMTD, so it is cited as “Lopez-Hilfiker et al., 2019”.
2. “Stefenelli et al. in prep”, the paper is now online in ACPD, so it is cited as “Stefenelli et al., 2019”.
3. “Bertrand et al., in prep”, the paper has been submitted, so here we change it to “submitted”.
4. “Lu et al., in prep”, status is unchanged.

Specific comments

P. 5, l. 9: What is “most”? Since the paper about the instrument is not available yet, this statement has to be made more quantitative/explicit. Which gas phase species are removed, based on what properties? The denuder only “reduces the gas phase background” – so what is left?

The referenced paper is now available from Atmospheric Measurement Techniques (<http://doi.org/10.5194/amt-2019-4>), and the reference has been updated. As a result, we have not otherwise modified the current paper but summarize here for reference.

The denuder has not been fully characterized on a compound-by-compound basis, but removes most gas-phase organics with high efficiency (e.g. pinonic acid, 99.6%).

Otherwise, the main source of background (i.e. non-particle-derived) signal is the working solution. This includes a variety of ions related to the NaI dopant and its clusters with acetonitrile and/or water. However, impurities in the working solution also generate detectable background signal. Finally, particles can pass through the denuder but then deposit on a surface rather than be extracted in the spray. Semi-volatile material desorbing from such deposited particles constitutes an additional source of background.

P. 5, l. 12: This might be discussed in the instrument paper, however, as this is not available, a short discussion should be included here: Are artefacts due to extraction to be expected, depending on solvent?

As noted in the previous comment, the instrument paper is now available and this issue is discussed in detail there. Briefly, the principal artifacts deriving from the use of the water, acetonitrile solvent are the potential for clusters of analyte ions with acetonitrile. These are weakly-bound clusters, and their prevalence depends strongly on voltage settings (i.e. collision energy) in the ion transfer optics. Formation of these clusters was found to be negligible at the settings used in the current study. We have clarified this as follows (P5, L25-26):

“Depending on voltage settings in the ion transfer optics (i.e. collision energy), clusters with acetonitrile can potentially be detected, however these clusters were observed to be negligible during the current study.”

P. 5, l. 15: This implies heating afterwards. Please clarify.

This is discussed in detail in the instrument paper and clarified in the manuscript as follows (P5, L20-22):

“The droplets then enter the mass spectrometer through a capillary heated to 250 C, however, the very short residence time in this capillary means that the effective temperature experienced by the analyte is much lower and no thermal decomposition is observed.”

P. 5, l. 26 – 32: Have the authors tried to relate the mass flux to ambient concentrations? Please discuss this. Do the authors expect a simple calibration with levoglucosan to be able to cover “instrument flow rate, EESI extraction/ionization efficiency, declustering probability, and ion transmission”?

The reviewer raises two issues here: (1) assessment of the EESI-TOF mass flux in terms of reference measurements, and (2) utility of the levoglucosan calibration. These points are discussed separately below.

The comparison of EESI-TOF mass flux and ambient OA concentrations is the subject of section 3.5 and Fig. 13. Fig. 13a presents the correlation 0.94 between the EESI-TOF mass flux and ambient concentrations. Figures 13c and 13d respectively show the O:C and H:C atomic ratios for the EESI-TOF as a function of those for the AMS. The EESI-TOF and AMS O:C ratios are correlated ($R=0.62$), however, the O:C ratios estimated by the EESI-TOF are systematically higher than those measured by the AMS. For H:C ratios, we do not observe a correlation. The EESI-TOF values are scattered around approximately 1.56, independent of the AMS H:C ratios which vary between 1.11 and 1.44. The cause for this discrepancy is not yet understood but may be related to differences in ion relative sensitivity.

As this is already a major section of the manuscript, we assume that the reviewer’s question was triggered by the sequence of discussion in the original manuscript rather than a general inadequacy in section 3.5. As a result, we have added the following statement to the initial discussion of EESI-TOF mass flux identified by the reviewer:

“A comparison of the EESI-TOF mass flux to the AMS signal in terms of total signal or mass, bulk properties, and source apportionment results in section 3.5.”

Regarding the second point, here it is important to distinguish between factors affecting the EESI-TOF sensitivity that are ion-dependent, and those which act uniformly across all ions. We use the levoglucosan calibration only to assess the stability of the instrument with respect to the second category (e.g. flow rate, effects of geometric overlap between aerosol and spray droplets on extraction efficiency, effective primary ion concentrations). Ion-specific considerations (extraction/ionization efficiency and ion transmission) cannot be characterized through this simple calibration. However, these are expected to be fundamental properties of the detected ions (in combination with specific instrument settings which are unchanged throughout the study (e.g. voltages in the ion optics), and although unknown are thus assumed to remain constant.

The statement on levoglucosan calibration has been revised for clarity as follows (P6, L7-8):

“EESI-TOF stability and linearity with mass were confirmed by periodic measurement of nebulized levoglucosan aerosol with quantification of the mass concentration with an SMPS.”

P. 6, l. 11 -13: Please include (e.g in the supplementary) more details on error calculations (show data periods chosen, values etc.) This can be very useful for readers / future users.

The original error matrix includes mass spectra from both direct ambient sampling and filter blank processed with Tofware. Then filter periods were interpolated to yield an estimated background spectrum during ambient measurements. We describe and add more clear detail in the main text as following (P6, L19-24):

“The corresponding error matrix σ_{ij} , which has the same dimensions as the data matrix, follows the model of Allan et al. (2003), which calculation includes the uncertainty deriving from electronic noise, ion-to-ion variability at the detector and ion counting statistics. The error estimates in this case incorporate the uncertainties related to both the ambient measurements (δ_i) (direct ambient sampling period) and the background (β_{ij}) (filter blank measuring period, both are processed with Tofware), which are combined in quadrature according to Eq. 2:”.

P. 8, l. 1-2: Why were exactly these factors constrained in the AMS PMF? Please clarify. Does that introduction of subjectivity distort your solution?

First, we correct a small mistake in the original manuscript, where it was stated that both traffic and cooking factors were constrained in the AMS PMF analysis whereas in fact only traffic was constrained.

With regards to the proposed introduction of subjectivity, we note that it is well-established that factor constraints select specific solutions (i.e., the selection environmentally reasonable subset) from a large set of solutions of approximately equal mathematical quality. These solutions may not be operationally accessible during analysis in the absence of factor constraints (or other rotational control allowing multidimensional exploration; note that rotation via the global f_{peak} parameter is insufficient). As a result, the solution returned by unconstrained PMF analysis is itself subject to distortion, as its selection by the model from among other solutions of similar quality is effectively arbitrary. Factor constraints address this problem and have been shown to significantly improve PMF model performance by minimizing such arbitrary distortions (Canonaco et al., 2013, Elser et al., 2016).

In the current study, the α -value for HOA was selected according to the correlations between the time series of HOA with the traffic species NO_x (P10, L9-10).

P. 11, l. 16 – 18: How do the diel patterns of the nicotine and COA factors compare? Could it be that they are similar due the influence of restaurant opening times, with people gathering outside the restaurants to smoke?

This is a good point and likely contributes to the necessity for constraining the CS-OA_{EESI} to obtain a clear separation. We have added diurnal plots of the EESI-TOF factors to the supplement (Fig. S6). The following statement has been added to the manuscript (P12, L9-13):

“The difficulty in separating these factors, despite their expected chemical differences, is likely due to strong temporal correlation between cooking and cigarette-smoking emissions due to the proximity of local restaurants (Fig. S6, the diurnal patterns of nicotine and COA_{EESI} factors), where people gather outside to smoke during mealtimes. We therefore attempted to obtain a clean cigarette smoking signature from the dataset to serve as an anchor profile with which to constrain this source.”

P. 12, l. 6-7: As Figure 2b shows, C₈H₁₂O₆ has a very prominent signal in the LABB spectra. The authors speculate that this ion represents hydroperoxides from the oxidation of phenolic compounds by OH radicals during daytime. Biomass burning seems to be mostly going on during evening/night times – how come daytime oxidation of compounds primarily emitted at night would have such a bit signal?

Here, we made a mistake. This was an early interpretation, but forgot to revise in the text. Oxidation typically leads to a large set chemically related compounds because all these reactive pathways branch in complex ways. In contrast, strong isolated peaks (e.g. levoglucosan) are more likely to result from a specific emissions source and/or process (e.g., because cellulose is a polymer, its pyrolysis leads to a relatively small number of discrete major products including levoglucosan). Although we are unsure of the compound(s) comprising C₈H₁₂O₆, it is very likely to be primary and not an oxidation product, since it is observed as an isolated peak with high relative intensity.

The incorrect interpretation is deleted in the text.

P. 12, l. 14-15: Already mention here what this “different” thing is

This statement related to the lack of correlation observed between primary/less aged AMS vs. EESI-TOF wood burning factors at the start of campaign, and has been clarified as follows (P13, L8-11):

“Fig. S8 compares the BBOA_{AMS} factor (Fig. 2a) with LABB1_{EESI}, LABB2_{EESI}, and the sum of LABB1_{EESI} + LABB2_{EESI}, with R 0.59, 0.79, and 0.82, respectively. The correlation is generally good except during the first part of the campaign (25 January to 27 January) which as discussed later relates to the complexity of wood burning classification between the EESI-TOF and AMS.”

P. 12, l. 23 – 25: January 27 – 29 was a weekend, and a quick google search revealed that the Zurich game festival (<http://www.ludicious.ch/ludicious-2017/>) was taking place then, which would mean a lot around Zurich Kaserne, eating, smoking: :Also LABB2 is high then, despite higher temperatures. How do the authors explain this?

Thanks for the significant information. The following statement is added to the manuscript (P14, L3-5):

“The Zurich game festival was taking place at the weekend (the event is apparently held in a building on the SW side of the courtyard), though no human activities in the immediate vicinity of the sampling inlet were evident by inspection of the on-site camera.”

LABB2 is the more event-driven WB and as such is likely not connected to regular (approximately temperature-driven) domestic heating but rather the activities of the large number of people nearby participating in this event. Probably some local wood burning is associated with this.

P. 15, l. 31 – 33: How sure can the authors be that the molecular formulae they measure correspond to the mentioned compounds? Please add a short discussion on this uncertainty.

We agree that this section requires clarification. In particular, the implication that the EESI-TOF identifies specific molecules is misleading, as the instrument can provide only a molecular formula. In some cases, e.g. $C_6H_{10}O_5$, we know that at a minimum several chemically similar isomers are present (i.e., not only levoglucosan but other sugars such as mannosan and galactosan). We have modified both the labels and caption of Fig. 10, as well as the accompanying text, to clarify this point.

Figure labels now highlight the molecular formula, for example: “ $C_6H_{10}O_5$ ” (~ levoglucosan).

The revised Fig. 10 caption is as follows:

“Fig. 10. Apportionment of selected ions by EESI-TOF PMF. (a) Time series of the mass flux ($ag\ s^{-1}$) and (b) mean fraction apportioned to each factor. Each ion is associated with a compound of interest having this molecular formula, however, the relative isomeric abundance of this compound cannot be confirmed by the EESI-TOF.”

Revised discussion (P16, L31):

“Here we investigate the apportionment of eight ions associated with compounds of interest: $C_6H_{10}O_5$ (approximately assigned to levoglucosan), $C_7H_7NO_4$ (methyl-nitrocatechol), $C_9H_{10}O_5$ (syringic acid), $C_8H_8O_4$ (vanillic acid), $C_8H_6O_4$ (phthalic acid), $C_5H_6O_4$ (glutaconic acid), $C_7H_8O_4$ (tetrahydroxy toluene) and $C_7H_{10}O_5$ (pentahydroxy toluene). Note that because the EESI-TOF can provide only a molecular formula, we cannot establish for certain the identity of a compound or assess the relative isomeric abundances. For example, $C_6H_{10}O_5$ is likely to consist not only of levoglucosan, but also other sugars such as mannosan and galactosan. The named compounds are thus provided for reference, but their identification should not be considered as conclusive and the ions cannot be assumed to be isomerically pure. Nevertheless, as these assignments are based on molecular

investigations of wood burning-related emissions they are likely to be qualitatively correct and provide a useful framework for interpreting molecular aspects of the source apportionment results.”

Technical corrections

P. 2, l. 19 – 21: Sentence structure

This sentence was modified in response to a comment by Reviewer #3, and now reads as follows (P2, L18-20):

*“This suggests the EESI-TOF apportionment **in the current study** can be approximately taken at face value, despite ion-by-ion differences in relative sensitivity.”*

P. 3, l. 16: Family?

Done. We change to **GC-family (P3, L16)**.

P. 3, l. 23: It would be beneficial if this paper was available once this manuscript is online

Done. The instrument paper “An Extractive Electrospray Ionization Time-of-Flight Mass Spectrometer (EESI-TOF) for online measurement of atmospheric aerosol particles” now is public on Atmospheric Measurement Techniques Discussions (**AMTD, <http://doi.org/10.5194/amt-2019-45>**).

P. 4, l. 24: I suggest removing this reference unless the paper is available at the time of publication of this one.

We believe there is small typo here, and the reviewer refers to a reference at P.4. l. 14. This paper is now available at ACPD, and the reference has been updated.

P. 6, l. 1: Number fitting?

Done (P6, L9-10). *“**The total number of 1125 fitted ions** (including 882 Na⁺ adducts, one H⁺ adduct, and 242 unknown ions) between m/z 135 and 400 were identified.”*

P. 6, l. 6: Servo and MS? Specify

The revised text reads (P6, L11-14):

*“Data were pre-averaged to 1 min time resolution, and high resolution peak fitting was performed. Individual 1-min spectra were classified as either ambient measurements, background sampling (through the particle filter), **or transitional measurements immediately after switching between ambient/background sampling. Transitional measurements were excluded from further analysis.**”*

P. 7, l. 20: Minimizes

Done (P7, L29). “Equation (3) is solved using a least squares algorithm that iteratively **minimizes** the quantity Q (Eq. 4),...”

P. 17, l. 7: separately?

We have revised the text for clarity (P18, L12-19):

The factor dendrogram identifies several groups of EESI-TOF PMF factors consistent with the interpretations provided above: (1) more aged biomass burning factors (MABB_LOWEESI, MABB_TRANSEESI and MABB_HIGHEESI), (2) less aged biomass burning factors (LABB1EESI and LABB2EESI), and (3) the cooking-related OA and cigarette smoking OA factors. The more aged and less aged biomass burning factor groups are themselves likewise grouped. This clustering is consistent with our interpretation of these factors, as discussed in the previous section. Ions are clustered to different groups using the standardized values. In each factor, there are distinguished molecules (lists of the specific ions (standardized value above 1.5) for each factor is shown in Table S2). The other two resolved groups, one group including SOA1 and EVENT factor, one group containing SOA2 and NSOA factor, apparently don't retrieve the common ions, which make less sense for the current study.”

Fig. 2, 6: Add arrows/lines to clarify the corresponding stick labels

Done. The arrows are added to the figures.

Fig. 10: The figure looks squished

Done. The shape of the figure is changed.

Response to the comments of anonymous referee #2

We thank the referee for the valuable comments which have greatly helped us improve the manuscript. Please find below our responses (in black) after the referee comments (in blue). The changes in the revised manuscript are written in *italic*.

Specific comments:

a) In Figure 2a, time delay seems to exist between LABB1 and LABB2 and levoglucosan (C₆H₁₀O₅) for peaks on 28-29 Jan. Also, in Figure 4a, LABB1 has a higher O:C and lower H:C compared to LABB2EESI. These might indicate LABB1 is more oxygenated. It could also originate from a different source from LABB2. How does the wind regression analysis for these factors show?

Concentrations of LABB2 are high only on three days, roughly corresponding to the EVENT_{EESI} factor that we now associate with a local festival (the Zurich game festival, the event is held in a building on the SW side of the courtyard in which the instrument is deployed). As a result, the reviewer's suggestion of a different source is likely correct. This is further supported by wind regression analysis of these two factors, shown below and added to the supplement as Fig. S7. LABB1 does not correspond to a specific wind direction, consistent with local, widespread domestic wood combustion. In contrast, LABB2 originates predominantly from a single wind direction while the smaller source to the SE is on the third day.

The sentences are added to the manuscript (P13, L5-11): “*The wind regression analysis of these two factors are shown in Fig. S7. LABB1_{EESI} does not correspond to a specific wind direction, in contrast, LABB2_{EESI} originates predominantly from a single wind direction, excluding the smaller source to the SE on the third day.*”

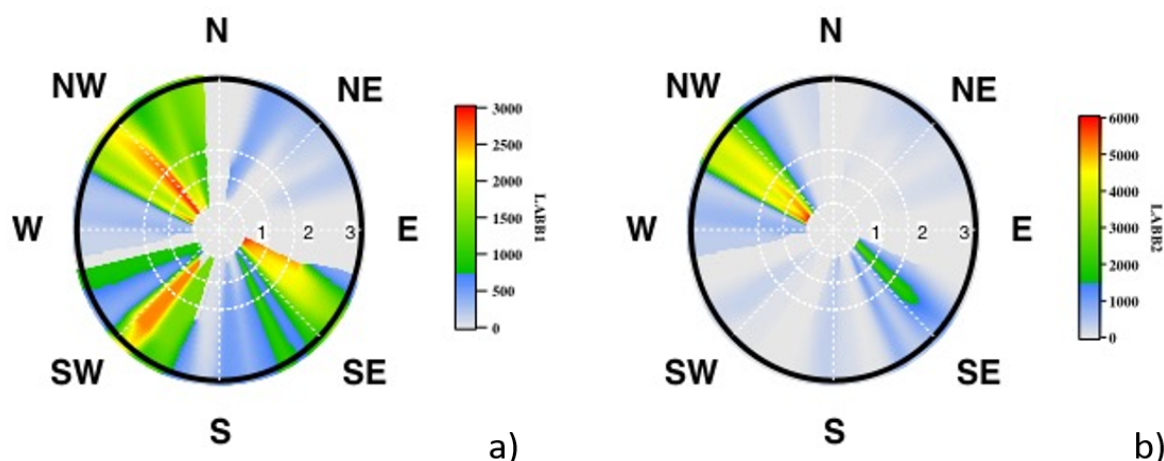


Fig. S7. Wind analysis results using the SWIM model on the concentrations of LABB1 (a) and LABB2 (b).

b) In the discussion of SOA factors (Pg. 15 Lns. 12-15), instead of a time series plot (Figure 6b), a diurnal plot will better show the daytime cycle of SOA₂. Also, I am not sure what is the evidence of that both factors (SOA₁ and SOA₂) are associated with SOA as opposed to the OOA-AMS factors. If it is due to similarities of the SOA

factors mass spectra to the monoterpene-related factors (Pg. 15 Lns. 5-6), I think it is more convincing to compare (plot correlation) of the mass spectra.

This is a good point, we added diurnal plots of the EESI-TOF factors to the supplement (Fig. S6), shown below. We have also added a comparison of the SOAEESI mass spectra with the monoterpene-related SOA factor from the Zurich summer campaign as Fig. S9.

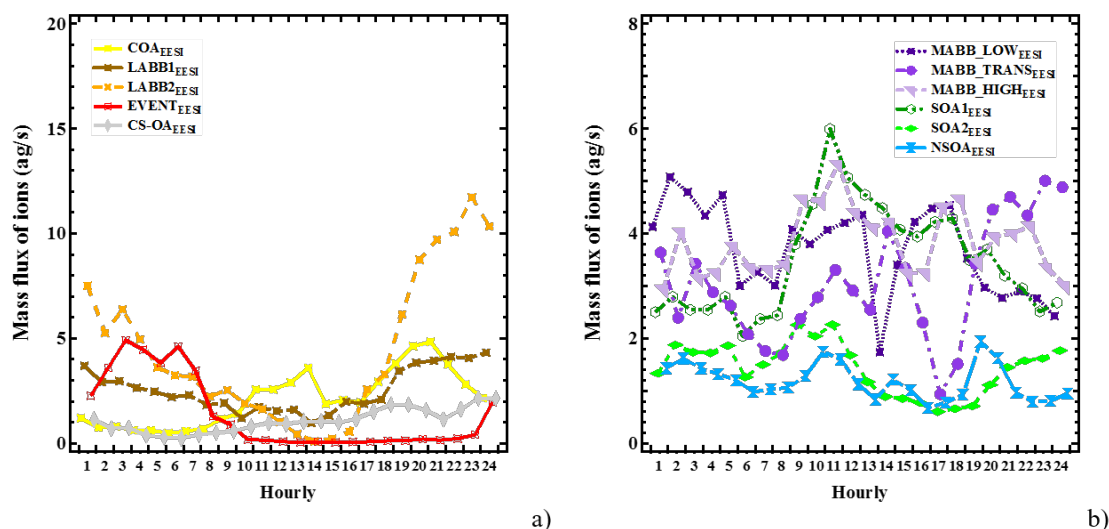
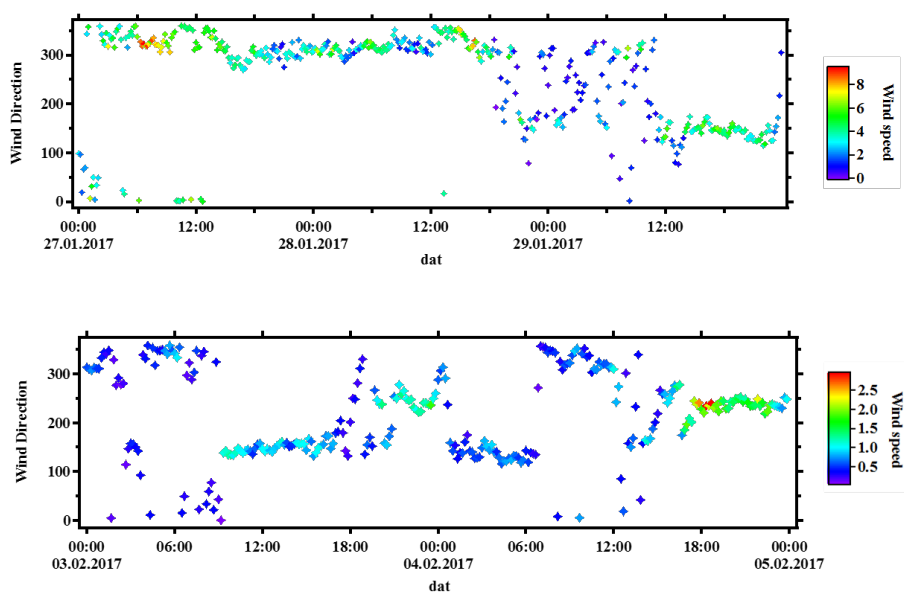


Fig. S6. The diurnal variation of EESI POA factors (a) and EESI SOA factors (b).

c) For the nitrogen-containing SOA factor, could the variability in time between the high peak at the night of 3-4 Feb and the small peak at the night of 28-29 Jan associated by a change in temperature, or was it caused by shifting of air masses? What the wind analysis or back-trajectory analysis suggest?

Yes, we agree with the comment, it is possible that the two nitrogen peaks are associated by a change in temperature. The temperature on 3-4 Feb was much higher than 28-29 Jan, but it was enhanced from 1 Feb. We assume the unique time series may also indicate other chemistry or emission process of the nitrogen-containing compounds, which we also plan to further study.

We plot the time series of wind speed and wind direction on 3-4 Feb and 27-29 Jan, shown below. The wind direction during these days are variable, especially on 3-4 Feb, which may not be a clear evidence.



d) The factor dendrogram seems to resolve five groups instead of three (Figure 11); SOA1 and EVENT factors are one group, and SOA2 and NSOA factors are another group. What do these groupings suggest in terms of characteristics? The discussion of factors dendrogram in Pg. 17 Lns. 6-10 could be expanded to include these groups.

We agree with the comment and have clarified the figure description. In the current study, the agglomerative hierarchical clustering is conducted based on the profiles from PMF. The dendrogram is generated with Euclidean distance metric and average linkage, showing relationships between each group and each factor. However, the dendrogram does not directly show which groups are “tight” (i.e. containing closely related factors or elements) and which are loose. With respect to the factors, the original text focused on three of the five groups where the grouping was consistent with factor definitions (implicitly assuming them to be tightly grouped) while not commenting on the other groups (assumed to be more loose).

We add a short illustration in the main text.

The revised text reads (P18, L12-19): *“The factor dendrogram identifies several groups of EESI-TOF PMF factors consistent with the interpretations provided above: (1) more aged biomass burning factors ($MABB_LOW_{EESI}$, $MABB_TRANS_{EESI}$ and $MABB_HIGH_{EESI}$), (2) less aged biomass burning factors ($LABB1_{EESI}$ and $LABB2_{EESI}$), and (3) the cooking-related OA and cigarette smoking OA factors. The more aged and less aged biomass burning factor groups are themselves likewise grouped. This clustering is consistent with our interpretation of these factors, as discussed in the previous section. Ions are clustered to different groups using the standardized values. In each factor, there are distinguished molecules (lists of the specific ions (standardized value above 1.5) for each factor is shown in Table S2). The other two resolved groups, one group including SOA1 and EVENT factor, one group containing SOA2 and NSOA factor, apparently don’t retrieve the common ions, which make less sense for the current study.”*

Technical comments:

a) Pg. 15 Ln. 21: Ratio of N:C of NSOA in Table S1 is 0.04.

Done (P16, L21). The value in **Table S1 (0.04)** is correct, and the value in the main text has been fixed.

b) Pg. 16 Lns. 13-14: Check the percentage contribution of syringic acid and vanillic acid that are apportioned to MABB factors. Based on Figure 10b, they are supposed to be 52% and 66%, respectively.

Done (P17, L19). "..., which in turn are a major component of biomass combustion emissions, and are apportioned primarily to the MABB_{EESI} factors **52 %** for syringic acid and **66 %** for vanillic acid)."

c) Pg. 16 Lns. 23-24: Be consistent with the decimal of percentage. The percentage can be off if the decimal is included.

Done (P17, L29). The main text is changed. "*Tetrahydroxy toluene (C₇H₈O₄) and pentahydroxy toluene (C₇H₈O₅) are apportioned mainly to secondary factors **85 % and 78 %**, respectively).*"

d) Table S2: LAWBI refers to LABB1? Check the acronyms of factors and make them consistent throughout the main text and supporting information.

Done. Yes, it should be **LABB1**. we correct the other names, **LABB2, MABB_LOW, MABB_TRANS, MABB_HIGH, CS-OA**.

Response to the comments of anonymous referee #3

We thank the referee for the valuable comments which have greatly helped us improve the manuscript. Please find below our responses (in black) after the referee comments (in blue). The changes in the revised manuscript are written in *italic*.

Technical comments:

P1, L19: “This suggests the EESI-TOF apportionment can be approximately taken at face value, despite ion-by-ion differences in relative sensitivity.” Perhaps this is too strong of a statement since this environment is under major influence of BB (and little HOA) and not a mix of very different sources as can be common in other environments, especially in the summer.

We have revised this statement to note that it applies specifically to the range of aerosol composition observed in the current study. We agree that similar analyses are required in different environments before a general conclusion can be drawn. However, even in the current study there is significant variation in the chemical composition (e.g., primary vs. secondary biomass burning, as well as SOA factors with terpene-like signatures that comprise nearly 20 % of the EESI-TOF signal).

The revised statement reads as follows (P2, L18-20):

“This suggests that the EESI-TOF source apportionment in the current study can be approximately taken at face value, despite ion-by-ion differences in relative sensitivity.”

P6, L3: why were the ions smaller than 135 amu small? Was tuning changed on purpose to increase transmission of larger ions? Or is there something different in the mass spec design compared to that of a typical CIMS/AMS?

For EESI-TOF, we aim to focus on the molecular compositions. The quads were operated such that the transmission decreases rapidly below approximately m/z 150.

P6, L8: Just out of curiosity, how stable was the background?

In this campaign, the background measurement is in the same level (almost the same value) during the whole measurement period.

P8, L2: why were different factors constrained for AMS and EESI-ToF?

Factors may be constrained to overcome a variety of issues compromising an unconstrained PMF solution, including factors with strong temporal correlation, two or more factors with similar chemical signatures, or factors with chemical features that due to the overall chemical variability within the dataset are not clearly mathematically

resolved. In the first case (temporal correlation), the reviewer is correct that one would expect similar factors to be constrained between AMS and EESI-TOF (with the exception of HOA_{AMS}, which is primarily composed of hydrocarbon species undetectable by the EESI-TOF). However, the remaining two cases depend on the nature of the chemical measurement by the AMS and EESI-TOF, which are fundamentally different. Therefore, the constrained factors are expected to vary between instruments. For example, in the current analysis, we note that the extensive fragmentation in the AMS results in both the long-chain hydrocarbons observed HOA_{AMS} and the fatty acids in COA_{AMS} yielding C_xH_y⁺ fragments, which makes these factors appear chemically similar (and requiring constraints). In contrast, the EESI-TOF directly detects cooking-derived fatty acids, making this factor appear chemically unique (and not requiring constraint). Meanwhile, the increased chemical specificity of the EESI-TOF allows identification of a cigarette-smoke related factor based largely on the distinctive C₁₀H₁₄N₂H⁺ ion, with the separation optimized by factor constraints, whereas the reduced chemical specificity necessitated the incorporation of cigarette smoke into a mixed factor.

We clarify this issue in the manuscript as follows (P8, L10-14):

“Different factors were constrained in the two datasets due to the fundamental differences between the AMS and EESI-TOF measurements. Specifically, the absence of fragmentation in the EESI-TOF allowed clear separation of cooking without the need for constraints, while separation of a cigarette smoke factor was only achieved for the EESI-TOF. In addition, constraining an AMS cigarette smoke factor was attempted but failed.”

P10, L1-2: If OOA1 has some of the C_xH_y fragments, shouldn't that be the more volatile OOA factor?

We agree with this comment.

The OOA1 factor is the less oxygenated factor (LO-OOA), while the current OOA2 factor is more oxygenated OOA (MO-OOA). We had fixed all the corresponding text and figures.

P15, L3: It's surprising that the SOAEESI factor is less oxidized than the oxidized BB factors. At least in the AMS-based PMF factors, the SOA (OOA) factors are quite more oxidized than the BBOA factor. Do the EESI data suggest that AMS OOA factors may contain the aged BB emissions too? Could the authors elaborate on this. After reading the paper, I realize the authors address this in Section 3.5. It will be good to include a sentence in P15 indicating that this surprising result is going to be further examined.

We agree with this suggestion.

Here we add a short sentence to guide readers (P16, L14-15), *“The more detailed comparison between EESI-TOF_SOA factors and AMS_OOA factors will be discussed in Sect. 3.5.”*

P17, L27-28: If the slopes of the mass defect vs. m/z points for both less and more aged BB is similar, how can one trust interpreting the slopes to understand types of functional groups added to the molecules included in the other factors?

We have clarified this discussion. The main point in these mass defect plots is that the BB-related factors (both LABB and MABB) exhibit slopes (and intercepts) that are significantly lower than those of the other investigated factors, suggesting increased aromaticity. Within the BB-related factors, LABB2_{EESI} and MABB_HIGH_{EESI} have similar slopes, which are slightly higher than LABB1_{EESI} and MABB_LOW_{EESI}.

Section 3.4 was revised as follows (P18-19):

“LABB1_{EESI} and LABB2_{EESI} have a lower mass defect and shallower slope than COA_{EESI} and CS-OA_{EESI}, consistent with increased aromaticity. The slopes are $(4.9\pm0.4)\cdot10^{-4}$, $(5.9\pm0.6)\cdot10^{-4}$, $(8\pm0.5)\cdot10^{-4}$ and $(8\pm0.3)\cdot10^{-4}$ for LABB1_{EESI}, LABB2_{EESI}, COA_{EESI} and CS-OA_{EESI}, respectively. The slopes of the two LABB factors as well as those of COA_{EESI} and CS-OA_{EESI} are very similar to each other and have a high possibility to be consistent with CH addition for the former (i.e. $C_{10+x}H_{14+x}O_{4.5}$, theoretical slope $6\cdot10^{-4}$), and CH₂ addition for the latter (i.e. $C_{10+x}H_{20+2x}O_{3.5}$ for COA_{EESI} and $C_{10+y}H_{15+2y}NO_{3.5}$ for CS-OA_{EESI} as nearly every CS-OA-specific ion contains a single N atom, theoretical slope $1.1\cdot10^{-3}$).

The MABB and LABB factors have similar slopes, despite different ion lists. The slopes of two MABB factors ($0.9\cdot10^{-3}$), as shown in Fig. 12b, are consistent with the addition of CHO functionality (theoretical slope = $0.1\cdot10^{-2}$). Due to the high variability of the slopes of the MABB factors, it may also contain the other potential possibility for the added functionalities.”

Section 3.5: I believe this section should be discussed earlier. As I was reading the paper, I kept thinking what if differences in sensitivity of the EESI to different molecules is playing a role in determining the identified factors, so it is reassuring if one reads this section before getting deep into the EESI-based PMF factors. Perhaps the first paragraph of this section that's not discussing the PMF factors yet can be moved to earlier parts of the paper.

We agree with the reviewer that molecule-dependent sensitivity of the EESI-TOF is an important point and that the reader should be aware from the start that an AMS/EESI-TOF comparison is presented. With that said, we prefer to retain the current order of sections because the bulk AMS/EESI-TOF comparisons cannot be well understood without also considering the factor-by-factor comparisons, and the factor comparisons in turn cannot be understood without first presenting the PMF analysis. However, we have added the following text to the beginning of section 3 to clarify the discussion structure (P9, L21-26):

“Results of AMS and EESI-TOF PMF analyses are presented in sections 3.1 and 3.2, respectively. Section 3.3 focuses on the EESI-TOF PMF results are then exploited to assess the apportionment of specific ions related to key marker compounds (section 3.3) and to identify groups of molecules uniquely characteristic of the retrieved factors (section 3.4). However, quantitative interpretation of the EESI-TOF PMF results is complicated by differences in the relative sensitivity of the EESI-TOF to different molecules. Therefore section 3.5 presents a comparison of the EESI-TOF and AMS results in terms of total signal, bulk atomic composition, and relative apportionment to the different factors.”

P18, L7-9: What's the explanation for a lower sensitivity of EESI for the times levoglucosan was low? Based on the AMS factors, the initial period is not dominated by HOA that EESI is blind to.

Laboratory measurements indicate that the EESI-TOF is likely more sensitive to levoglucosan than to typical SOA components (Lopez-Hilfiker et al., 2019). This has been clarified in the text as follows (P19, L16-19):

“An SOA-dominated period with low levoglucosan concentrations (red line) toward the beginning of the campaign exhibits a lower sensitivity than during a period with higher levoglucosan concentrations (black line), which includes the events on 28.01.2017 and 29.01.2017 characteristic of $EVENT_{EESI}$ (Lopez-Hilfiker et al., 2019).”

Editorial comments: Some correlation coefficients were presented as R, some as R2. Please use one consistently.

Done. We change all the R2 to R. R2 is focus on the section 3.2.2, LABB factors.

Quality of some figures was not good when viewed at 100% and the legends/axis labels were blurry.

Done. Fig. 10 and Fig. 12 are changed to the high resolution.

P 1. L15: “: : was derived: : :”

Done. “While the AMS attributed slightly over half the OA mass to SOA but did not identify its source, the EESI-TOF showed that most (> 70 %) of the SOA was derived from biomass burning.” (P2, L15)

P1, L21: consider changing “..utilize a : : :” to “: : :utilization of a : : :”

Done. “The apportionment of specific ions measured by the EESI-TOF (e.g. levoglucosan, nitrocatechol, and selected organic acids), and utilization of a cluster analysis-based approach to identify key marker ions for the EESI-TOF factors are investigated.” (P2, L21)

P2, L14: delete “of” in “: : :fragments typical SOA molecules”.

Done. “The chemical analysis of aerosol online-proton transfer reaction mass spectrometer (CHARON-PTR-MS) has no significant thermal decomposition but the ionization scheme fragments typical SOA molecules.” (P3, L15-16)

P6, L2: change “The total number fitting of 1125 ions : : :” to “The total number of 1125 fitted ions : : :”.

Done. “The total number of 1125 fitted ions (including 882 Na^+ adducts, one H^+ adduct, and 242 unknown ions) between m/z 135 and 400 were identified.” (P6, L9-10)

P6, L9: delete “the” to read “: : :were removed from further analysis.”

Done. “Ions with a mean signal-to-noise ratio (SNR) below 2 were removed from further analysis.” (P6, L17-18)

P6, L19: “An HR-ToF-AMS: : :”

Done. “An HR-TOF-AMS was deployed for online measurements of non-refractory (NR) $PM_{2.5}$.” (P6, L28)

P6, L21: “spent”

Done. “The AMS recorded data with 1 min time resolution, of which 30 s was spent recording the ensemble mass spectrum (mass spectrum (MS) mode) and 30 s recording size-resolved mass spectra.” (P6, L29-31)

P14, L4/5: it should be NOAAMS (not NSOAAMS). Related to this, the discussion on NOAAMS and the EESI-based factor is provided after this sentence, not before.

Done. In the section 3.1, the AMS source apportionment, we suggest this factor is a mixed factor, so here we don't include it into the calculation of AMS OOA contribution. “NOA_{AMS} is excluded from this calculation due to the contribution from primary cigarette smoke discussed above.” (P15, L2-3)

Fig. 6b- unit for precipitation is not included.

Done. The unit for precipitation has been added (mm/h).

P14, L12: “period 1” should be move to “: : :study, period 1, occurs : : :”

Done. “As shown in Fig. 6b, the coldest part of the study, period 1, occurs from 25 to 27 January.” (P15, L9-10)

P15, L25: I believe you mean EESI-CHON fragments correlate better NSOA_EESI. I don't think AMS_CHON fragments are displayed.

Done. “Figure S10 shows a comparison of the NSOA_{EESI} time series and CS-OA_{EESI} time series with the CHON ions from the EESI and CHN ions from the AMS, respectively. The group of EESI_CHON ions shows the same temporal variation as the NSOA_{EESI} factor (Fig. S10) while the AMS_CHN group is more correlated to the primary organic group.” (P16, L24-26)

Fig. 12b. Green color for more aged secondary BB factor is too hard to see against the white background.

Done. We change to the black color.

P18, L10: consider replacing “big events” to some other phrase

Done. “An SOA-dominated period with low levoglucosan concentrations (red line) toward the beginning of the campaign exhibits a lower sensitivity than during a period with higher levoglucosan concentrations (black line), which includes the events on 28.01.2017 and 29.01.2017 characteristic of $EVENT_{EESI}$.” (P19, L16-19)

Fig. 13b: intercept of the black line appears to have two negative signs in front

Done. We delete one negative sign.

P18, L31: change “primarily” to “primary”

Done. “Both AMS and EESI-TOF factors stacked time series (Fig. 14) show clearly that biomass burning is dominated by secondary fractions early in the campaign, mixed fractions in the middle of the campaign, and primary fractions late in the campaign.” (P20, L6)

P18, L34: replace “WB-related” by “BB-related”?

Done. “..., it is hard to define how much of AMS OOA is BB-related as a function of time.” (P20, L9)

Supplement Information

Organic aerosol source apportionment in Zurich using an extractive electrospray ionization time-of-flight mass spectrometer (EESI-TOF): Part II, biomass burning influences in winter

Lu Qi^{1,2}, Mindong Chen², Giulia Stefenelli¹, Veronika Pospisilova¹, Yandong Tong¹, Amelie Bertrand¹, Christoph Hueglin³, Xinlei Ge², Urs Baltensperger¹, André S. H. Prévôt¹, Jay G. Slowik¹

¹Laboratory of Atmospheric Chemistry, Paul Scherrer Institute (PSI), Switzerland

²Nanjing University of Information Science & Technology, Nanjing, China

³EMPA, Dübendorf 8600, Switzerland

Correspondence to: Jay G. Slowik (jay.slowik@psi.ch) and André S. H. Prévôt (andre.prevot@psi.ch)

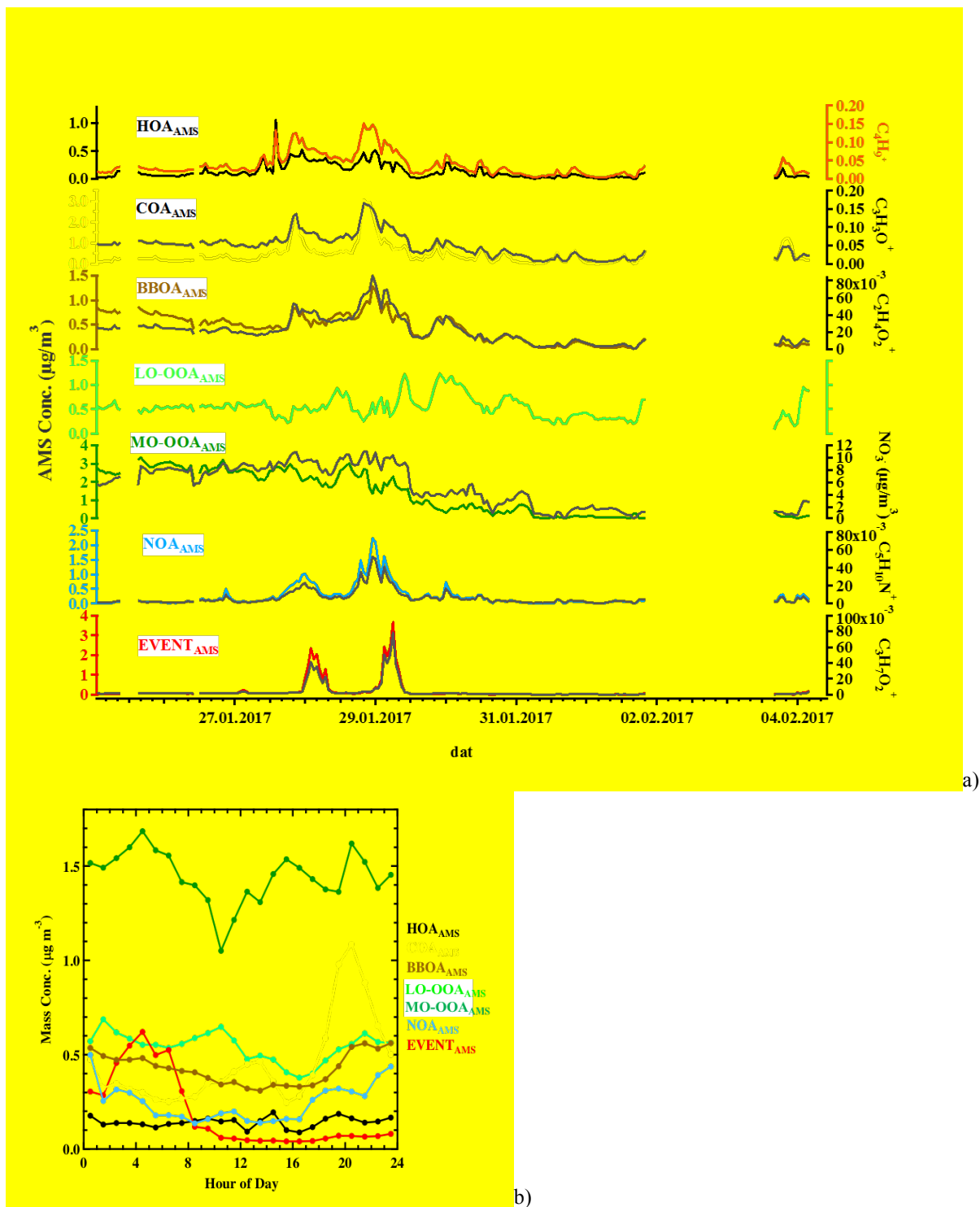


Fig. S1 a) Time-series of the AMS factors. b) Diurnal variations of the AMS factors.

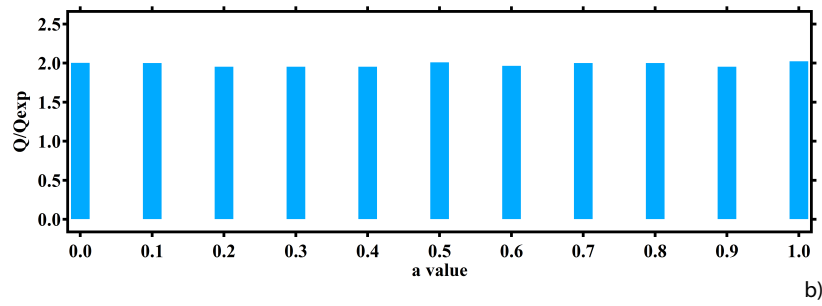
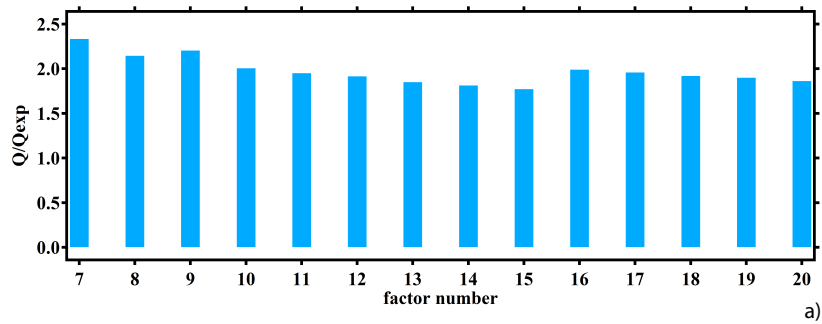
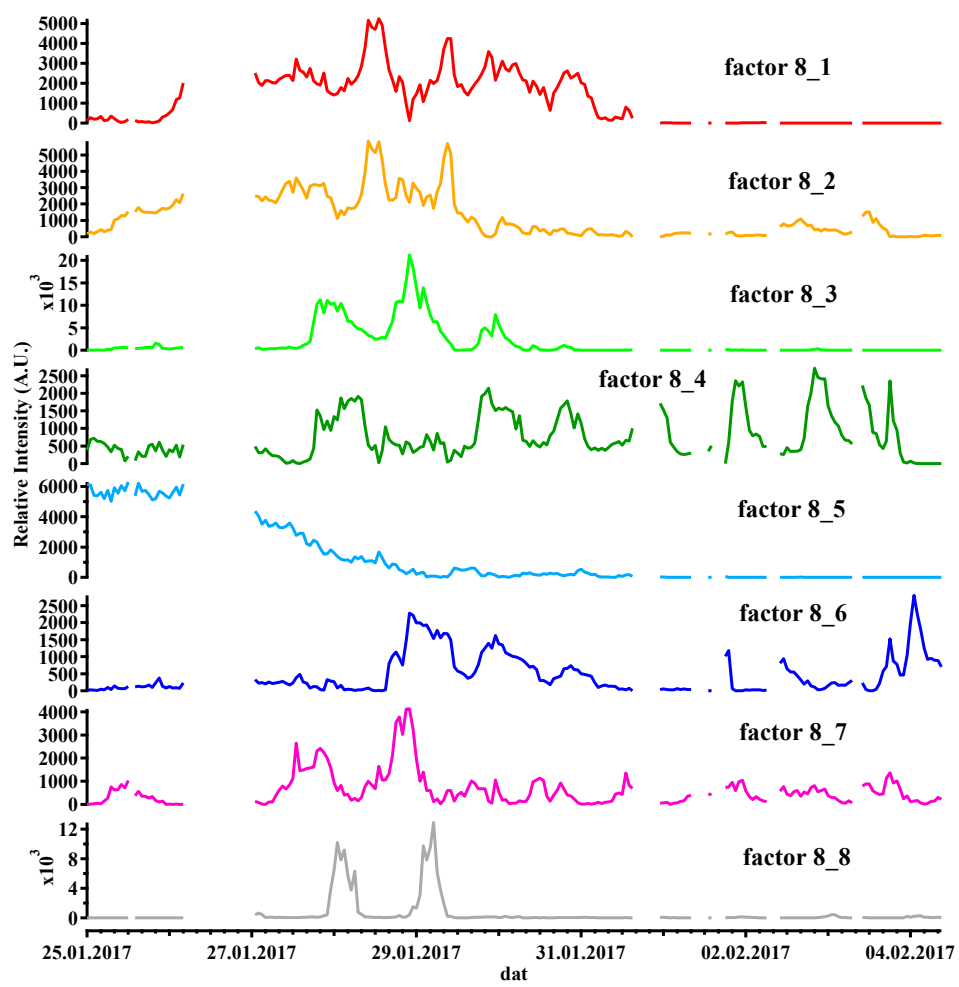
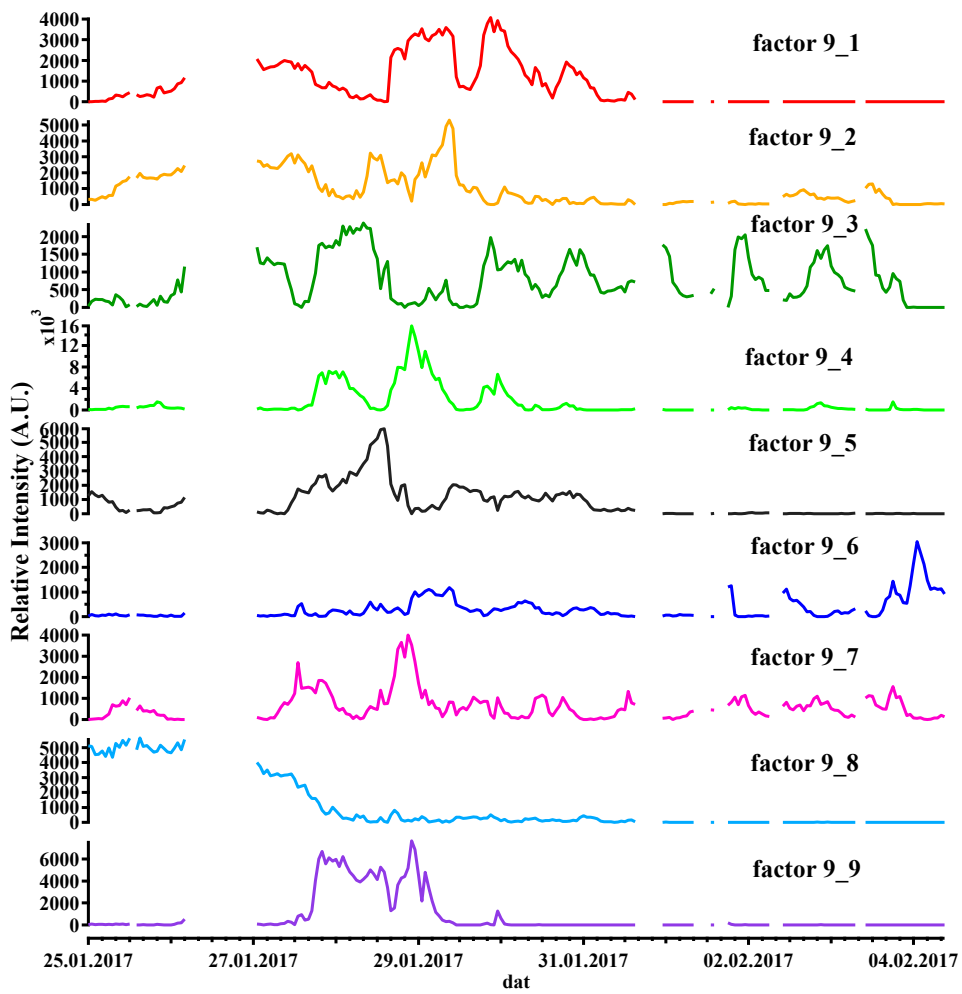


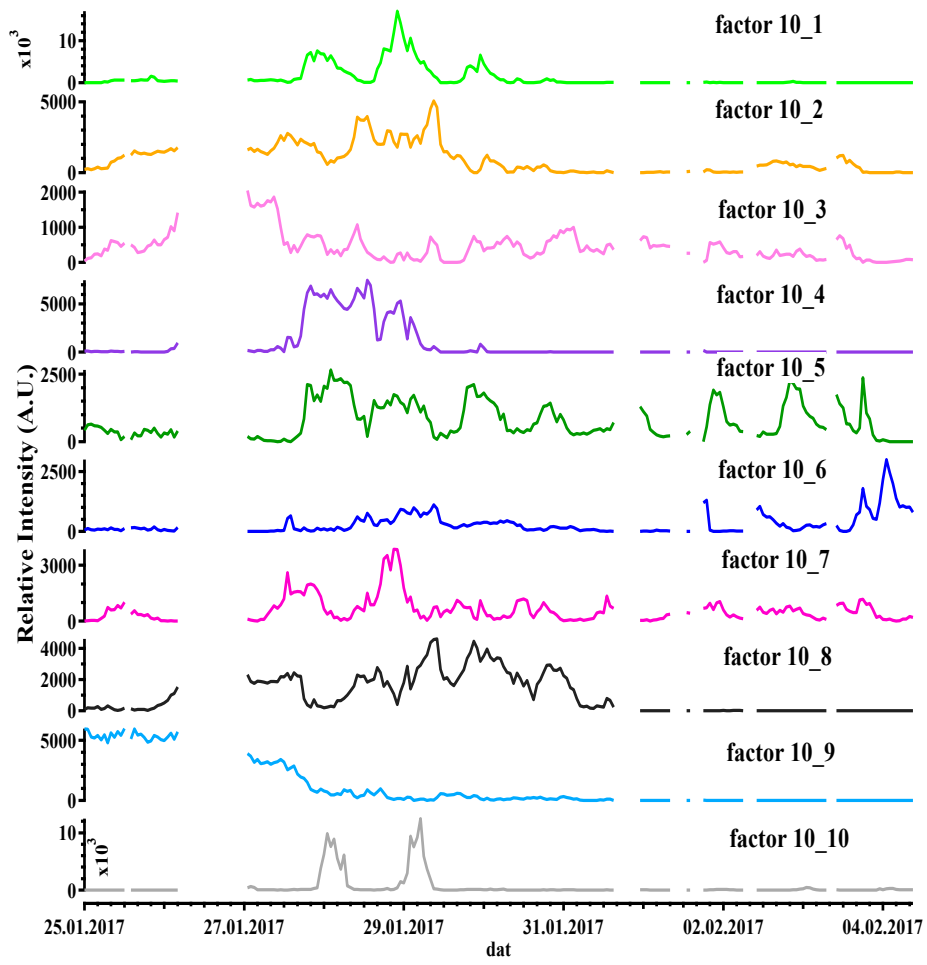
Fig. S2 a) Q/Q_{exp} for the unconstrained solutions from 7 to 20 factors. b) Q/Q_{exp} for the set of final 11-factor solutions (with CSOA constrained).



a)



b)



c)

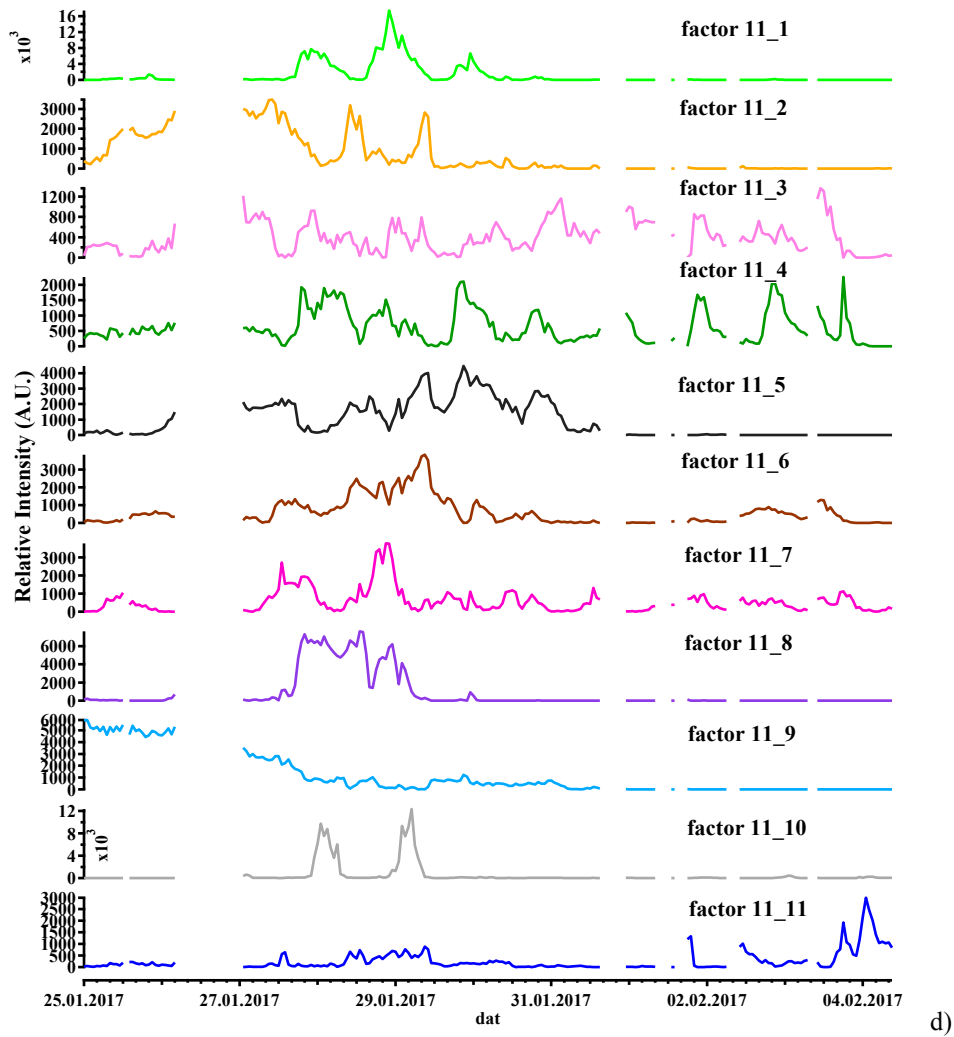
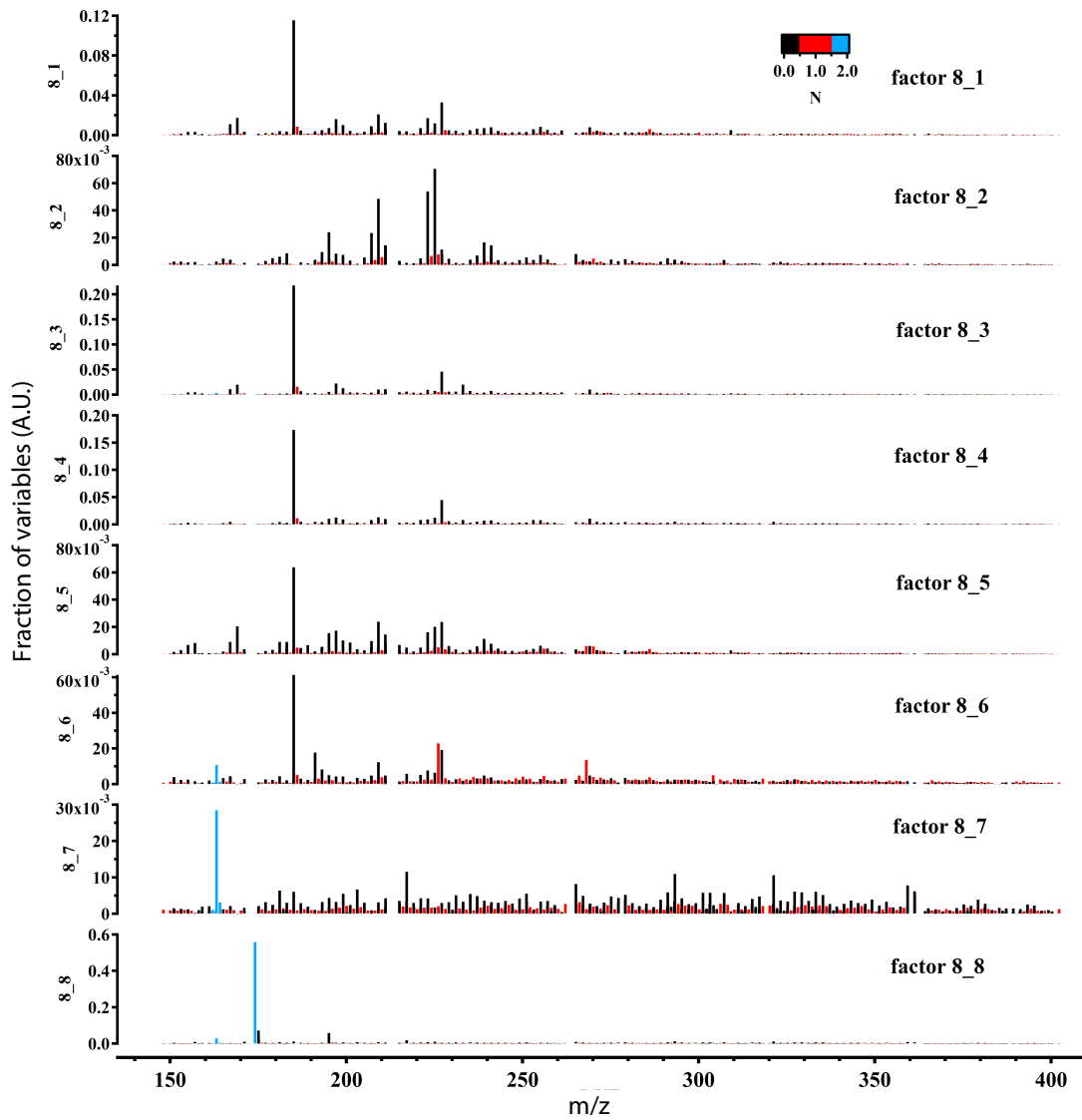
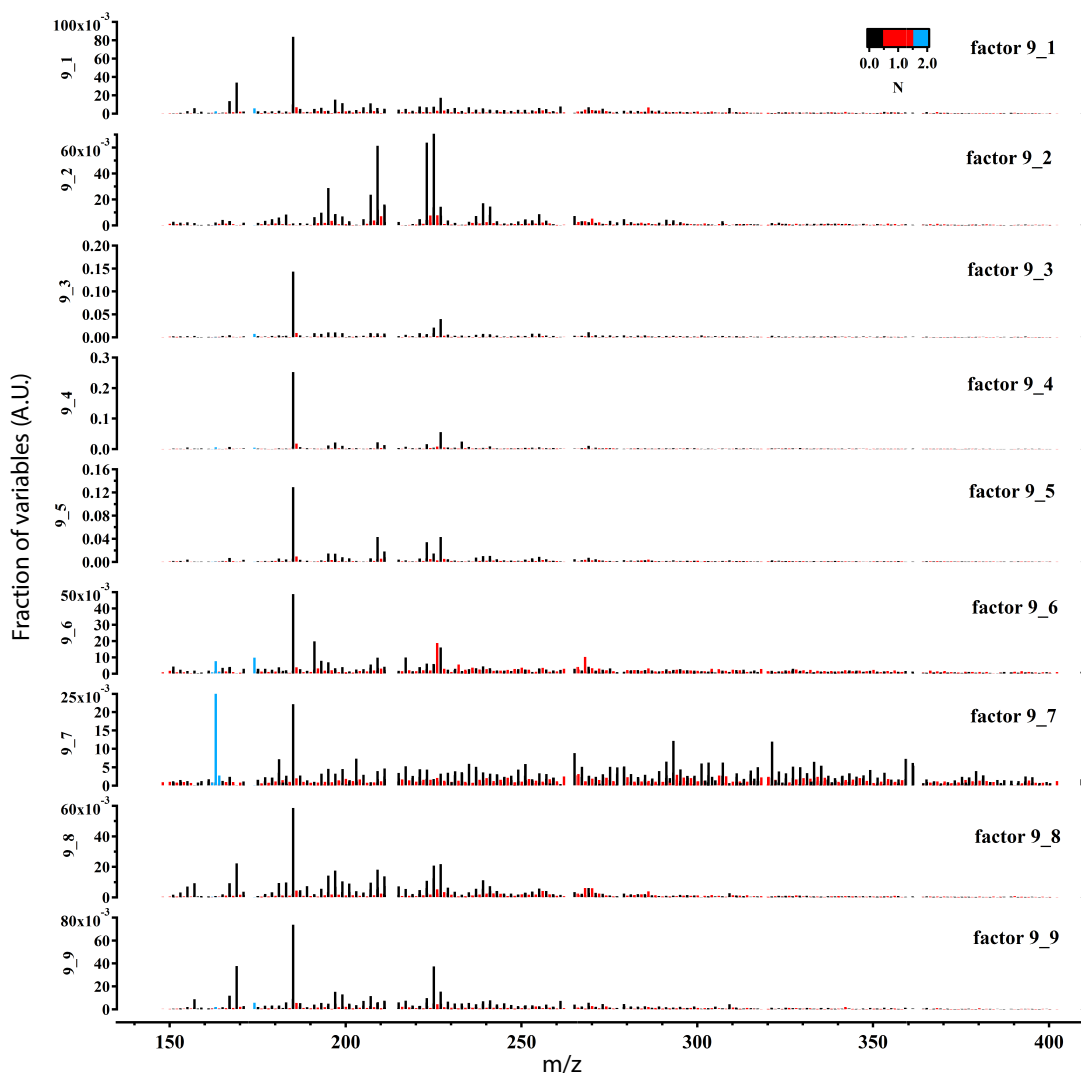


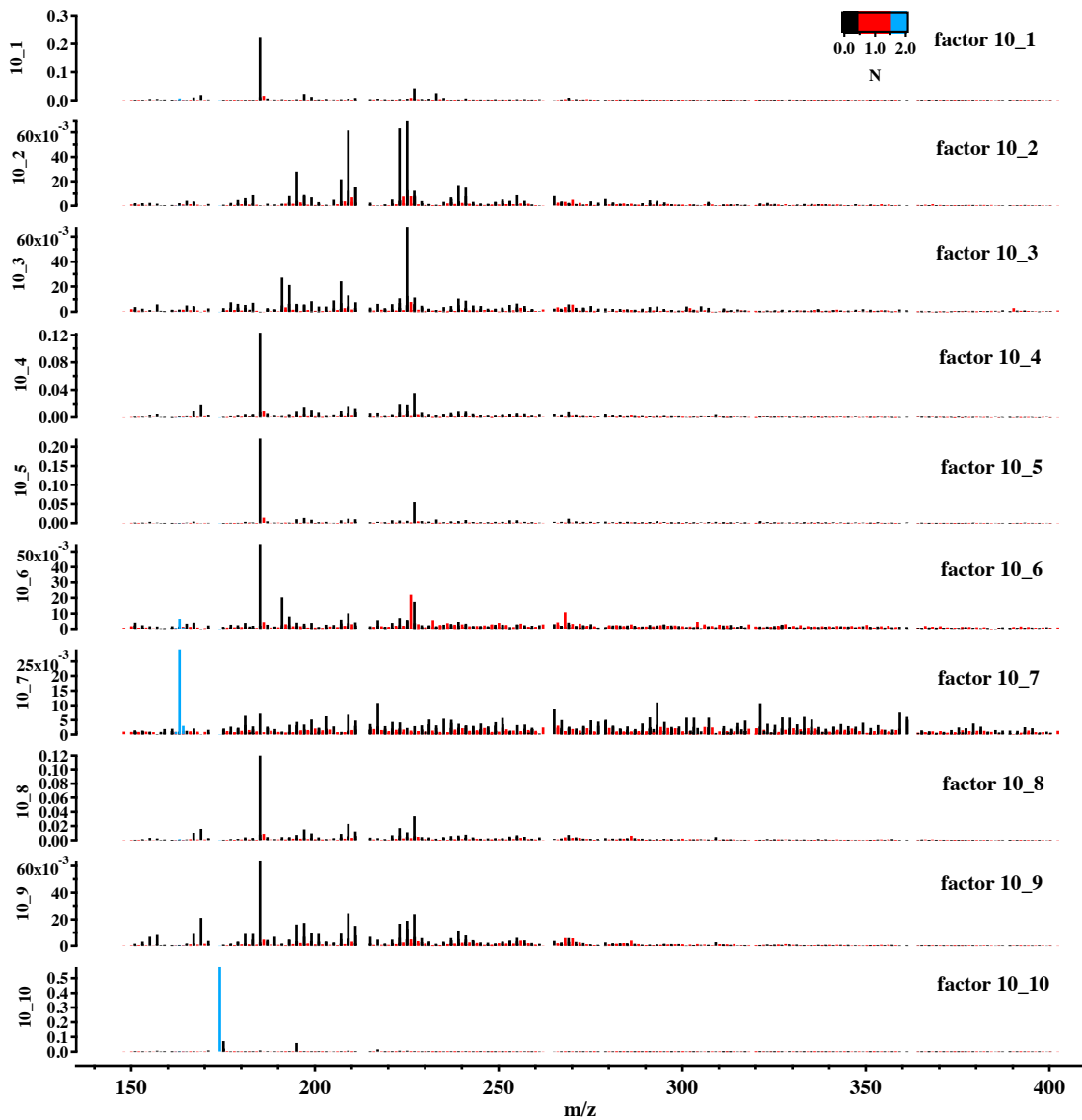
Fig. S3 Time series of solutions for 8 to 11 factors without constraining CSOA.



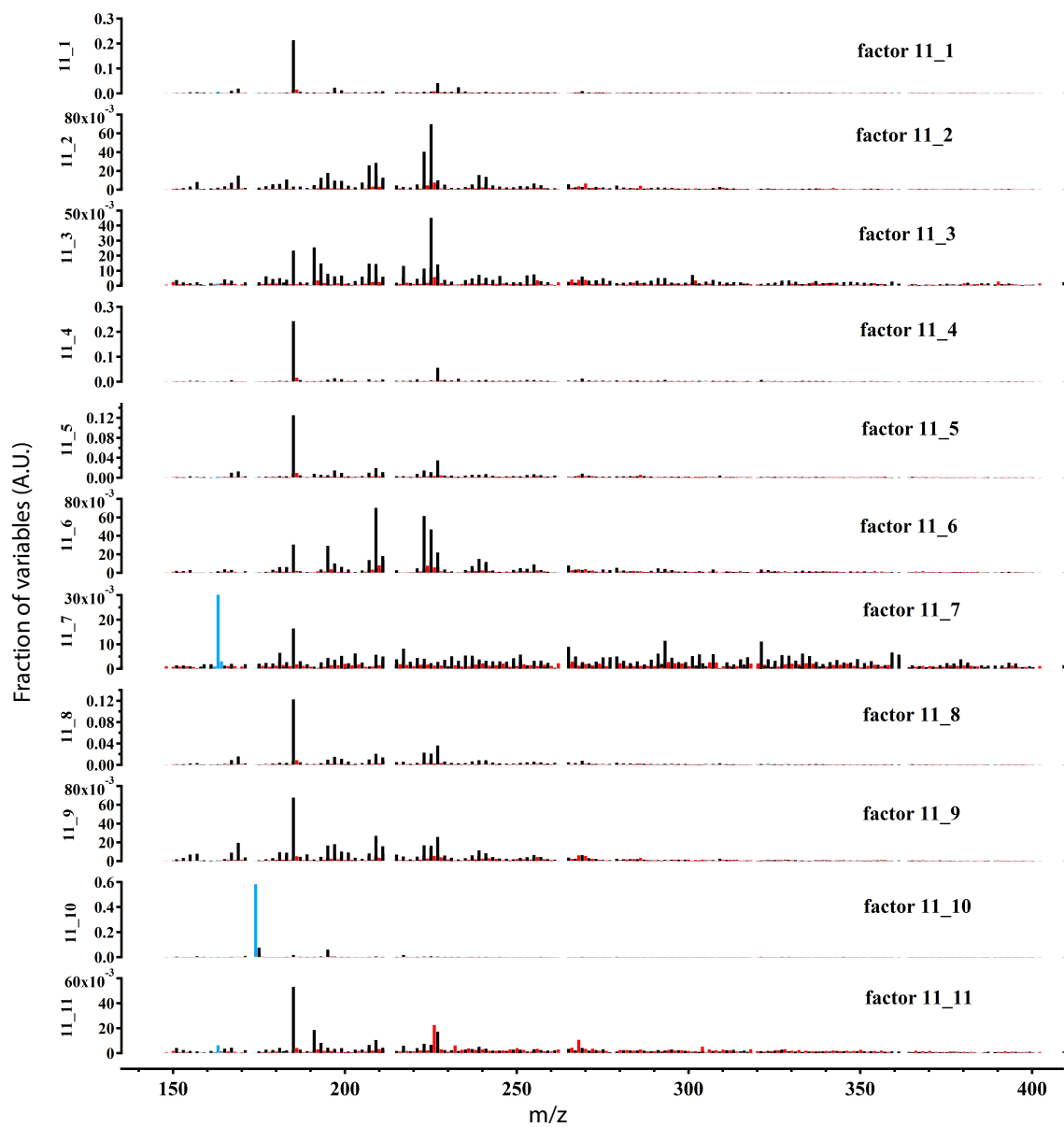
a)



b)



c)



d)

Fig. S4 Profiles of solutions for 8 to 11 factors without constraining CS-OA.

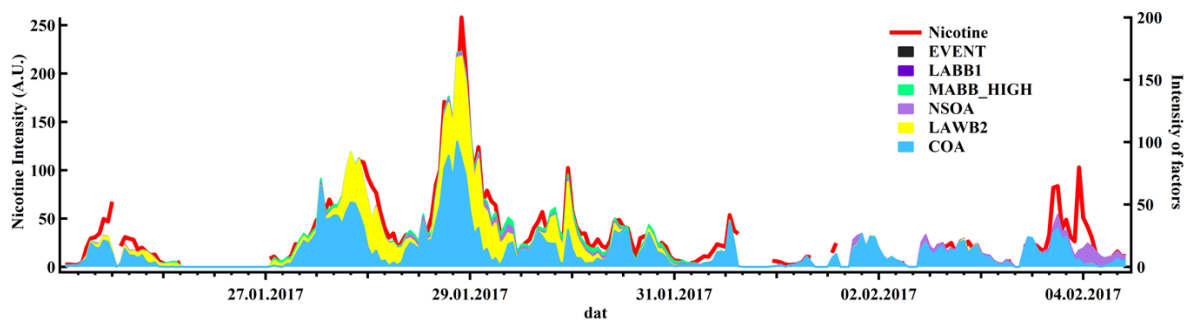


Fig. S5. Comparison between time series of the intensity of nicotine composition and the intensity of contributions of nicotine to each factor (10 factors' solution).

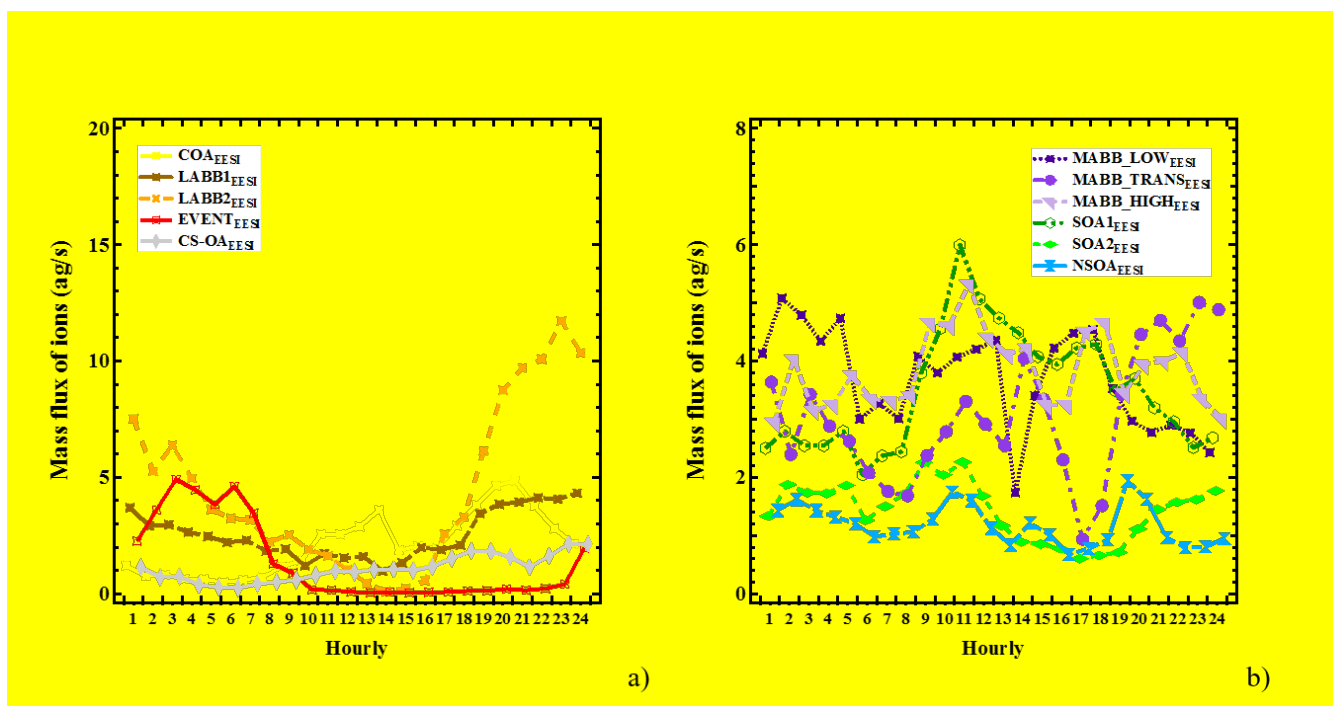


Fig. S6. The diurnal variation of EESI POA factors (a) and EESI SOA factors (b).

Table S1. The O:C, H:C, and N:C values for the EESI and AMS factors (excluding the C₆H₁₀O₅ and C₈H₁₂O₆ ions).

	O:C	H:C	N:C
EESI-TOF			
LABB1	0.35	1.04	0.02
MABB_LOW	0.50	1.39	0.02
SOA1	0.42	1.61	0.02
COA	0.30	1.56	0.02
MABB_HIGH	0.45	1.26	0.02
EVENT	0.23	1.44	0.15
LABB2	0.37	1.09	0.02
MABB_TRANS	0.43	1.28	0.02
SOA2	0.43	1.54	0.02
NSOA	0.39	1.41	0.04
CS-OA	0.31	1.51	0.05
AMS			
HOA	0.04	1.79	0.01
OOA1	0.58	1.01	0.02
OOA2	0.84	0.84	0.02
EVENT	0.27	1.89	0.03
COA	0.10	1.55	0.02
NOA	0.43	1.33	0.05
BBOA	0.39	1.49	0.04

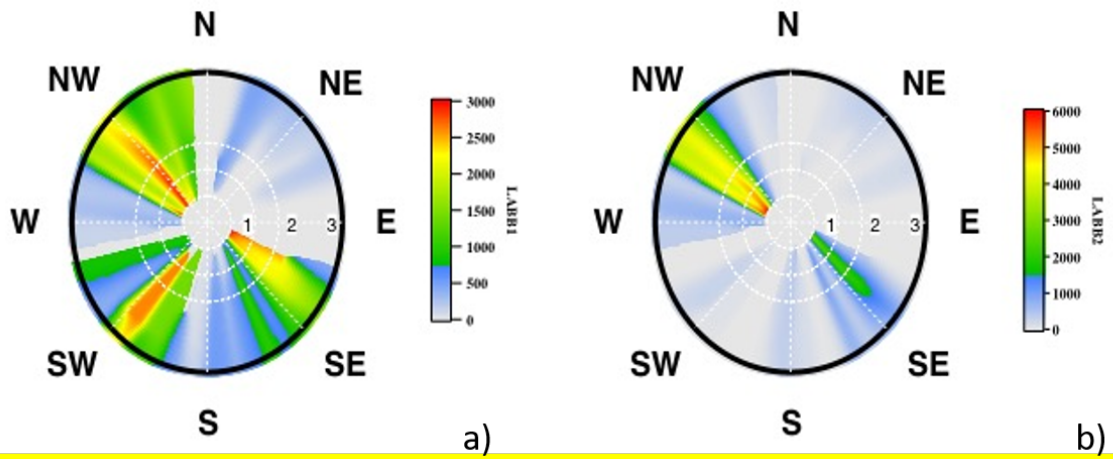


Fig.S7. Wind analysis results using the SWIM model on the concentrations of LABB1 (a) and LABB2 (b).

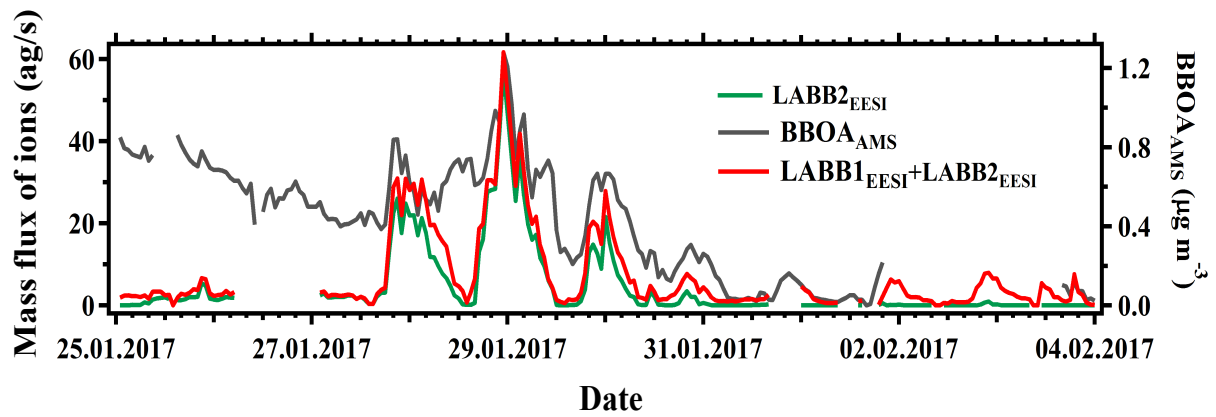


Fig.S8. Comparison between the LABB_{EESI} factors and the WBOA_{AMS} factor.

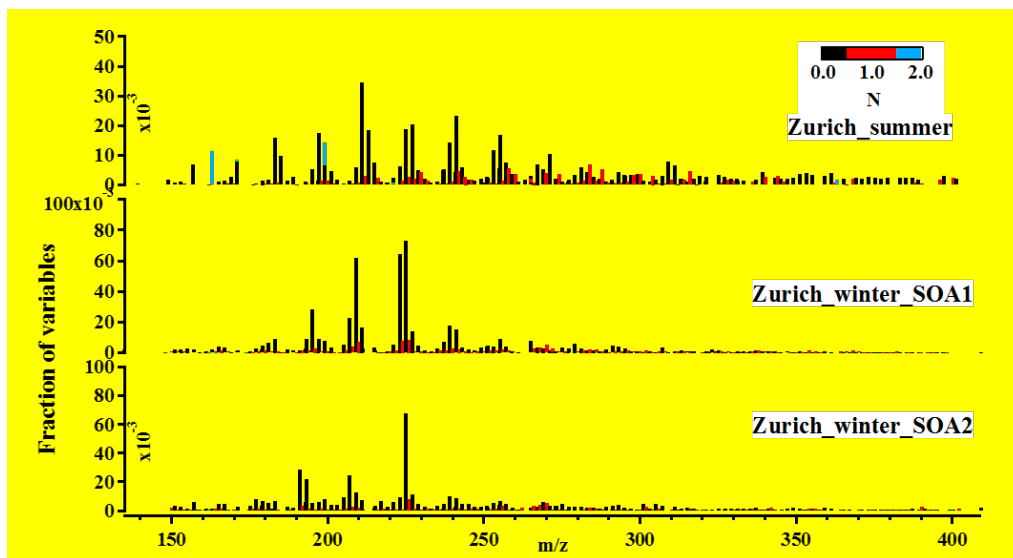
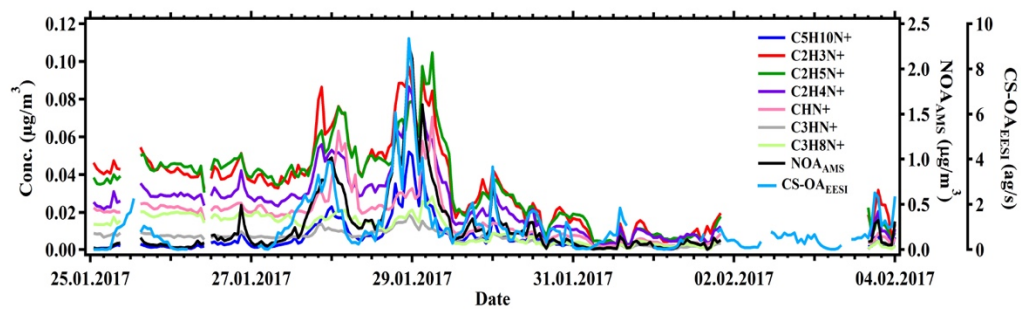


Fig. S9. Mass spectra comparison between SOA factors and reference mass spectra from Zurich summer source apportionment.



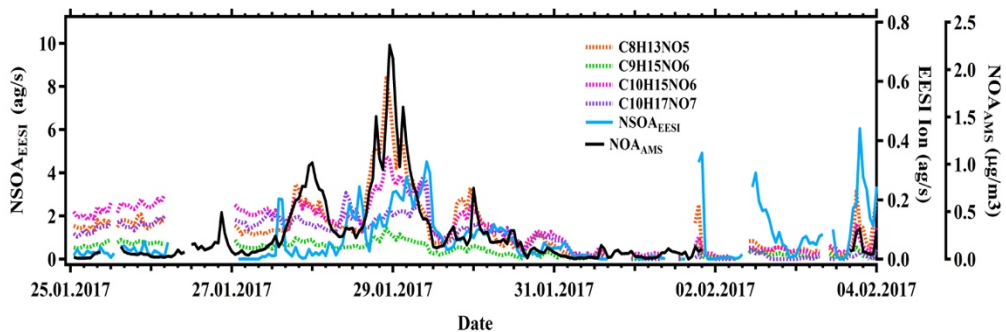
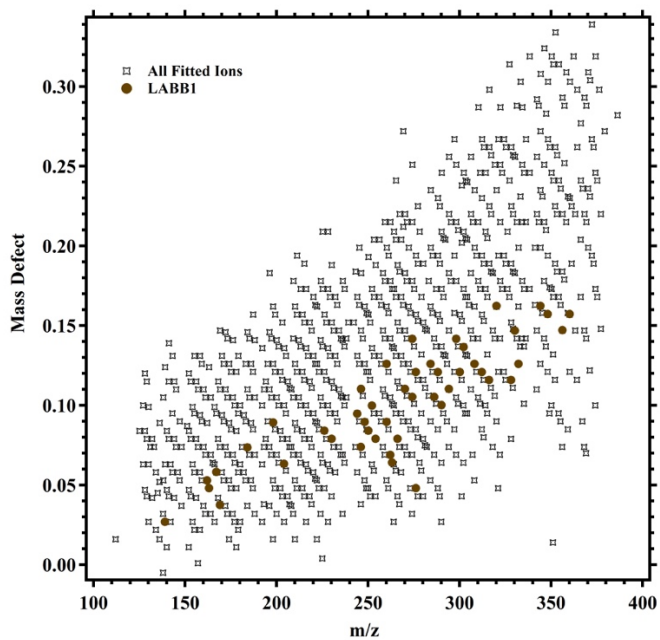
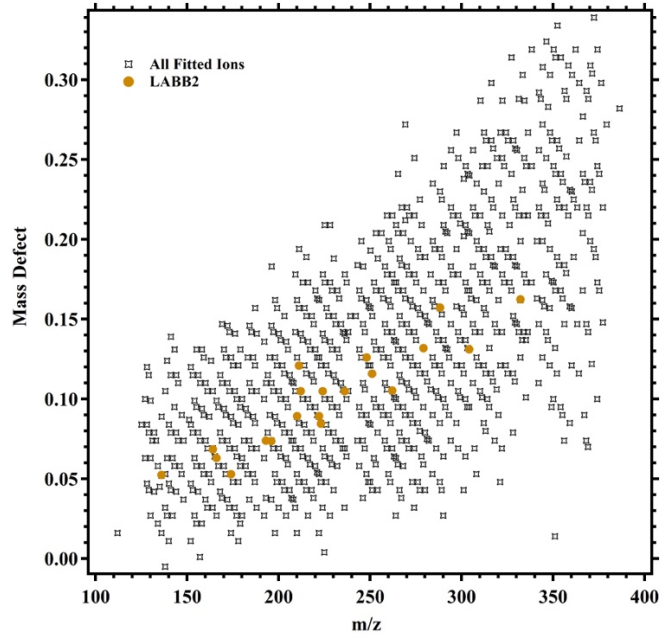
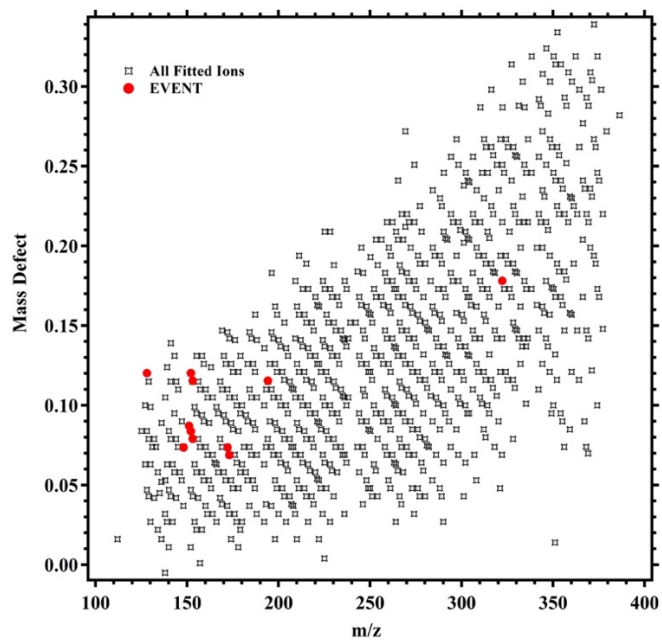
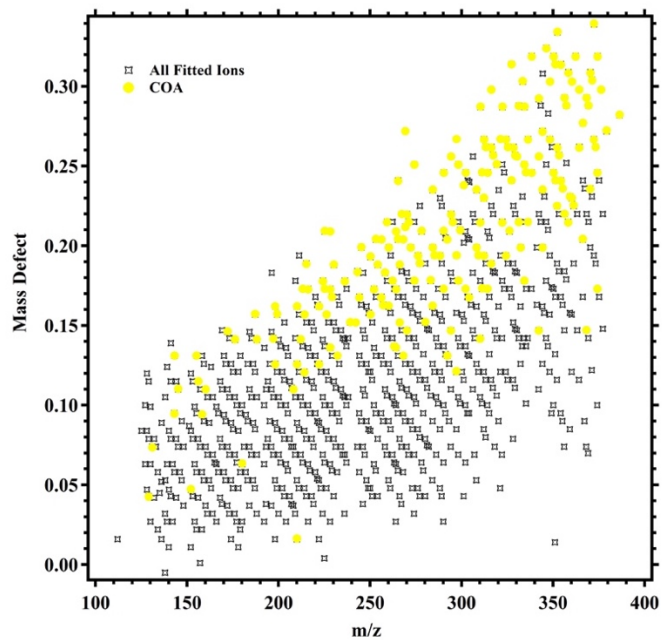
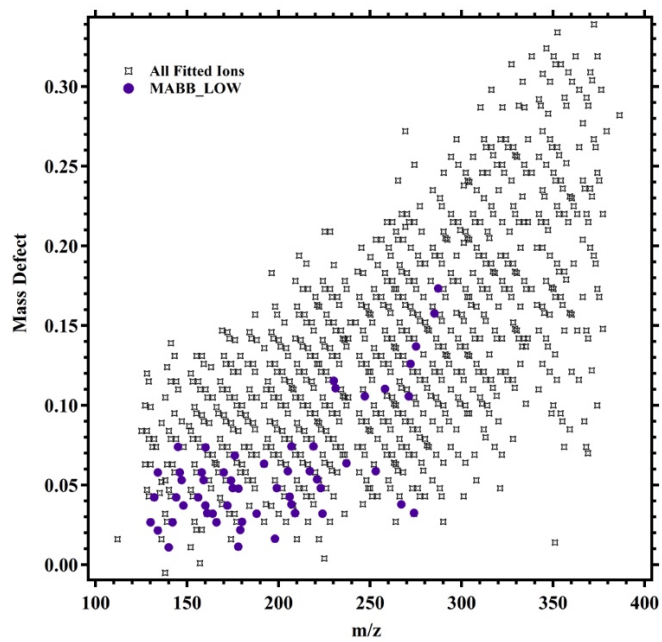
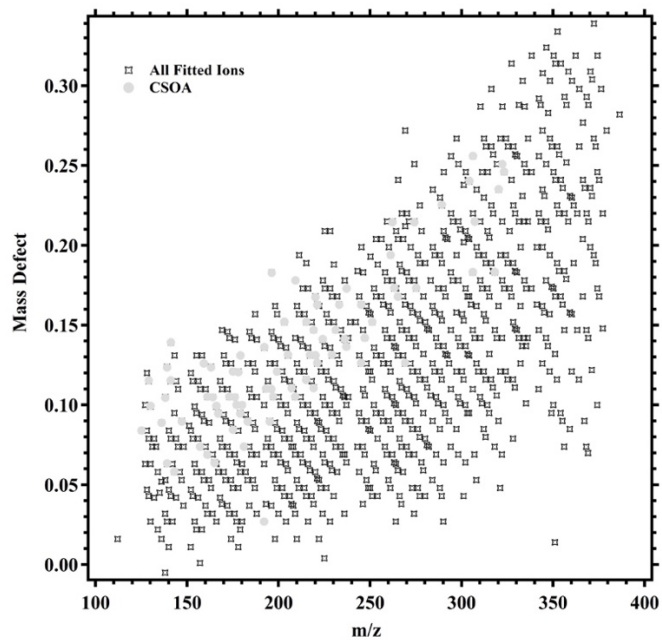


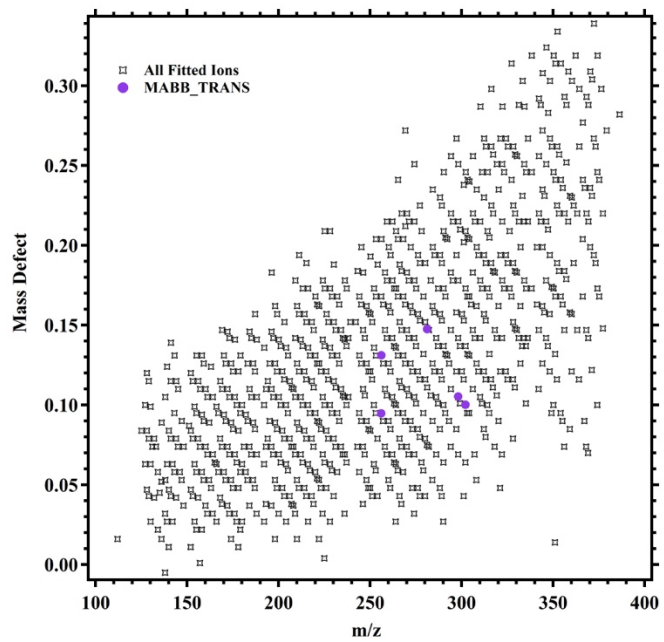
Fig. S10. Time series of fragments group of AMS CHON and AMS CHN compared to the time series of NSOA_{EESI} factor and CS-OA_{EESI} factor, respectively.

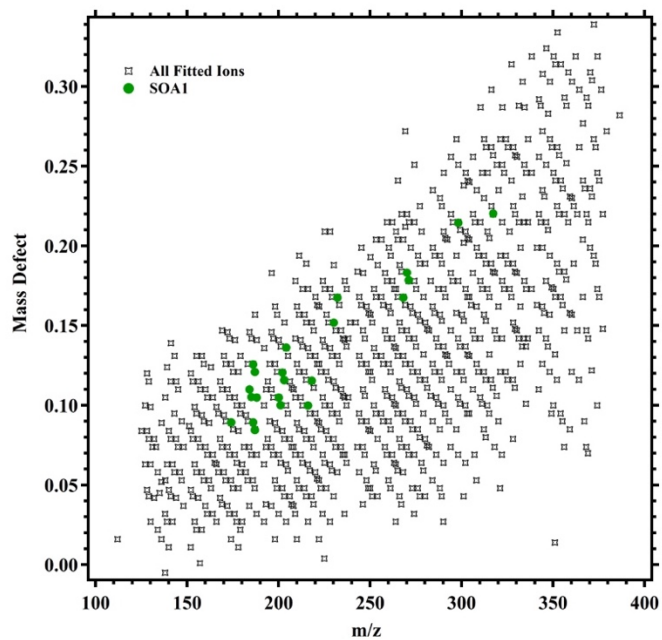
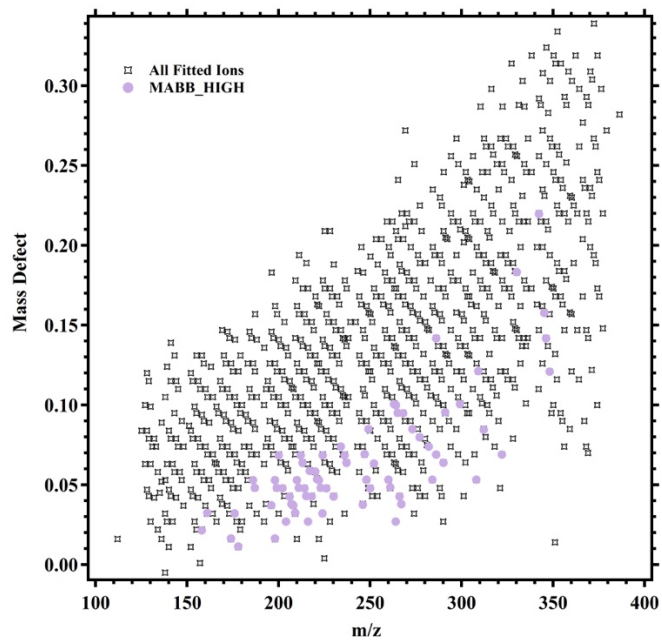












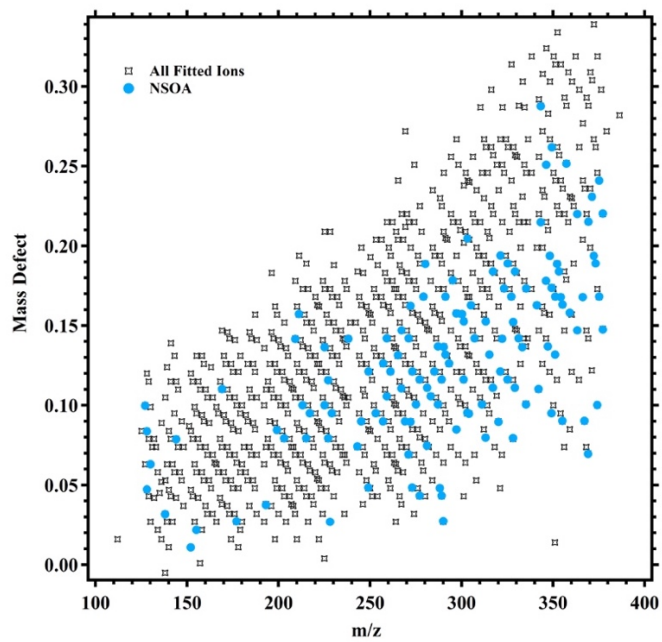
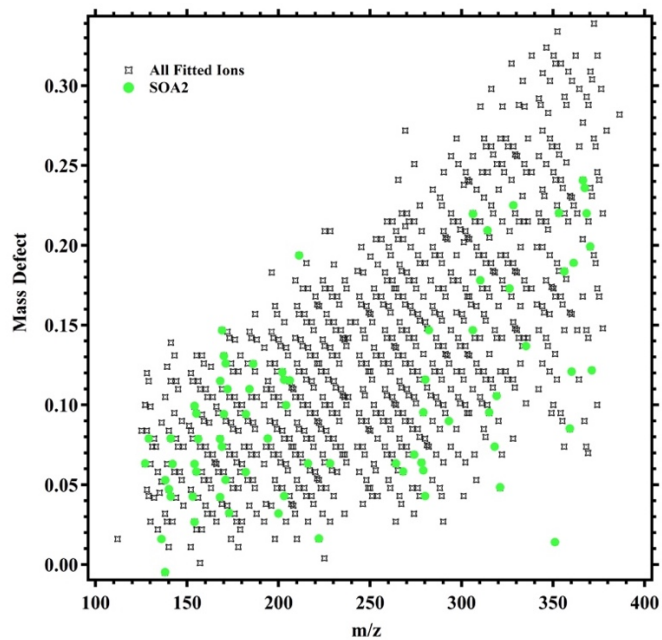


Fig. S11. Mass defect plots for each factor, with the unique ions marked in colors.

Table S2. Tentative formula assignment of MS peaks with m/z values for cluster groups.

Factor Name	Ion formula	m/z
COA		
	C5H4O3	112.016
	C5H7NO3	129.043
	C9H9N	131.074
	C7H13NO2	143.095
	C8H17NO	143.131
	C7H15NO2	145.11
	C8H8O3	152.047
	C9H17NO	155.131
	C9H16O2	156.115
	C8H14O3	158.094
	C8H16O3	160.11
	C10H20O2	172.146
	C9H19NO2	173.142
	C9H20O3	176.141
	C6H12O6	180.063
	C11H20O2	184.146
	C10H19NO2	185.142
	C10H21NO2	187.157
	C10H20O3	188.141
	C11H19NO2	197.142
	C11H18O3	198.126
	C12H22O2	198.162
	C11H21NO2	199.157
	C11H20O3	200.141
	C12H16O3	208.11
	C9H6O6	210.016
	C12H18O3	210.126
	C13H22O2	210.162
	C12H20O3	212.141
	C12H23NO2	213.173
	C11H18O4	214.121
	C12H22O3	214.157
C12H25NO2	215.189	
C12H24O3	216.173	
C13H18O3	222.126	
C14H22O2	222.162	
C14H24O2	224.178	

C13H23NO2	225.173
C14H27NO	225.209
C13H22O3	226.157
C12H20O4	228.136
C13H24O3	228.173
C14H28O2	228.209
C12H23NO3	229.168
C13H26O3	230.188
C11H20O5	232.131
C15H24O2	236.178
C13H21NO3	239.152
C13H22O4	242.152
C13H25NO3	243.184
C13H24O4	244.168
C13H27NO3	245.199
C15H22O3	250.157
C16H26O2	250.193
C15H24O3	252.173
C15H27NO2	253.204
C15H26O3	254.188
C14H24O4	256.168
C15H28O3	256.204
C13H23NO4	257.163
C14H26O4	258.183
C14H29NO3	259.215
C13H24O5	260.162
C14H28O4	260.199
C13H26O5	262.178
C11H21NO6	263.137
C15H20O4	264.136
C16H24O3	264.173
C17H28O2	264.209
C16H27NO2	265.204
C17H31NO	265.241
C15H22O4	266.152
C16H26O3	266.188
C16H29NO2	267.22
C14H20O5	268.131
C16H28O3	268.204
C16H29O3	269.212
C17H35NO	269.272

C14H22O5	270.147
C16H30O3	270.22
C15H29NO3	271.215
C15H28O4	272.199
C14H26O5	274.178
C16H34O3	274.251
C14H28O5	276.194
C13H27NO5	277.189
C14H30O5	278.209
C12H24O7	280.152
C15H25NO4	283.178
C15H24O5	284.162
C16H28O4	284.199
C17H32O3	284.235
C15H27NO4	285.194
C15H28O5	288.194
C14H26O6	290.173
C15H30O5	290.209
C16H34O4	290.246
C16H20O5	292.131
C18H28O3	292.204
C16H22O5	294.147
C18H30O3	294.22
C19H34O2	294.256
C17H29NO3	295.215
C14H19NO6	297.121
C16H27NO4	297.194
C18H35NO2	297.267
C16H26O5	298.178
C18H34O3	298.251
C16H29NO4	299.21
C17H33O4	301.238
C15H26O6	302.173
C17H34O4	302.246
C18H24O4	304.168
C18H28O4	308.199
C19H32O3	308.235
C17H27NO4	309.194
C16H22O6	310.142
C18H30O4	310.215
C20H38O2	310.287

C16H25NO5	311.173
C18H33NO3	311.246
C17H28O5	312.194
C18H32O4	312.23
C19H36O3	312.267
C18H35NO3	313.262
C16H26O6	314.173
C18H34O4	314.246
C16H28O6	316.189
C18H36O4	316.262
C19H40O3	316.298
C17H35NO4	317.257
C20H33NO2	319.251
C20H35NO2	321.267
C19H30O4	322.215
C21H38O2	322.287
C18H28O5	324.194
C20H36O3	324.267
C19H35NO3	325.262
C18H30O5	326.209
C18H33NO4	327.241
C20H41NO2	327.314
C19H36O4	328.262
C18H35NO4	329.257
C22H34O2	330.256
C20H29NO3	331.215
C22H37NO	331.288
C20H28O4	332.199
C22H39NO	333.303
C19H26O5	334.178
C21H34O3	334.251
C22H38O2	334.287
C20H33NO3	335.246
C16H32O7	336.215
C21H36O3	336.267
C20H34O4	338.246
C22H42O2	338.319
C20H22O5	342.147
C23H34O2	342.256
C24H38O	342.292
C21H28O4	344.199

C22H32O3	344.235
C23H36O2	344.272
C24H42O	346.324
C22H36O3	348.267
C23H40O2	348.303
C21H34O4	350.246
C23H42O2	350.319
C20H33NO4	351.241
C22H41NO2	351.314
C20H32O5	352.225
C21H36O4	352.262
C23H44O2	352.334
C20H35NO4	353.257
C20H34O5	354.241
C22H42O3	354.314
C19H33NO5	355.236
C19H32O6	356.22
C21H40O4	356.293
C20H39NO4	357.288
C22H30O4	358.215
C21H42O4	358.309
C18H33NO6	359.231
C22H32O4	360.23
C24H40O2	360.303
C21H31NO4	361.225
C24H42O2	362.319
C22H36O4	364.262
C23H40O3	364.298
C20H30O6	366.204
C22H38O4	366.277
C18H24O8	368.147
C22H40O4	368.293
C21H39NO4	369.288
C20H34O6	370.236
C22H42O4	370.309
C21H41NO4	371.304
C24H36O3	372.267
C26H44O	372.339
C23H35NO3	373.262
C21H26O6	374.173
C23H34O4	374.246

	C25H42O2	374.319
	C24H40O3	376.298
	C22H37NO4	379.272
	C25H38O3	386.282
LABBI		
	C6H5NO3	139.027
	C6H10O5	162.053
	C5H9NO5	163.048
	C8H9NO3	167.058
	C7H7NO4	169.038
	C9H12O4	184.074
	C10H14O4	198.089
	C8H12O6	204.063
	C10H14O6	230.079
	C13H14O5	250.084
	C13H16O5	252.1
	C10H14O8	262.069
	C9H13NO8	263.064
	C13H14O6	266.079
	C13H18O6	270.11
	C12H18O7	274.105
	C13H22O6	274.142
	C10H12O9	276.048
	C12H20O7	276.121
	C14H20O6	284.126
	C13H18O7	286.105
	C13H20O7	288.121
	C12H18O8	290.1
	C15H18O6	294.11
	C15H22O6	298.142
	C14H20O7	300.121
	C14H22O7	302.137
	C16H20O6	308.126
	C15H20O7	312.121
	C14H20O8	316.116
	C18H24O5	320.162
	C15H20O8	328.116
	C19H22O5	330.147
	C18H20O6	332.126
	C20H24O5	344.162
	C19H24O6	348.157

	C17H24O8	356.147
	C20H24O6	360.157
LABB2		
	C8H8O2	136.052
	C6H12O5	164.069
	C9H10O3	166.063
	C10H11NO3	193.074
	C10H12O4	196.074
	C11H14O4	210.089
	C11H17NO3	211.121
	C11H16O4	212.105
	C12H14O4	222.089
	C11H13NO4	223.085
	C12H16O4	224.105
	C13H16O4	236.105
	C11H20O6	248.126
	C13H17NO4	251.116
	C11H18O7	262.105
	C11H21NO7	279.132
	C14H24O6	288.157
	C17H20O5	304.131
	C19H24O5	332.162
EVENT		
	C8H16O	128.12
	C6H12O4	148.074
	C8H11N2O	151.087
	C9H12O2	152.084
	C10H16O	152.12
	C8H11NO2	153.079
	C9H15NO	153.115
	C8H12O4	172.074
	C7H11NO4	173.069
	C8H18O5	194.115
	C11H17NO2	195.126
	C18H26O5	322.178
CS-OA		
	C7H11NO	125.084
	C7H15NO	129.115
	C7H14O2	130.099
	C9H12O	136.089
	C9H14O	138.105

C7H9NO2	139.063
C8H15N2	139.124
C8H15NO	141.115
C8H17N2	141.139
C6H9NO3	143.058
C6H13NO3	147.09
C7H11NO3	157.074
C8H17NO2	159.126
C6H11NO4	161.069
C7H15NO3	161.105
C10H15N2	163.124
C7H16O4	164.105
C5H11NO5	165.064
C10H14O2	166.099
C9H13NO2	167.095
C8H15NO3	173.105
C7H13NO4	175.085
C8H17NO3	175.121
C8H16O4	176.105
C7H15NO4	177.1
C8H18O4	178.121
C10H13NO2	179.095
C11H17NO	179.131
C7H16O5	180.1
C9H11NO3	181.074
C9H13NO3	183.09
C6H8O7	192.027
C9H20O4	192.136
C11H15NO2	193.11
C10H13NO3	195.09
C11H16O3	196.11
C13H24O	196.183
C10H15NO3	197.105
C10H17NO3	199.121
C10H21NO3	203.152
C9H19NO4	205.131
C8H17NO5	207.111
C11H15NO3	209.105
C13H23NO	209.178
C11H21NO3	215.152
C10H19NO4	217.131

	C9H17NO5	219.111
	C10H21NO4	219.147
	C10H20O5	220.131
	C11H24O4	220.168
	C9H19NO5	221.126
	C10H23NO4	221.163
	C13H20O3	224.141
	C11H21NO4	231.147
	C11H23NO4	233.163
	C14H20O3	236.141
	C13H19NO3	237.137
	C14H23NO2	237.173
	C12H23NO4	245.163
	C11H21NO5	247.142
	C14H21NO3	251.152
	C13H27NO4	261.194
	C14H30O4	262.215
	C12H25NO5	263.173
	C15H23NO3	265.168
	C13H19NO5	269.126
	C15H30O4	274.215
	C13H25NO5	275.173
	C15H31NO4	289.225
	C20H32O2	304.24
	C18H26O4	306.183
	C20H34O2	306.256
	C18H29NO3	307.215
	C19H26O4	318.183
	C20H32O3	320.235
	C20H34O3	322.251
	C19H33NO3	323.246
	MABB_LOW	
	C5H6O4	130.027
	C5H8O4	132.042
	C4H6O5	134.022
	C5H10O4	134.058
	C6H4O4	140.011
	C6H6O4	142.027
	C6H8O4	144.042
	C6H11NO3	145.074
	C6H10O4	146.058

C5H9NO4	147.053
C5H8O5	148.037
C7H8O4	156.042
C7H10O4	158.058
C6H9NO4	159.053
C6H8O5	160.037
C7H12O4	160.074
C5H7NO5	161.032
C5H8O6	164.032
C8H6O4	166.027
C8H10O4	170.058
C7H8O5	172.037
C7H10O5	174.053
C6H9NO5	175.048
C7H12O5	176.069
C5H6O7	178.011
C6H10O6	178.048
C8H5NO4	179.022
C5H8O7	180.027
C7H8O6	188.032
C7H12O6	192.063
C8H6O6	198.016
C8H9NO5	199.048
C7H11NO6	205.059
C7H10O7	206.043
C6H9NO7	207.038
C7H13NO6	207.074
C9H7NO5	209.032
C8H11NO6	217.059
C8H13NO6	219.074
C7H11NO7	221.054
C10H9NO5	223.048
C10H8O6	224.032
C11H18O5	230.115
C10H17NO5	231.111
C11H11NO5	237.064
C10H17NO6	247.106
C11H11NO6	253.059
C12H18O6	258.11
C11H9NO7	267.038
C12H17NO6	271.106

	C13H20O6	272.126
	C10H10O9	274.032
	C12H21NO6	275.137
	C14H23NO5	285.158
	C14H25NO5	287.173
MABB_TRANS		
	C12H16O6	256.095
	C13H20O5	256.131
	C11H23NO7	281.148
	C14H18O7	298.105
	C13H18O8	302.1
MABB_HIGH		
	C6H6O5	158.022
	C5H7NO5	161.032
	C6H6O6	174.016
	C6H8O6	176.032
	C5H6O7	178.011
	C8H10O5	186.053
	C7H9NO5	187.048
	C9H8O5	196.037
	C8H6O6	198.016
	C9H10O5	198.053
	C8H9NO5	199.048
	C9H12O5	200.069
	C8H10O6	202.048
	C7H8O7	204.027
	C7H10O7	206.043
	C6H9NO7	207.038
	C10H8O5	208.037
	C9H7NO5	209.032
	C10H10O5	210.053
	C9H9NO5	211.048
	C10H12O5	212.069
	C9H11NO5	213.064
	C9H10O6	214.048
	C8H9NO6	215.043
	C8H8O7	216.027
	C8H11NO6	217.059
	C8H10O7	218.043
	C8H12O7	220.058
	C7H11NO7	221.054

C11H10O5	222.053
C10H9NO5	223.048
C10H8O6	224.032
C11H12O5	224.069
C10H10O6	226.048
C9H10O7	230.043
C9H14O7	234.074
C12H12O5	236.069
C11H11NO5	237.064
C9H10O8	246.038
C9H13NO7	247.069
C9H12O8	248.053
C9H15NO7	249.085
C12H10O6	250.048
C12H12O6	252.063
C10H12O8	260.053
C9H11NO8	261.048
C10H17NO7	263.101
C12H8O7	264.027
C14H16O5	264.1
C13H15NO5	265.095
C12H10O7	266.043
C11H9NO7	267.038
C13H16O6	268.095
C11H15NO7	273.085
C10H15NO8	277.08
C13H14O7	282.074
C12H12O8	284.053
C12H14O8	286.069
C14H22O6	286.142
C11H14O9	290.064
C11H17NO8	291.095
C13H17NO7	299.101
C14H12O8	308.053
C15H19NO6	309.121
C14H16O8	312.085
C15H14O8	322.069
C20H26O4	330.183
C22H30O3	342.22
C19H23NO5	345.158
C19H22O6	346.142

	C18H20O7	348.121
SOA1		
	C8H14O4	174.089
	C9H15NO3	185.105
	C9H14O4	186.089
	C8H13NO4	187.085
	C9H17NO3	187.121
	C9H16O4	188.105
	C10H16O4	200.105
	C9H15NO4	201.1
	C10H20O4	204.136
	C10H16O5	216.1
	C10H18O5	218.115
	C12H22O4	230.152
	C12H24O4	232.168
	C14H25NO4	271.178
	C17H30O4	298.215
	C16H31NO5	317.22
SOA2		
	C6H9NO2	127.063
	C6H11NO2	129.079
	C7H4O3	136.016
	C6H2O4	137.995
	C4H10O5	138.053
	C7H8O3	140.047
	C6H7NO3	141.043
	C7H11NO2	141.079
	C7H10O3	142.063
	C7H7NO3	153.043
	C7H6O4	154.027
	C8H10O3	154.063
	C9H14O2	154.099
	C7H9NO3	155.058
	C8H13NO2	155.095
	C8H12O3	156.079
	C8H8O4	168.042
	C9H12O3	168.079
	C10H16O2	168.115
	C8H11NO3	169.074
	C10H19NO	169.147
	C9H14O3	170.094

C10H18O2	170.131
C7H9NO4	171.053
C9H17NO2	171.126
C9H16O3	172.11
C6H7NO5	173.032
C9H10O4	182.058
C10H14O3	182.094
C8H8O5	184.037
C10H16O3	184.11
C10H18O3	186.126
C7H14O6	194.079
C8H8O6	200.032
C10H18O4	202.121
C7H9NO6	203.043
C9H17NO4	203.116
C9H16O5	204.1
C9H18O5	206.115
C13H25NO	211.194
C9H12O6	216.063
C10H6O6	222.016
C9H5O7	225.004
C10H12O6	228.063
C9H11NO6	229.059
C9H12O7	232.058
C10H18O6	234.11
C11H8O6	236.032
C10H12O7	244.058
C11H10O7	254.043
C11H14O7	258.074
C13H12O6	264.063
C12H12O7	268.058
C15H24O4	268.168
C12H14O7	270.074
C15H26O4	270.183
C11H14O8	274.069
C10H14O9	278.064
C9H13NO9	279.059
C10H17NO8	279.095
C9H12O10	280.043
C11H20O8	280.116
C15H22O5	282.147

	C13H16O7	284.09
	C14H15NO6	293.09
	C13H14O8	298.069
	C17H22O5	306.147
	C19H30O3	306.22
	C15H18O7	310.105
	C17H26O5	310.178
	C16H24O6	312.157
	C14H18O8	314.1
	C17H30O5	314.209
	C13H17NO8	315.095
	C16H14O7	318.074
	C16H17NO6	319.106
	C14H11NO8	321.048
	C17H26O6	326.173
	C18H32O5	328.225
	C15H23NO7	329.148
	C17H21NO6	335.137
	C18H26O6	338.173
	C19H20O6	344.126
	C18H7O8	351.014
	C19H31NO5	353.22
	C16H18O9	354.095
	C15H16O10	356.074
	C18H28O7	356.184
	C14H17NO10	359.085
	C19H20O7	360.121
	C20H27NO5	361.189
	C21H34O5	366.241
	C20H33NO5	367.236
	C20H32O6	368.22
	C17H23NO8	369.142
	C19H30O7	370.199
	C16H21NO9	371.122
	NSOA	
	C7H13NO	127.1
	C6H8O3	128.047
	C7H12O2	128.084
	C6H10O3	130.063
	C7H6O3	138.032
	C7H12O3	144.079

C7H4O4	152.011
C6H5NO4	155.022
C9H15NO2	169.11
C5H7NO6	177.027
C8H9NO4	183.053
C8H11NO4	185.069
C9H7NO4	193.038
C9H11NO4	197.069
C9H13NO4	199.085
C8H11NO5	201.064
C8H13NO5	203.079
C8H15NO5	205.095
C12H19NO2	209.142
C10H13NO4	211.085
C12H21NO2	211.157
C10H15NO4	213.1
C11H19NO3	213.137
C9H13NO5	215.079
C10H17NO4	215.116
C9H15NO5	217.095
C7H9NO7	219.038
C8H15NO6	221.09
C12H17NO3	223.121
C10H11NO5	225.064
C11H15NO4	225.1
C12H19NO3	225.137
C12H18O4	226.121
C10H13NO5	227.079
C11H17NO4	227.116
C9H8O7	228.027
C10H15NO5	229.095
C11H19NO4	229.131
C9H15NO6	233.09
C9H17NO6	235.106
C10H21NO5	235.142
C12H15NO4	237.1
C10H22O6	238.142
C10H13NO6	243.074
C12H20O5	244.131
C10H15NO6	245.09
C11H19NO5	245.126

C8H11NO8	249.048
C10H19NO6	249.121
C14H20O4	252.136
C12H15NO5	253.095
C13H19NO4	253.131
C11H15NO6	257.09
C12H19NO5	257.126
C13H22O5	258.147
C10H13NO7	259.069
C11H17NO6	259.106
C12H21NO5	259.142
C11H19NO6	261.121
C12H23NO5	261.158
C12H22O6	262.142
C12H11NO6	265.059
C14H19NO4	265.131
C12H13NO6	267.074
C13H17NO5	267.111
C14H21NO4	267.147
C12H15NO6	269.09
C11H13NO7	271.069
C13H21NO5	271.142
C12H16O7	272.09
C14H24O5	272.162
C10H11NO8	273.048
C12H19NO6	273.121
C11H17NO7	275.101
C9H11NO9	277.043
C11H19NO7	277.116
C14H31NO4	277.225
C12H25NO6	279.168
C13H28O6	280.189
C9H15NO9	281.075
C10H19NO8	281.111
C13H17NO6	283.106
C13H19NO6	285.121
C12H17NO7	287.101
C13H21NO6	287.137
C11H12O9	288.048
C10H11NO9	289.043
C12H19NO7	289.116

C13H23NO6	289.153
C10H10O10	290.027
C13H22O7	290.137
C12H21NO7	291.132
C13H25NO6	291.168
C14H29NO5	291.205
C15H19NO5	293.126
C14H14O7	294.074
C16H25NO4	295.178
C13H15NO7	297.085
C15H23NO5	297.158
C14H21NO6	299.137
C15H24O6	300.157
C11H11NO9	301.043
C13H19NO7	301.116
C14H23NO6	301.153
C16H29O5	301.202
C12H14O9	302.064
C12H17NO8	303.095
C15H29NO5	303.205
C16H16O6	304.095
C17H23NO4	305.163
C14H13NO7	307.069
C16H21NO5	307.142
C14H17NO7	311.101
C13H15NO8	313.08
C15H23NO6	313.153
C16H27NO5	313.189
C14H21NO7	315.132
C16H29NO5	315.205
C13H19NO8	317.111
C15H27NO6	317.184
C16H16O7	320.09
C16H19NO6	321.121
C18H27NO4	321.194
C17H22O6	322.142
C17H25NO5	323.173
C15H19NO7	325.116
C17H27NO5	325.189
C16H25NO6	327.168
C14H16O9	328.079

C16H24O7	328.152
C14H19NO8	329.111
C16H27NO6	329.184
C18H21NO5	331.142
C21H19NO3	333.137
C20H31NO3	333.231
C20H30O4	334.215
C16H17NO7	335.101
C18H25NO5	335.173
C20H23NO4	341.163
C19H18O6	342.11
C21H29NO3	343.215
C23H37NO	343.288
C21H31NO3	345.231
C20H26O5	346.178
C22H34O3	346.251
C18H21NO6	347.137
C20H29NO4	347.21
C22H37NO2	347.283
C20H28O5	348.194
C20H15NO5	349.095
C15H27NO8	349.174
C21H35NO3	349.262
C17H18O8	350.1
C19H26O6	350.173
C17H21NO7	351.132
C18H25NO6	351.168
C17H20O8	352.116
C19H28O6	352.189
C18H27NO6	353.184
C18H26O7	354.168
C15H17NO9	355.09
C17H25NO7	355.163
C19H35NO5	357.252
C16H25NO8	359.158
C22H21NO4	363.147
C24H29NO2	363.22
C18H20O8	364.116
C19H26O7	366.168
C16H17NO9	367.09
C16H16O10	368.074

C15H15NO10	369.07
C19H31NO6	369.215
C19H33NO6	371.231
C22H28O5	372.194
C21H27NO5	373.189
C19H18O8	374.1
C20H25NO6	375.168
C22H33NO4	375.241
C19H23NO7	377.148
C21H31NO5	377.22